NASA Contractor Report 172308

THE CRACK-INCLUSION INTERACTION PROBLEM

Liu Xue-Hui and F. Erdogan

LEHIGH UNIVERSITY
Bethlehem, Pennsylvania 18015

Grant NGR 39-007-011
February 1984

NASA
National Aeronautics and
Space Administration

Langley Research Center
Hampton, Virginia 23665

ENTER:

16 1 1 RN/NASA-CR-172308

DISPLAY 16/6/1

84N19928*# ISSUE 10 PAGE 1516 CATEGORY 39 RPT*: NASA-CR-172308 NAS 1.26:172308 CNT*: NGR-39-007-011 DTRS56-82-C-00014 84/02/00 71 PAGES UNCLASSIFIED DOCUMENT

UTTL: The crack-inclusion interaction problem

AUTH: A/XUE-HUI, L.; B/ERDOGAN, F.

CORP: Lehigh Univ., Bethlehem, Pa. AVAIL.NTIS SAP: HC A04/MF A01 Hampton, Va. NASA. Langley Research Center

MAJS: /*CRACKS/*ELASTOSTATICS/*INCLUSIONS/*STRESS INTENSITY FACTORS

MINS: / CRACK GEOMETRY/ GREEN'S FUNCTIONS/ INTEGRAL EQUATIONS/ INTERSECTIONS/ STIFFNESS

ABA: A.R.H.

THE CRACK-INCLUSION INTERACTION PROBLEM*

by

Liu Xue-Hui and F. Erdogan

Lehigh University, Bethlehem, PA

ABSTRACT

In this study the general plane elastostatic problem of interaction between a crack and an inclusion is considered. The Green's functions for a pair of dislocations and a pair of concentrated body forces are used to generate the crack and the inclusion. The integral equations of the problem is obtained for a line crack and an elastic line inclusion having an arbitrary relative orientation and size. The nature of stress singularity around the end points of rigid and elastic inclusions is described. A question of specific interest which is studied is the nature of stress singularity around the point of intersection of the crack and the inclusion. Three special cases of this intersection problem which have been studied are a crack and an inclusion which are collinear and have a common end point, a crack perpendicular to an inclusion with a common end point (the L configuration), and a crack perpendicular to an inclusion terminating at its midpoint (the T configuration). The problem is solved for an arbitrary uniform stress state away from the crack-inclusion region. First, the non-intersecting crack-inclusion problem is considered for various relative size, orientation, and stiffness parameters and the stress intensity factors at the ends of the inclusion and the crack are calculated. Then for the crack-inclusion intersection case special stress intensity factors are defined and are calculated again for various values of the parameters defining the relative size and orientation of the crack and the inclusion and the stiffness of the inclusion.

(*) This work was supported by NASA-Langley under the Grant NGR 39 007 011 and by the U.S. Department of Transportation, Office of University Research under the Contract DTRS 5682-C-00014.

1. Introduction

In studying the fracture of multi-phase materials, structures composed of bonded dissimilar solids, and welded joints it is necessary to take into account the effect of the imperfections in the medium. Generally such imperfections are in the form of either geometric discontinuities or material inhomogeneities. For example, in welded joints various shapes of voids, cracks, notches and regions of lack of fusion may be mentioned as examples for the former and variety of inclusions for the latter. From the viewpoint of fracture mechanics two important classes of imperfections are the planar flaws which may be idealized as cracks and relatively thin inhomogeneities which may be idealized as flat inclusions with "sharp" boundaries. In both cases the edges of the defects are lines of stress singularity and, consequently, regions of potential crack initiation and propagation.

The technical literature on cracks, voids and inclusions which exist in the material separately is quite extensive. However, the problems concerning the interaction of cracks, voids and inclusions do not seem to be as widely studied (see, for example, [1] for the results of crack-circular inclusion or void interaction problem and for some references). In this paper the relatively simple problem of an elastic plane containing a crack and an arbitrarily oriented flat elastic inclusion is considered. Of special interest is the examination of the asymptotic stress field in the neighborhood of inclusion ends and the problems of intersecting cracks and inclusions. The basic dislocation and concentrated force solutions are used to formulate the problem [2]. Hence, the formulation can easily be extended to study problems involving multiple cracks and inclusions.

2. Integral Equations of the Problem

The geometry of the crack-inclusion interaction problem under consideration is shown in Figure 1. It is assumed that the medium is under a state of plane strain or generalized plane stress and the in-plane dimensions of the medium are large compared to the lengths of and the distance between the crack and the inclusion so that the effect of the remote boundaries on the

perturbed stress state may be neglected. Thus, the Green's functions for the concentrated forces and dislocations in an infinite plane may be used to formulate the problem. It is further assumed that the inclusion is sufficiently "thin" so that its bending stiffness may also be neglected.

Referring to Figure 1 we consider the stresses and displacements due to a pair of edge dislocations on the x axis, a pair of concentrated forces on the line θ=constant and the applied loads acting on the medium away from the crack-inclusion region. Let the subscripts d, p and a designate these three stress and deformation states, i.e., let σ_{dij}, σ_{pij} and σ_{aij}, (i,j) = (x,y) or (i,j) = (r,θ), be the stress components due to dislocations, concentrated forces, and applied loads, respectively. The total stress state in the elastic plane may, therefore, be expressed as

$$\sigma_{ij}(x,y) = \sigma_{dij}(x,y) + \sigma_{pij}(x,y) + \sigma_{aij}(x,y), \quad (i,j = x,y) \tag{1}$$

Let us now assume that the dislocations are distributed along a<x<b, y=0 forming a crack. If g(x) and h(x) refer to the dislocation densities defined by

$$\frac{\partial}{\partial x}\left[u_y(x,+0) - u_y(x,-0)\right] = g(x) \ , \ a < x < b \ ,$$

$$\frac{\partial}{\partial x}\left[u_x(x,+0) - u_x(x,-0)\right] = h(x) \ , \ a < x < b \ , \tag{2a,b}$$

the corresponding stress components at a point (x,y) in the plane may be expressed as

$$\sigma_{dxx}(x,y) = \int_a^b \left[G_{xx}(x,y,t)g(t) + H_{xx}(x,y,t)h(t)\right]dt \ ,$$

$$\sigma_{dyy}(x,y) = \int_a^b \left[G_{yy}(x,y,t)g(t) + H_{yy}(x,y,t)h(t)\right]dt \ , \tag{3a-c}$$

$$\sigma_{dxy}(x,y) = \int_a^b \left[G_{xy}(x,y,t)g(t) + H_{xy}(x,y,t)h(t)\right]dt \ ,$$

where

$$G_{xx} = \frac{2\mu}{\pi(\kappa+1)} \cdot \frac{(t-x)[(t-x)^2 - y^2]}{[(t-x)^2 + y^2]^2} ,$$

$$G_{yy} = \frac{2\mu}{\pi(\kappa+1)} \cdot \frac{(t-x)[3y^2 + (t-x)^2]}{[(t-x)^2 + y^2]^2} ,$$

$$G_{xy} = \frac{2\mu}{\pi(\kappa+1)} \cdot \frac{y[y^2 - (t-x)^2]}{[(t-x)^2 + y^2]^2} ,$$

$$H_{xx} = \frac{2\mu}{\pi(\kappa+1)} \cdot \frac{y[y^2 + 3(t-x)^2]}{[(t-x)^2 + y^2]^2} , \qquad (4a-f)$$

$$H_{yy} = \frac{2\mu}{\pi(\kappa+1)} \cdot \frac{y[y^2 - (t-x)^2]}{[(t-x)^2 + y^2]^2} ,$$

$$H_{xy} = \frac{2\mu}{\pi(\kappa+1)} \cdot \frac{(t-x)[(t-x)^2 - y^2]}{[(t-x)^2 + y^2]^2} .$$

In (4) μ and κ are the elastic constants of the medium, μ the shear modulus, $\kappa = 3-4\nu$ for plane strain and $\kappa = (3-\nu)/(1+\nu)$ for plane stress ν being the Poisson's ratio.

Similarly, from the concentrated force solution as given, for example, in [2] the stress components $\sigma_{pij} = S_{ij}$ due to a pair of forces P_x and P_y acting at the point (x_o, y_o) may be written as

$$S_{xx}(x,y,x_o,y_o) = \frac{1}{2\pi(\kappa+1)} \frac{(A_1+A_2)P_x + (B_1+B_2)P_y}{[(x-x_o)^2 + (y-y_o)^2]^2} ,$$

$$S_{yy}(x,y,x_o,y_o) = \frac{1}{2\pi(\kappa+1)} \frac{(A_1-A_2)P_x + (B_1-B_2)P_y}{[(x-x_o)^2 + (y-y_o)^2]^2} , \qquad (5a-c)$$

$$S_{xy}(x,y,x_o,y_o) = \frac{1}{2\pi(\kappa+1)} \frac{A_3P_x + B_3P_y}{[(x-x_o)^2 + (y-y_o)^2]^2} ,$$

$$A_1 = -2(x-x_o)[(x-x_o)^2 + (y-y_o)^2]$$

$$A_2 = -\kappa(x-x_o)[(x-x_o)^2 + (y-y_o)^2] - (x-x_o)[(x-x_o)^2 - (y-y_o)^2] + 2(y-y_o)^2(x-x_o)$$

$$B_1 = -2(y-y_0)[(x-x_0)^2 + (y-y_0)^2]$$

$$B_2 = +\kappa(y-y_0)[(x-x_0)^2+ (y-y_0)^2]-(y-y_0)[(x-x_0)^2-(y-y_0)^2]-2(x-x_0)^2(y-y_0)$$

$$A_3 = -\kappa(y-y_0)[(x-x_0)^2+(y-y_0)^2]-(y-y_0)[(x-x_0)^2-(y-y_0)^2]-2(x-x_0)^2(y-y_0)$$

$$B_3 = -\kappa(x-x_0)[(x-x_0)^2+(y-y_0)^2]+(x-x_0)[(x-x_0)^2-(y-y_0)^2]-2(y-y_0)^2(x-x_0)$$

(6a-f)

If the inclusion is located along the line $c < r < d$, θ = constant, and if its bending stiffness is neglected, then the following conditions are valid:

$$u_r(r,\theta+0) = u_r(r,\theta-0),\ u_\theta(r,\theta+0) = u_\theta(r,\theta-0)\ ,$$

$$-P_\theta(r,\theta) = \sigma_{\theta\theta}(r,\theta+0) - \sigma_{\theta\theta}(r,\theta-0) = 0\ , \qquad (7a\text{-}d)$$

$$-P_r(r,\theta) = -p(r) = \sigma_{r\theta}(r,\theta+0) - \sigma_{r\theta}(r,\theta-0)\ ,\ (c<r<d).$$

Thus, to formulate the problem it is sufficient to consider only the radial component $P_r=p$ of the concentrated force. For $P_\theta=0$ and $P_r=p$ observing that

$$P_x = p\cos\theta\ ,\ P_y = p\sin\theta\ , \qquad (8a,b)$$

and substituting $x_0 = r_0\cos\theta$, $y_0 = r_0\sin\theta$, by using the kernels S_{ij} given by (5) the stress components σ_{pij} are found to be

$$\sigma_{pxx}(x,y) = \frac{1}{2\pi(\kappa+1)}\int_c^d \frac{(A_1'+A_2')\cos\theta+(B_1'+B_2')\sin\theta}{[(x-r_0\cos\theta)^2+(y-r_0\sin\theta)^2]^2}\,p(r_0)dr_0\ ,$$

$$\sigma_{pyy}(x,y) = \frac{1}{2\pi(\kappa+1)}\int_c^d \frac{(A_1'-A_2')\cos\theta+(B_1'-B_2')\sin\theta}{[(x-r_0\cos\theta)^2+(y-r_0\sin\theta)^2]^2}\,p(r_0)dr_0\ , \qquad (9a\text{-}c)$$

$$\sigma_{pxy}(x,y) = \frac{1}{2\pi(\kappa+1)}\int_c^d \frac{A_3'\cos\theta + B_3'\sin\theta}{[(x-r_0\cos\theta)^2+(y-r_0\sin\theta)^2]^2}\,p(r_0)dr_0\ ,$$

where the functions A_i', B_i', (i=1,2,3) are obtained from (6) by substituting $x_o = r_o\cos\theta$ and $y_o = r_o\sin\theta$, e.g.,

$$A_1'(x,y,r_o) = -2(x-r_o\cos\theta)[(x-r_o\cos\theta)^2 + (y-r_o\sin\theta)^2] \ . \qquad (10)$$

Since the stresses σ_{aij} due to the applied loads are known, from (1), (3) and (9) it is seen that once the functions g(x), h(x) and p(r) are determined the problem is solved. These unknown functions may be determined by expressing the stress boundary conditions on the crack surfaces and the displacement compatibility condition along the inclusion, namely

$$\sigma_{yy}(x,0) = \sigma_{dyy}(x,0) + \sigma_{pyy}(x,0) + \sigma_{ayy}(x,0) = 0 \ , \quad (a<x<b),$$

$$\sigma_{xy}(x,0) = \sigma_{dxy}(x,0) + \sigma_{pxy}(x,0) + \sigma_{axy}(x,0) = 0 \ , \quad (a<x<b), \qquad (11a\text{-}c)$$

$$\varepsilon_{rr}(r,\theta) = \varepsilon_{drr}(r,\theta) + \varepsilon_{prr}(r,\theta) + \varepsilon_{arr}(r,\theta) = \varepsilon_i(r), \ (c<r<d)$$

where $\varepsilon_i(r)$ is the (longitudinal) strain in the inclusion. If, for example, the stress state away from the crack inclusion region is given by σ_{ij}^{∞}, (i,j) = (x,y), then the applied quantities in (11) may be expressed as

$$\sigma_{ayy}(x,0) = \sigma_{yy}^{\infty} \ , \ \sigma_{axy}(x,0) = \sigma_{xy}^{\infty} \ ,$$

$$\varepsilon_{arr}(r,\theta) = \frac{1+\kappa}{8\mu}\left[\sigma_{xx}^{\infty}\left(\cos^2\theta - \frac{3-\kappa}{1+\kappa}\sin^2\theta\right)\right.$$

$$\left. + \sigma_{yy}^{\infty}\left(\sin^2\theta - \frac{3-\kappa}{1+\kappa}\cos^2\theta\right) + \frac{4}{1+\kappa}\sigma_{xy}^{\infty}\sin 2\theta\right] . \qquad (12a\text{-}c)$$

We now note that if p(r) is the body force acting on the elastic medium then -p(r) would be the force acting on the inclusion distributed along its length. Thus, the strain in the inclusion may be obtained as

$$\varepsilon_i(r) = -\frac{1+\kappa_s}{8\mu_s A_s}\int_r^d p(r_o)dr_o \qquad (13)$$

where μ_s and κ_s are the elastic constants, and A_s is the cross-sectional area of the inclusion corresponding to unit thickness of the medium in z-direction. From the expression of ε_{rr} given by the Hooke's law

$$\varepsilon_{rr} = \frac{1+\kappa}{8\mu}\left(\sigma_{rr} - \frac{3-\kappa}{1+\kappa}\sigma_{\theta\theta}\right) , \tag{14}$$

from (9) and the corresponding stress transformation it can be shown that

$$\varepsilon_{prr}(r,\theta) = \frac{\kappa}{2\pi(1+\kappa)\mu}\int_c^d \frac{p(r_o)}{r_o - r}\, dr_o . \tag{15}$$

Similarly, from (3), (4) and (14) we find

$$\varepsilon_{drr}(r,\theta) = \frac{1+\kappa}{8\mu}\int_a^b [G_\varepsilon(r,t)g(t) + H_\varepsilon(r,t)h(t)]dt \tag{16}$$

where

$$\begin{aligned} G(r,t) = \frac{2\mu}{\pi(1+\kappa)}\frac{1}{R^4}\{&\cos^2\theta - \frac{3-\kappa}{1+\kappa}\sin^2\theta)(t - r\cos\theta) \times \\ &\times[(t-r\cos\theta)^2 - r^2\sin^2\theta] + (\sin^2\theta - \frac{3-\kappa}{1+\kappa}\cos^2\theta) \times \\ &\times(t-r\cos\theta)[3r^2\sin^2\theta + (t-r\cos\theta)^2] \\ &+ \frac{4}{1+\kappa}\sin 2\theta\, r\sin\theta[r^2\sin^2\theta - (t-r\cos\theta)^2]\} , \end{aligned} \tag{17}$$

$$\begin{aligned} H_\varepsilon(r,t) = \frac{2\mu}{\pi(1+\kappa)}\frac{1}{R^4}\{&(\cos^2\theta - \frac{3-\kappa}{1+\kappa}\sin^2\theta) r\sin\theta[r^2\sin^2\theta \\ &+ 3(t-r\cos\theta)^2] + (\sin^2\theta - \frac{3-\kappa}{1+\kappa}\cos^2\theta) r\sin\theta \times \\ &\times[r^2\sin^2\theta - (t - r^2\cos^2\theta)^2] + \frac{4}{1+\kappa}\sin 2\theta \times \\ &\times(t-r\cos\theta)[(t-r\cos\theta)^2 - r^2\sin^2\theta] , \end{aligned} \tag{18}$$

$$R^2 = (t - r\cos\theta)^2 + r^2\sin^2\theta . \tag{19}$$

Finally, by substituting from (3), (4), (9), (12), (13), (15) and (16) into (11), the integral equations of the problem may be obtained as follows:

$$\frac{1}{\pi}\int_a^b \frac{g(t)dt}{t-x} + \frac{1}{4\pi\mu}\int_c^d \frac{(A_1'-A_2')\cos\theta+(B_1'-B_2')\sin\theta}{[(x-r_o\cos\theta)^2+(r_o\sin\theta)^2]^2}\, p(r_o)dr_o = -\frac{1+\kappa}{2\mu}\sigma_{yy}^{\infty} ,$$

$$(a<x<b) ,$$

$$\frac{1}{\pi}\int_a^b \frac{h(t)dt}{t-x} + \frac{1}{4\pi\mu}\int_c^d \frac{(A_3'\cos\theta+B_3'\sin\theta)p(r_o)}{[(x-r_o\cos\theta)^2+(r_o\sin\theta)^2]^2}\, dr_o = -\frac{1+\kappa}{2\mu}\sigma_{xy}^{\infty} ,$$

$$(a<x<b) ,$$

$$\frac{c_o}{\pi}\int_a^b G_\varepsilon(r,t)g(t)dt + \frac{c_o}{\pi}\int_a^b H_\varepsilon(r,t)h(t)dt + \frac{1}{\pi}\int_c^d \frac{p(r_o)}{r_o-r}\, dr_o$$

$$+ \frac{\gamma c_o}{\pi}\int_c^d H(r_o-r)p(r_o)dr_o = -\frac{c_o}{\pi}[(\cos^2\theta - \frac{3-\kappa}{1+\kappa}\sin^2\theta)\sigma_{xx}^{\infty}$$

$$+ (\sin^2\theta - \frac{3-\kappa}{1+\kappa}\cos^2\theta)\sigma_{yy}^{\infty} + \frac{4}{1+\kappa}\sigma_{xy}^{\infty}\sin 2\theta], \quad (c<r<d) , \qquad (20a\text{-}c)$$

where

$$c_o = \frac{\pi(1+\kappa)^2}{4\kappa} , \quad \gamma = \frac{\mu(1+\kappa_s)}{A_s\mu_s(1+\kappa)} . \qquad (21a,b)$$

From the definition of g and h given by (2) it follows that

$$\int_a^b g(t)dt = 0 , \quad \int_a^b h(t)dt = 0 . \qquad (22a,b)$$

Also, the static equilibrium of the inclusion requires that

$$\int_c^d p(r)dr = 0 . \qquad (23)$$

Thus, the system of singular integral equations must be solved under the conditions (22) and (23). From the function-theoretic examination of the integral equations (20) it can be shown that the unknown functions g, h and p are of the following form [2]:

$$g(t) = \frac{F_1(t)}{(b-t)^{\frac{1}{2}}(t-a)^{\frac{1}{2}}} , \quad h(t) = \frac{F_2(t)}{(b-t)^{\frac{1}{2}}(t-a)^{\frac{1}{2}}} , \quad p(r) = \frac{F_3(r)}{(d-r)^{\frac{1}{2}}(r-c)^{\frac{1}{2}}} ,$$

(24a-c)

where F_1, F_2 and F_3 are bounded functions. The solution of (20) subject to (22) and (23) may easily be obtained by using the numerical method described in [3].

3. Stress Singularities

After solving (20) the Modes I and II stress intensity factors k_1 and k_2 at the crack tips x=a and x=b, y=0 which are defined by

$$k_1(a) = \lim_{x\to a} \sqrt{2(a-x)}\, \sigma_{yy}(x,0) , \quad k_1(b) = \lim_{x\to b} \sqrt{2(x-b)}\, \sigma_{yy}(x,0) ,$$

$$k_2(a) = \lim_{x\to a} \sqrt{2(a-x)}\, \sigma_{xy}(x,0) , \quad k_2(b) = \lim_{x\to b} \sqrt{2(x-b)}\, \sigma_{xy}(x,0) ,$$

(25a-d)

may be obtained as follows:

$$k_1(a) = \frac{2\mu}{1+\kappa} \lim_{x\to a} \sqrt{2(x-a)}\, g(x) , \quad k_1(b) = -\frac{2\mu}{1+\kappa} \lim_{x\to b} \sqrt{2(b-x)}\, g(x) ,$$

$$k_2(a) = \frac{2\mu}{1+\kappa} \lim_{x\to a} \sqrt{2(x-a)}\, h(x) , \quad k_2(b) = -\frac{2\mu}{1+\kappa} \lim_{x\to b} \sqrt{2(b-x)}\, h(x) .$$

(26a-d)

The constants k_1 and k_2 are related to the asymptotic stress fields near the crack tips through the well-known expressions (see, for example, [4] and [5]). However, not so well-known is the asymptotic behavior of the stress fields near the inclusions having sharp edges. From (24c) and (7d) it is seen that the shear stress $\sigma_{r\theta}$ has a square-root singularity at the

tip of the inclusion. However, if one is interested in crack initiation around such singular points, one needs to know the direction and the magnitude of the maximum local cleavage stress. This, in turn, requires the investigation of the complete asymptotic stress field near the singular points. By using the basic form of the solution of the related density functions given by (24) and going back to the original stress expressions, the asymptotic stress fields may be developed by following the general techniques described in, for example, [6] or [7].

In an elastic medium containing an elastic line inclusion under plane strain or generalized plane stress conditions, the asymptotic analysis gives the near tip stress field as follows [7](*):

$$\sigma_{yy}(r,\theta) \tilde{=} \frac{k_1}{\sqrt{2r}} \cos\frac{\theta}{2} ,$$

$$\sigma_{xx}(r,\theta) \tilde{=} -\frac{3+\kappa}{\kappa-1} \frac{k_1}{\sqrt{2r}} \cos\frac{\theta}{2} ,$$

$$\sigma_{xy}(r,\theta) \tilde{=} -\frac{\kappa+1}{\kappa-1} \frac{k_1}{\sqrt{2r}} \sin\frac{\theta}{2} , \qquad (27a\text{-}c)$$

where x,y and r,θ are the standard rectangular and polar coordinates, the origin of coordinate axes is at the inclusion tip and the inclusion lies along the negative x axis or along $\theta=\pi$, $r>0$. Equations (27) suggest that similar to crack problems one may define a (Mode I) "stress intensity factor" in terms of the (tensile) cleavage stress as follows:

$$k_1 = \lim_{r\to 0} \sqrt{2r}\, \sigma_{yy}(r,0) . \qquad (28)$$

From (7) by observing that (at the right end of the inclusion)

$$\sigma_{xy}(r,+\pi) - \sigma_{xy}(r,-\pi) = -p(r) , \qquad (29)$$

(*) Note the misprints in (4.6) of [7].

in terms of the function $p(x)$ k_1 may be expressed as

$$k_1 = -\lim_{r\to 0} \frac{1}{2}\frac{\kappa-1}{\kappa+1}\sqrt{2r}\, p(r) \ . \tag{30}$$

It should be noted that in the case of flexible elastic line inclusions there is no antisymmetric singular stress field. For example, in a plane under pure shear (σ^{∞}_{xy}) parallel to the inclusion, the perturbed stress field is zero. Physically this of course follows from the fact that the normal strain (ε_{xx}) parallel to the plane of shear is zero.

Similarly, for a rigid line inclusion (i.e., for an inclusion having infinite bending as well as tensile stiffness) it can be shown that for small values of r the asymptotic stress field is given by

$$\sigma_{yy}(r,\theta) \cong \frac{1}{\sqrt{2r}}\left(k_1 \cos\frac{\theta}{2} + \frac{\kappa+1}{\kappa-1} k_2 \sin\frac{\theta}{2}\right) ,$$

$$\sigma_{xx}(r,\theta) \cong \frac{1}{\sqrt{2r}}\left(-\frac{3+\kappa}{\kappa-1} k_1 \cos\frac{\theta}{2} + \frac{3-\kappa}{\kappa-1} k_2 \sin\frac{\theta}{2}\right) , \tag{31a-c}$$

$$\sigma_{xy}(r,\theta) \cong \frac{1}{\sqrt{2r}}\left(-\frac{\kappa+1}{\kappa-1} k_1 \sin\frac{\theta}{2} + k_2 \cos\frac{\theta}{2}\right) \ .$$

Again, the stress intensity factors k_1 and k_2 are defined in terms of the tensile and shear cleavage stresses at $\theta=0$ plane as follows:

$$k_1 = \lim_{r\to 0} \sqrt{2r}\, \sigma_{yy}(r,0) \ , \ k_2 = \lim_{r\to 0} \sqrt{2r}\, \sigma_{xy}(r,0) \ . \tag{32a,b}$$

As in the crack problems, the antiplane shear component of the asymptotic stress field around flat elastic and rigid inclusions is uncoupled. Defining a Mode III stress intensity factor by

$$k_3 = \lim_{r\to 0} \sqrt{2r}\, \sigma_{xz}(r,0) \ , \tag{33}$$

the asymptotic stress field may be expressed as

$$\sigma_{xz}(r,\theta) \cong \frac{k_3}{\sqrt{2r}} \cos\frac{\theta}{2} ,$$

$$\sigma_{yz}(r,\theta) \cong \frac{k_3}{\sqrt{2r}} \sin\frac{\theta}{2} , \qquad (34a,b)$$

where again the inclusion lies along $\theta=\pi$ plane(*).

4. Crack-Inclusion Intersection

Analytically as well as from a practical viewpoint intersection of cracks and inclusions presents some interesting problems. In these problems the point of intersection is a point of irregular singularity with a power other than 1/2. Even though the general intersection problems for an arbitrary value of θ may be treated in a relatively straightforward manner, in this paper only some special cases will be considered.

4.1 The case of $\theta = \frac{\pi}{2}$, a = 0, c = 0

In this case the system of singular integral equations (20) becomes

$$\frac{1}{\pi}\int_0^b \frac{g(t)}{t-x}\,dt + \frac{1}{\pi}\int_0^d \left[\frac{c_1 t}{x^2+t^2} - \frac{c_2 t x^2}{(x^2+t^2)^2}\right]p(t)dt = f_1(x) , \quad (0<x<b) ,$$

$$\frac{1}{\pi}\int_0^b \frac{h(t)}{t-x}\,dt + \frac{1}{\pi}\int_0^d \left[\frac{c_2 x^3}{(x^2+t^2)^2} - \frac{c_1 x}{x^2+t^2}\right]p(t)dt = f_2(x) , \quad (0<x<b) ,$$

(*) Note that in this case if the remote stress is decomposed into σ^{∞}_{xz} and σ^{∞}_{yz}, the perturbed stress field due to σ^{∞}_{yz} would be zero. For the cleavage plane θ the shear cleavage stress may be written as $\sigma_{\theta_0}(r,\theta)=\sigma_{xz}\sin\theta-\sigma_{yz}\cos\theta= -(k_3/\sqrt{2r})\sin(\theta/2)$, $\theta_0 = \theta+\pi/2$, indicating that $\theta=\mp\pi/2$ is the maximum cleavage planes.

$$\frac{1}{\pi}\int_0^b \left[\frac{c_3 t}{t^2+r^2} + \frac{c_4 t r^2}{(t^2+r^2)^2}\right] g(t)dt + \frac{1}{\pi}\int_0^b \left[\frac{c_3 r}{t^2+r^2} - \frac{c_4 r t^2}{(t^2+r^2)^2}\right] h(t)dt$$

$$+ \frac{1}{\pi}\int_0^d \frac{p(t)}{t-r}\,dt + \frac{c_5}{\pi}\int_0^d H(t-r)p(t)dt = f_3(r)\ ,\ (0<r<d), \qquad (35a\text{-}c)$$

where

$$c_1 = \frac{3+\kappa}{4\mu}\ ,\ c_2 = \frac{1}{\mu}\ ,\ c_3 = \frac{\mu(\kappa-1)}{\kappa}\ ,$$

$$c_4 = \frac{4\mu}{\kappa}\ ,\ c_5 = \frac{\pi(1+\kappa)(1+\kappa_s)\mu}{4A_s\kappa\mu_s}\ , \qquad (36)$$

and f_1, f_2 and f_3 are known input functions (see, for example, the right hand side of (20)). Note that aside from the simple Cauchy kernels, (35) has kernels which become unbounded as the variables (t,x,r) approach the point of irregular singularity (x=0=t=r). Thus, defining the unknown functions by

$$g(t) = \frac{F_1(t)}{t^\alpha(b-t)^{\beta_1}}\ ,\ h(t) = \frac{F_2(t)}{t^\alpha(b-t)^{\beta_2}}\ ,\ p(t) = \frac{F_3(t)}{t^\alpha(c-t)^{\beta_3}}\ ,$$

$$0<\mathrm{Re}(\alpha,\beta_k)<1,\ (k=1,2,3)\ , \qquad (37a\text{-}c)$$

and by using the function-theoretic technique described in [3], the characteristic equations for β_1, β_2, β_3 and α may be obtained as follows:

$$\cot\pi\beta_k = 0\ ,\ (k = 1,2,3) \qquad (38)$$

$$b_1\cos^2\pi\alpha - (b_2+8\alpha-b_3\alpha^2)\cos^2\frac{\pi\alpha}{2}$$

$$-(b_4-b_5\alpha+b_3\alpha^2)\sin^2\frac{\pi\alpha}{2} = 0\ , \qquad (39)$$

where

$$b_1 = 8\kappa/(1+\kappa)\ ,\ b_2 = 2(3+\kappa)(\kappa-1)/(\kappa+1)\ ,$$
$$b_3 = 8/(\kappa+1)\ ,\ b_4 = 2(3-\kappa)\ ,\ b_5 = 16/(1+\kappa)\ . \tag{40}$$

Note that the properties of the inclusion (as expressed by the constant c_5 in (36)) enter the integral equations (35) only through a Fredholm kernel and, therefore, have no influence on the singular behavior of the solution, and α is dependent on κ or on the Poisson's ratio of the medium only. From (38) it is seen that the acceptable roots are $\beta_k = 0.5$, (k = 1,2,3). The numerical examination of (39) indicates that in this special case of $\theta = \frac{\pi}{2}$ we have $0.5<\alpha<1$, meaning that the stress state at r=0=x has a stronger singularity than the conventional crack tip singularity of $1/\sqrt{r}$. This may be due to the fact that in this problem two singular stress fields are combined at r=0. Also, it turns out that for $0<\nu\leq 5$ the characteristic equation (39) has two roots in $0<\mathrm{Re}(\alpha)<1$ and both are real. These roots are given in Table 1 for various values of the Poisson's ratio.

Table 1. Powers of stress singularity α for a crack and an inclusion: a = 0, c = 0, $\theta = \pi/2$ (Fig. 1).

ν	plane strain		plane stress	
	α_1	α_2	α_1	α_2
0.0	0.63627093	0	0.63627093	0
0.1	0.64489401	0.09571474	0.64408581	0.08990596
0.2	0.65405762	0.14825371	0.65095281	0.13249000
0.3	0.66352760	0.18953334	0.65695651	0.16176440
0.4	0.67270080	0.22567265	0.66217253	0.18404447
0.5	0.67996342	0.26027940	0.66666667	0.20196313

The stress intensity factors at the crack tip x=b, y=0 and at the end of the inclusion x=0, y=d may be obtained by using the relations (26) and (30). At the singular point x=0, y=0 the following useful stress intensity factors are defined;

$$k_1(0) = \lim_{x\to-0} \sqrt{2}\, x^{\alpha}\, \sigma_{yy}(-0,0) \ ,$$

$$k_2(0) = \lim_{x\to-0} \sqrt{2}\, x^{\alpha}\, \sigma_{xy}(-0,0) \ , \qquad (41a,b)$$

for the crack, and

$$k_1(0) = \lim_{y\to+0} \frac{\sqrt{2}}{2}\, y^{\alpha}\, p(0,+0) \qquad (42)$$

for the inclusion.

4.2 The Special Case of $\theta = \frac{\pi}{2}$, $c = -d$, $a = 0$.

In this case the problem is further simplified by assuming "symmetric" external loads (for example, $\sigma^{\infty}_{xy}=0$ in (20)). Thus, the plane of the crack is a plane of symmetry, $h(x) = 0$, and (20) would reduce to

$$\frac{1}{\pi}\int_0^b \frac{g(t)}{t-x}\,dt + \frac{2}{\pi}\int_0^d \left[\frac{c_1 t}{t^2+x^2} - \frac{c_2 t x^2}{(t^2+x^2)^2}\right]p(t)dt = f_1(x), \ (0<x<b) \ ,$$

$$\frac{1}{\pi}\int_0^b \left[\frac{c_3 t}{t^2+y^2} + \frac{c_4 t y^2}{(t^2+y^2)^2}\right]g(t)dt + \frac{1}{\pi}\int_0^d \left[\frac{1}{t-y} + \frac{1}{t+y}\right.$$

$$\left. + c_5 H(t-y)\right]p(t)dt = f_3(y) \ , \ (0<y<d) \ , \qquad (43a,b)$$

where, again the input functions f_1 and f_3 are known and, for example, are given in (20) (with $\sigma^{\infty}_{xy} = 0$) and the constants $c_1,\ldots,c_5$ are defined by (36).

By defining

$$g(t) = \frac{G_1(t)}{t^{\alpha}(b-t)^{\beta_1}} \ , \ p(t) = \frac{G_2(t)}{t^{\alpha}(d-t)^{\beta_2}} \ , \ 0<\mathrm{Re}(\alpha,\beta_1,\beta_2)<1 \qquad (44)$$

from (43) it may be shown that

$$\cot\beta_k = 0 \ , \ (k=1,2) \ , \qquad (45)$$

$$\cos\pi\alpha-(c_3 + \frac{1}{2} c_4\alpha)(c_1 - \frac{1}{2} c_2\alpha) = 0 \ . \qquad (46)$$

From (45) it is seen that $\beta_k = 0.5$. A close examination of (46) shows that it has only one root for which $0<\mathrm{Re}(\alpha)<1$. Furthermore, this root turns out to be real and highly dependent on the Poisson's ratio (see Table 2). The characteristic equation (46) and the roots given in Table 2 are identical to those found in [8] where an infinitely long stringer in cracked plate was considered.

Table 2. Power of stress singularity α at the crack-inclusion intersection for $\theta=\pi/2$, $c=-d$, $a=0$ and for symmetric loading.

ν	α	
	plane strain	plane stress
0	0	0
0.1	0.10964561	0.10263043
0.2	0.17432137	0.15468088
0.3	0.22678790	0.19132495
0.4	0.27392547	0.21972274
0.5	0.31955800	0.24288552

In this problem, too, the stress intensity factors for the crack and the inclusion may be defined as in (41) and (42).

4.3 The Special Case of $\theta=\pi$, $a=0$, $c=0$

In this case the crack and the inclusion are on the x axis and occupy $(y=0,\ 0<x<b)$ and $(y=0,\ -d<x<0)$, respectively. Restricting our attention again to the symmetric loading for which $h(x) = 0$ and observing that for the variables along the inclusion $r = -x$, $r_o = -t$, $p(r_o) = -p_x(t)$, the integral equations of the problem may be expressed as

$$\frac{1}{\pi}\int_0^b \frac{g(t)}{t-x}\,dt - \frac{1}{\pi}\frac{\kappa-1}{4\mu}\int_{-d}^0 \frac{p_x(t)}{t-x}\,dt = f_1(x)\ ,\ (0<x<b)$$

$$\frac{c_3}{\pi}\int_0^b \frac{g(t)}{t-x}\,dt + \frac{1}{\pi}\int_{-d}^0 \frac{p_x(t)}{t-x}\,dt - \frac{c_5}{\pi}\int_{-d}^x p_x(t)dt = f_3(x),\ (-d<x<0) \qquad (47a,b)$$

where the constants c_3 and c_5 are defined by (36) and the known functions f_1 and f_3 are given by the right hand sides of (20a) and (20c) (with $\sigma_{xy}^{\infty}=0$). If we now let

$$g(t) = \frac{H_1(t)}{t^{\alpha}(b-t)^{\beta_1}}\ ,\ p_x(t) = \frac{H_2(t)}{(-t)^{\alpha}(t+d)^{\beta_2}}\ ,\ 0<\mathrm{Re}(\alpha,\beta_1,\beta_2)<1\ , \qquad (48)$$

from (47) the characteristic equations for α, β_1 and β_2 may be obtained as follows:

$$\cot\pi\beta_k = 0\ ,\ (k = 1,2)\ , \qquad (49)$$

$$\cos 2\pi\alpha = -\left(\frac{\kappa-1}{2\sqrt{\kappa}}\right)^2\ . \qquad (50)$$

Equation (49) again gives $\beta_1 = \beta_2 = 0.5$. From (50) it may easily be seen that α is complex and its value for which $0<\mathrm{Re}(\alpha)<1$ is found to be

$$\alpha = \frac{1}{2} + i\left(\frac{\log\kappa}{2\pi}\right)\ . \qquad (51)$$

This value of α turns out to be identical to the power of singularity for a perfectly rough rigid stamp with a sharp corner pressed against an elastic half plane having κ as an elastic constant [2] (e.g., $\kappa = 3-4\nu$ for the plane strain case). At first this result may be somewhat unexpected. However, upon closer examination of the problem first, from (47b) it may be seen that the elasticity of the inclusion (i.e., the term containing the constant c_5) has no effect on the nature of the stress singularity. Thus, if one assumes the inclusion to be inextensible, for the symmetric problem under consideration it can be shown that the conditions in the neighborhood of the

crack tip x=0, y=0, for example, for y<0, are identical to the conditions around the corner of the stamp in the elastic half plane occupying y<0. It, therefore, appears that for the elastic inclusion collinear with a crack, the stress state around the common end point would have the standard complex singularity found in the rigid stamp problem.

5. The Results

The crack-inclusion problem described in previous sections is solved for a uniform stress state σ_{ij}^{∞}, (i,j=x,y), away from the crack-inclusion region. For simplicity the results are obtained by assuming one stress component (σ_{xx}^{∞} or σ_{yy}^{∞} or σ_{xy}^{∞}) to be nonzero at a time. The solution for a more general loading may then be obtained by superposition. Even though the stress state everywhere in the plane can be calculated after solving the integral equations (e.g., (20)) and determining the density functions g, h, and p, only the stress intensity factors are given in this section. For nonintersecting cracks and inclusions the stress intensity factors defined by (26) and (28) are normalized as follows:

$$k_i'(x_j) = \frac{k_i(x_j)}{\sigma_a^{\infty}\sqrt{(b-a)/2}} \quad , \quad (i=(1,2);\ x_j=(a,b);\ \sigma_a^{\infty}=(\sigma_{yy}^{\infty},\sigma_{xx}^{\infty},\sigma_{xy}^{\infty})), \tag{52}$$

for the crack and

$$k_1'(r_j) = \frac{k_1(r_j)}{k_o} \ , \ k_o = \frac{1-\kappa}{2(1+\kappa)}\ \sigma_a^{\infty}\ \sqrt{(d-c)/2}\ ,$$

$$(r_j = (c,d)\ ,\ \sigma_a^{\infty} = (\sigma_{yy}^{\infty},\ \sigma_{xx}^{\infty},\ \sigma_{xy}^{\infty})) \tag{53}$$

for the inclusion.

Referring to Figure 1, for c=a, d=b, and (b/a)=5 the effect of the angle θ on the stress intensity factors is shown in Table 3. These results are given for two values of the stiffness parameter γ defined by (21), namely γ=0 (the inextensible inclusion) and γ=10.

Table 3. Normalized stress intensity factors in a plane containing a crack and an inclusion subjected to a uniform stress state σ_{ij}^{∞} away from the crack-inclusion region (c=a,d=b,a=b/5,Fig. 1).

γ	k'	θ						
		1°	30°	60°	90°	120°	150°	180°
		(a) $\sigma_{yy}^{\infty} \neq 0$, $\sigma_{xx}^{\infty} = 0$, $\sigma_{xy}^{\infty} = 0$						
0	$k_1'(a)$	.8905	1.0083	1.0298	1.0049	.9912	1.0001	1.0076
	$k_2'(a)$	-.2152	-.0098	-.0661	-.0830	-.0367	.0004	.0000
	$k_1'(b)$	1.0221	.9967	.9570	.9617	.9857	1.0001	1.0033
	$k_2'(b)$	.4327	-.0065	-.0002	.0007	-.0001	.0001	.0000
	$k_1'(c)$	.9570	-.3273	-1.1324	-1.3970	-.8879	-.0310	.3850
	$k_1'(d)$	.8012	.1552	-.6989	-1.1134	-.7336	.0428	.4320
10	$k_1'(a)$	.9691	.9999	1.0016	.9988	.9978	1.0000	1.0014
	$k_2'(a)$	-.0517	-.0047	-.0136	-.0153	-.0066	.0001	.0000
	$k_1'(b)$	.9862	.9997	.9919	.9928	.9973	1.0000	1.0006
	$k_2'(b)$	.0742	-.0020	.0001	.0005	.0002	.0000	.0000
	$k_1'(c)$	.2619	-.1277	-.3979	-.4735	-.2989	-.0220	.1106
	$k_1'(d)$	-.0269	.1001	-.1848	-.3269	-.2177	.0171	.1354
		(b) $\sigma_{xx}^{\infty} \neq 0$, $\sigma_{yy}^{\infty} = 0$, $\sigma_{xy}^{\infty} = 0$						
0	$k_1'(a)$	.1237	.0704	-.0034	-.0034	.0008	-.0117	-.0203
	$k_2'(a)$	.2355	.0122	.0052	.0310	.0036	-.0161	.0000
	$k_1'(b)$	-.0806	-.0365	.0036	.0142	.0014	-.0072	-.0086
	$k_2'(b)$	-.5321	-.0140	.0001	.0001	.0000	-.0003	.0000
	$k_1'(c)$	-1.1068	-.6949	.0766	.4620	.0774	-.6988	-1.0877
	$k_1'(d)$	-1.4785	-.6941	.0772	.4644	.0776	-.6994	-.0884
10	$k_1'(a)$	.0385	.0106	-.0005	-.0001	.0002	-.0023	-.0038
	$k_2'(a)$	.0587	.0004	.0010	.0056	.0006	.0029	.0000
	$k_1'(b)$	-.0252	-.0068	.0007	.0026	.0003	-.0013	-.0016
	$k_2'(b)$	-.1128	-.0030	.0000	.0000	.0000	.0000	.0000
	$k_1'(c)$	-.3440	-.2152	.0239	.1432	.0239	-.2151	-.3346
	$k_1'(d)$	-.3885	-.2154	.0239	.1434	.0239	-.2151	-.3347

Table 3 - cont.

γ	k'	θ						
		1°	30°	60°	90°	120°	150°	180°
		(c) $\sigma^{\infty}_{yy} \neq 0$, $\sigma^{\infty}_{xx} = 0$, $\sigma^{\infty}_{xy} = 0$						
0	$k'_1(a)$	.1289	.1428	.0669	.0028	.0134	.0223	0.0000
	$k'_2(a)$	1.0849	1.0180	.9054	.9950	1.0599	1.0304	1.0000
	$k'_1(b)$	.1641	-.0754	-.0670	-.0021	0.0231	.0136	0.0000
	$k'_2(b)$	1.4055	.9685	.9974	.9995	1.0005	1.0005	1.0000
	$k'_1(c)$	-1.0246	-1.6348	-1.3085	.0533	1.3767	1.3606	0.0000
	$k'_1(d)$	2.0539	-1.3808	-1.4661	-.1076	1.2735	.3117	.0000
10	$k'_1(a)$	.0858	.0198	.0100	.0010	.0032	.0043	.0000
	$k'_2(a)$	1.0527	.9967	.9826	.9992	1.0108	1.0054	1.0000
	$k'_1(b)$	.1044	-.0140	-.0121	-.0003	.0043	.0025	.0000
	$k'_2(b)$	1.1662	.9929	.9994	.9998	.9999	1.0000	1.0000
	$k'_1(c)$	-.6916	-.5492	-.3731	.0557	.4513	-.4316	.0000
	$k'_1(d)$	1.1639	-.4179	-.4533	-.0342	.3912	-.4029	.0000

Some sample results for an inclusion collinear with a crack (i.e, for $\theta=0$) are given in Table 4. Note that for this configuration under the

Table 4. Normalized stress intensity factors for an inclusion collinear with a crack. Relative dimensions: $\theta=0$, d-c = b-a, c = b+s. Applied loads: σ^{∞}_{ij}, (i,j=x,y) (Fig. 1).

σ^{∞}_{ij}	k'	s = (b-a)/100		s = (b-a)/2	
		γ = 0	γ = 10	γ = 0	γ = 10
σ^{∞}_{xx}	$k_1'(a)$	-0.0202	-0.0040	-0.0019	-0.0004
	$k_1'(b)$	-0.1338	-0.0300	-0.0027	-0.0005
	$k_1'(c)$	-1.0482	-0.3296	-1.0889	-0.3347
	$k_1'(d)$	-1.0845	-0.3345	-1.0889	-0.3347
σ^{∞}_{yy}	$k_1'(a)$	1.0047	1.0006	1.0008	1.0002
	$k_1'(b)$	1.0200	0.9987	1.0011	1.0002
	$k_1'(c)$	-0.0861	-0.1571	0.4559	0.1397
	$k_1'(d)$	0.3841	0.1273	0.4590	0.1413

loads shown in the table, that is, for σ^{∞}_{yy} and σ^{∞}_{xx}, because of symmetry the Mode II stress intensity factors $k_2(a)$ and $k_2(b)$ are zero. Also, for the shear loading σ^{∞}_{xy} it is found that $k_2'(a) = 1$, $k_2'(b) = 1$ and $k_1(a) = k_1(b) = k_1(c) = k_1(d) = 0$. This follows from the fact that in the cracked plane under pure shear σ^{∞}_{xy} the strain component $\varepsilon_{xx}(x,0)$ is zero and hence an inextensible inclusion on the x axis would have no effect on the stress distribution.

Another special configuration is an inclusion parallel to the crack for which Table 5 shows some sample results. In the two special configurations considered in Tables 4 and 5 the effect of the crack-inclusion interaction on the stress intensity factors does not seem to be very significant.

The results for an elastic medium for which xz plane is a plane of symmetry with respect to the crack-inclusion geometry as well as the

Table 5. Normalized stress intensity factors in a plane containing an inclusion parallel and equal in length to a crack, both symmetrically located with respect to the y axis. The crack is along the x axis and H is the distance between the crack and the inclusion in y direction (Fig. 1).

σ^{∞}_{ij}	k'	H = b-a		H = 10(b-a)	
		$\gamma = 0$	$\gamma = 10$	$\gamma = 0$	$\gamma = 10$
σ^{∞}_{xx}	$k'_1(a)=k'_1(b)$	-0.0182	-0.0070	-0.0007	-0.0002
	$k'_2(a)=-k'_2(b)$	0.0281	-0.0011	0.0006	0.0000
	$k'_1(c)=k'_1(d)$	-1.0834	-1.0887	-0.0683	-0.0683
σ^{∞}_{yy}	$k'_1(a)=k'_1(b)$	1.0063	1.0028	1.0004	1.0001
	$k'_2(a)=-k'_2(b)$	-0.0060	0.0004	-0.0001	0.0000
	$k'_1(c)=k'_1(d)$	0.3917	0.4387	0.0411	0.0276
σ^{∞}_{xy}	$k'_1(a)=-k'_1(b)$	-0.0042	0.0000	-0.0002	0.0000
	$k'_2(a)=k'_2(b)$	0.9965	1.0000	0.9998	1.0000
	$k'_1(c)$	-0.1131	0.0033	-0.0123	0.0004
	$k'_1(d)$	0.1129	-0.0052	0.0123	-0.0006

applied loads are given in Figures 2-12. In this example the crack is perpendicular to the inclusion and the external load is a uniform tension parallel or perpendicular to the crack and away from the crack-inclusion region (see the insert in the figures). The results shown in the figures are self-explanatory. However, the solution also has some unusual features among which, for example, one may mention the tendency of the crack tip stress intensity factors k'(a) and k'(b) to "peaking" as γ decreases and as d/ℓ increases (where 2d and 2ℓ are the lengths of the inclusion and the crack, respectively and $\gamma = 0$ corresponds to an inextensible inclusion).

The results for the limiting case of the crack touching the inclusion are given in Figures 8-12. In this case at the singular point x=0, y=0 the stress intensity factor $k_1(a)$ and the normalized stress intensity factor $k_1'(a)$ are defined by

$$k_1(a) = \lim_{x\to 0^-} \sqrt{2}\, x^{\alpha}\sigma_{yy}(x,0) \ , \ (x < 0) \ , \tag{54}$$

$$k_1'(a) = k(a)/\sigma_{ii}^{\infty}\sqrt{\ell} \ , \ (i=(x,y);\ \ell=b/2) \tag{55}$$

where the power of singularity α is given in Table 2. The results shown in Figures 8-12 are obtained for $\nu = 0.3$.

The stress intensity factors for the other symmetric crack inclusion problem, namely for the problem in which y axis is the line of symmetry with regard to loading and geometry are given in Figures 13-28. In this problem $a=-\ell$, $b=\ell$, $d>c>0$ and the external load is either σ_{yy}^{∞} or σ_{xx}^{∞} (see the insert in Figure 13). Note that the figures show the crack tip stress intensity factors at $x=a=-\ell$ and $k_1(b)=k_1(a)$, $k_2(b)=-k_2(a)$. Generally the magnitude of $k_1(a)$ and $k_2(a)$ seem to increase with increasing length and stiffness of the inclusion (i.e., with increasing $(d-c)/2\ell$ and decreasing $\gamma = \mu(1+\kappa_s)/A_s\mu_s(1+\kappa)$, where μ_s is the shear modulus of the inclusion). Also, as expected, $k_1(c)$ and $k_1(d)$ describing the intensity of the stress field at inclusion ends tend to increase as the stiffness of the inclusion increases. However, their dependence on the relative length parameters is somewhat more complicated (see, for example, Figure 16 for change in behavior of the variation of $k_1(d)$ at $(d-c)/2\ell=5$). Figures 13-20 show the effect

of the inclusion length for constant crack length 2ℓ and constant distance c (Figure 13). The effect of the distance c for constant inclusion and crack lengths is shown in Figures 13-28.

The results of the nonsymmetric problem showing the effect of the relative location of the inclusion are shown in Table 6. Referring to Figure 1, in these calculations it is assumed that $\theta = \frac{\pi}{2}$, d-c = 2ℓ, $c/2\ell = 0.1$ and $a/2\ell$ is variable.

Finally, the stress intensity factors for the crack-inclusion intersection problem considered in Section 4.1 are given in Figures 29-43. The normalized stress intensity factors shown in these figures are defined by (see (41), (52) and (53))

$$k'_{1B} = \frac{1}{\sigma^{\infty}_{ij}\sqrt{\ell}} \lim_{x\to b} \sqrt{2(x-b)}\, \sigma_{yy}(x,0) ,$$

$$k'_{2B} = \frac{1}{\sigma^{\infty}_{ij}\sqrt{\ell}} \lim_{x\to b} \sqrt{2(x-b)}\, \sigma_{xy}(x,0) ,$$

$$k'_{1A} = \frac{1}{\sigma^{\infty}_{ij}\sqrt{\ell}} \lim_{x\to -0} \sqrt{2}\, x^{\alpha}\, \sigma_{yy}(-0,0) ,$$

$$k'_{2A} = \frac{1}{\sigma^{\infty}_{ij}\sqrt{\ell}} \lim_{x\to -0} \sqrt{2}\, x^{\alpha}\, \sigma_{xy}(-0,0) , \qquad (56)$$

$$k'_{1D} = \frac{1}{k_o} \lim_{y\to d} \sqrt{2(y-d)}\, \sigma_{xx}(0,y) ,$$

$$k_o = \frac{1-\kappa}{2(1+\kappa)}\, \sigma^{\infty}_{ij}\, \sqrt{d/2} \quad .$$

In this case too, generally the magnitude of the stress intensity factors increases with increasing length and stiffness of the inclusion. However, since the crack and the inclusion are located in each other's "shadow", the relative dimensions seem to have considerable influence on the variation as well as the magnitude of the stress intensity factors.

Table 6. The effect of the relative location of inclusion on the stress intensity factors; $\theta = \pi/2$, $(d-c)/2\ell = 1$, $c/2\ell = 0.1$ (Figure 1).

σ^{∞}_{ij}	$\frac{a}{2\ell}$	$k_1'(a)$	$k_2'(a)$	$k_1'(b)$	$k_2'(b)$	$k_1'(c)$	$k_1'(d)$
σ^{∞}_{xx}	0.1	-0.0202	0.0490	0.0161	0.0003	0.4450	0.4471
	0.0	-0.1033	0.0425	0.0133	0.0039	0.4192	0.4402
	-0.1	-0.0849	-0.0044	0.0076	0.0081	0.3538	0.4285
	-0.3	-0.0349	-0.0308	0.0023	0.0060	0.3348	0.4163
	-0.5	-0.0363	-0.0114	-0.0363	0.0114	0.3195	0.4109
σ^{∞}_{yy}	+0.1	1.0458	-0.1396	0.9545	0.0012	-1.5217	-1.0543
	0.0	1.2652	-0.1090	0.9667	-0.0078	-1.2922	-0.9497
	-0.1	1.1548	0.0064	0.9865	-0.0150	-0.5345	-0.8136
	-0.3	1.0448	0.0294	1.0013	-0.0102	-0.2308	-0.6378
	-0.5	1.0313	0.0129	1.0313	-0.0129	-0.1959	-0.5801
σ^{∞}_{xy}	0.1	0.0098	0.9905	-0.0033	0.9992	0.1050	-0.1338
	0.0	0.0493	0.9796	-0.0065	0.9983	-0.1734	-0.1675
	-0.1	0.0463	1.0019	-0.0041	0.9960	-0.1054	-0.1648
	-0.3	0.0123	1.0066	-0.0007	0.9971	-0.0236	-0.0977
	-0.5	0	1	0	1	0	0

References

1. F. Erdogan and G.D. Gupta, "The Inclusion Problem with a Crack Crossing the Boundary", Int. J. of Fracture, Vol. 11, pp. 13-27, 1975.

2. I.N. Muskhelishvili, Some Basic Problems of the Mathematical Theory of Elasticity, Noordhoff, Groningen, The Netherlands, 1953.

3. F. Erdogan, "Mixed Boundary Value Problems in Mechanics", Mechanics Today, Vol. 4, S. Nemat-Nasser, ed. pp. 1-86, Pergamon Press Inc., 1978.

4. G.R. Irwin, "Analysis of Stresses and Strains Near the End of a Crack Traversing a Plate", J. Appl. Mech., Vol. 24, Trans. ASME, pp. 361-364, 1957.

5. M.L. Williams, "On the Stress Distribution at the Base of a Stationary Crack", J. Appl. Mech., Vol. 24, Trans. ASME, pp. 109-114, 1957.

6. F. Delale and F. Erdogan, "Transverse Shear Effect in a Circumferentially Cracked Cylindrical Shell", Quarterly of Applied Mathematics, Vol. 37, pp. 239-258, 1979.

7. F. Erdogan and G.D. Gupta, "Stresses near a Flat Inclusion in Bonded Dissimilar Materials", Int. J. Solids Structures, Vol. 8, pp. 533-547, 1972.

8. O.S. Yahsi and F. Erdogan, "A Note on the Cracked Plates Reinforced by a Line Stiffener", Engineering Fracture Mechanics, (to appear) 1984.

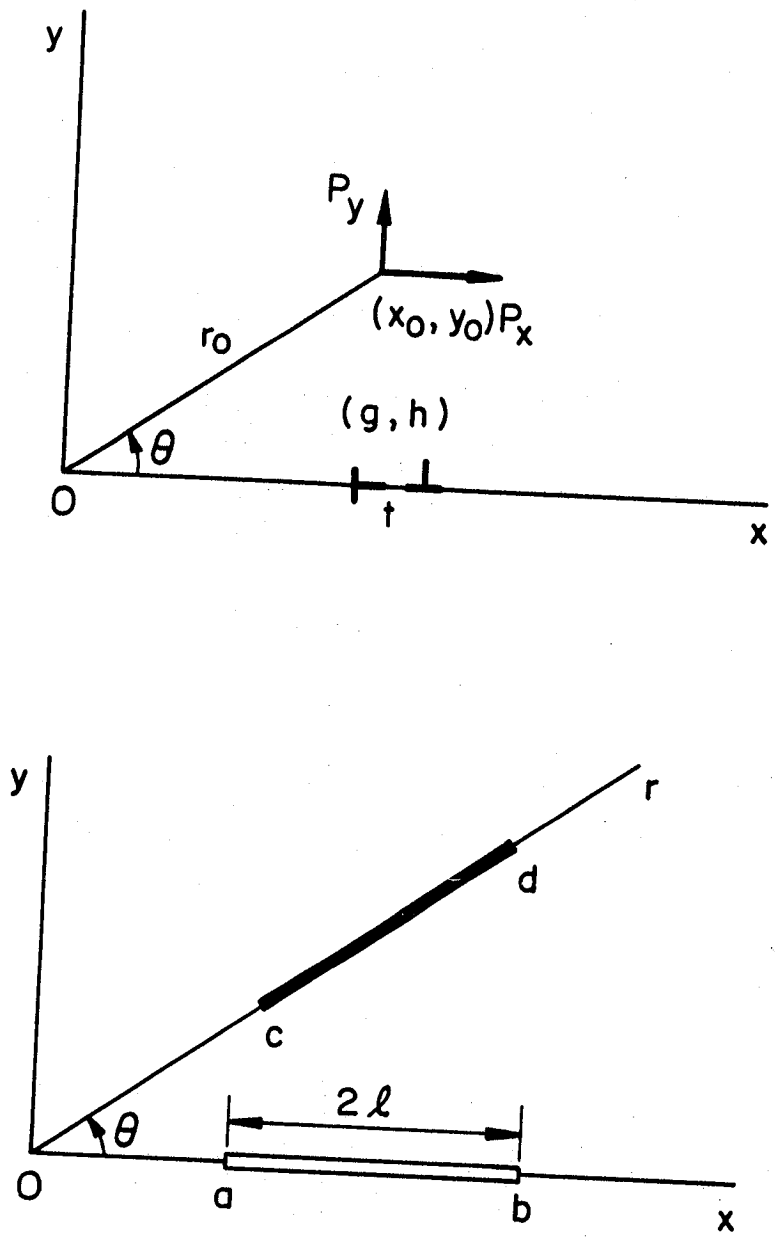

Figure 1. The geometry and notation for the crack-inclusion problem.

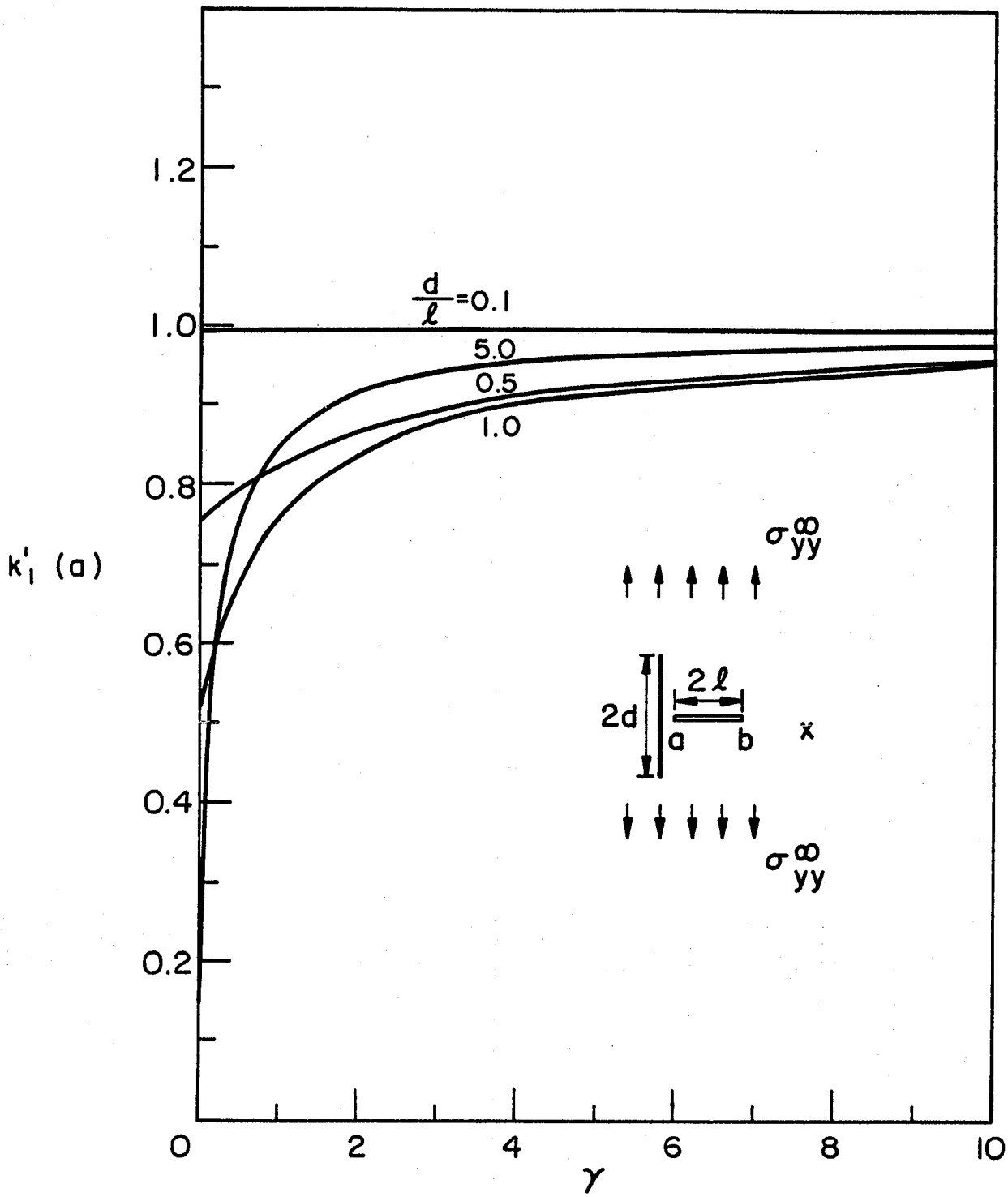

Figure 2. The effect of the stiffness and the relative length of the inclusion on the normalized stress intensity factor $k_1'(a)$; $\sigma_{yy}^{\infty} \neq 0$, $\sigma_{xx}^{\infty} = 0$, $\sigma_{xy}^{\infty} = 0$; $a/\ell = 0.5$, $\nu = 0.3$.

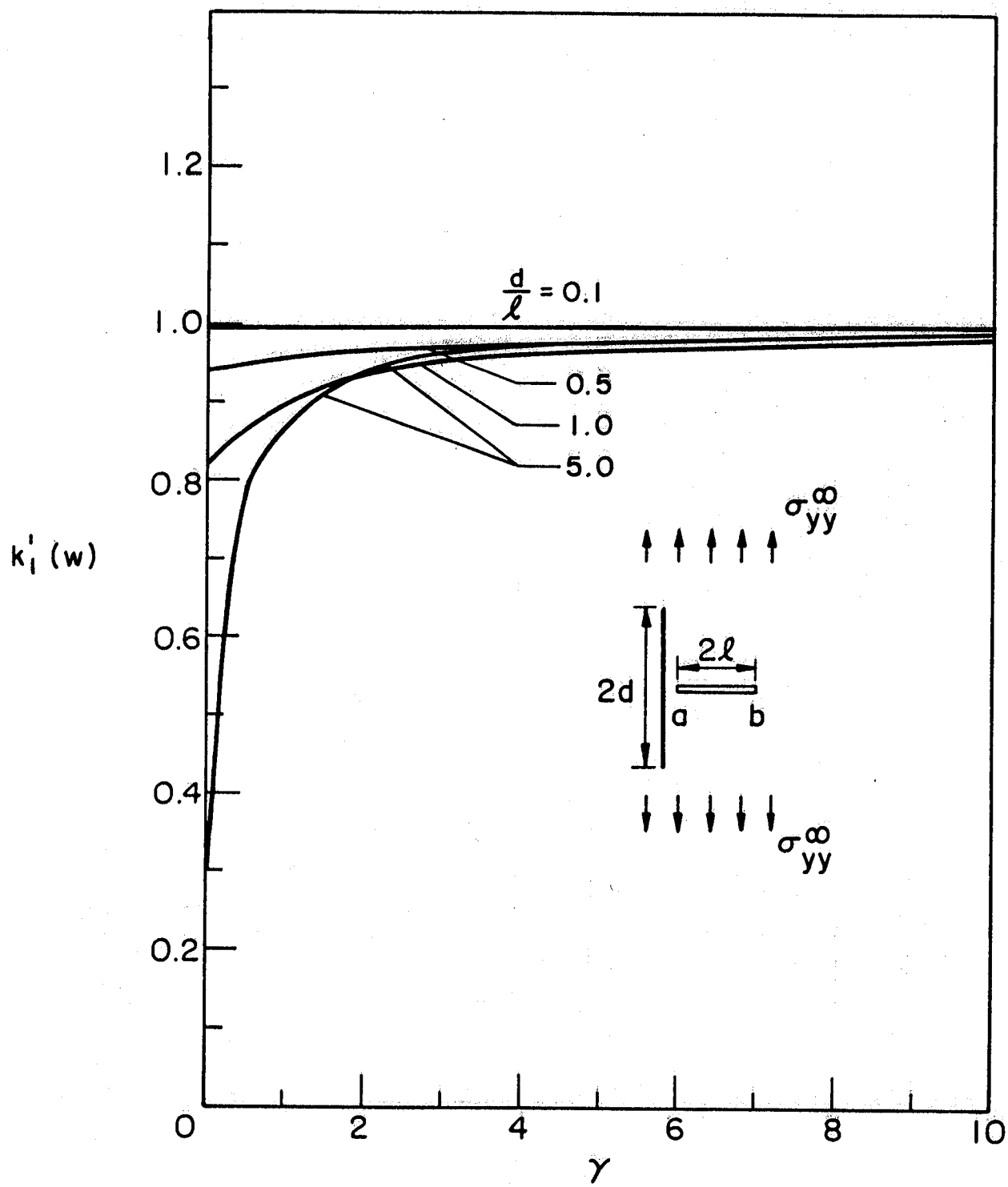

Figure 3. Normalized stress intensity factor $k_1'(b)$; $\sigma_{yy}^{\infty} \neq 0$, $\sigma_{xx}^{\infty} = 0 = \sigma_{xy}^{\infty}$, $a/\ell = 0.5$, $\nu = 0.3$.

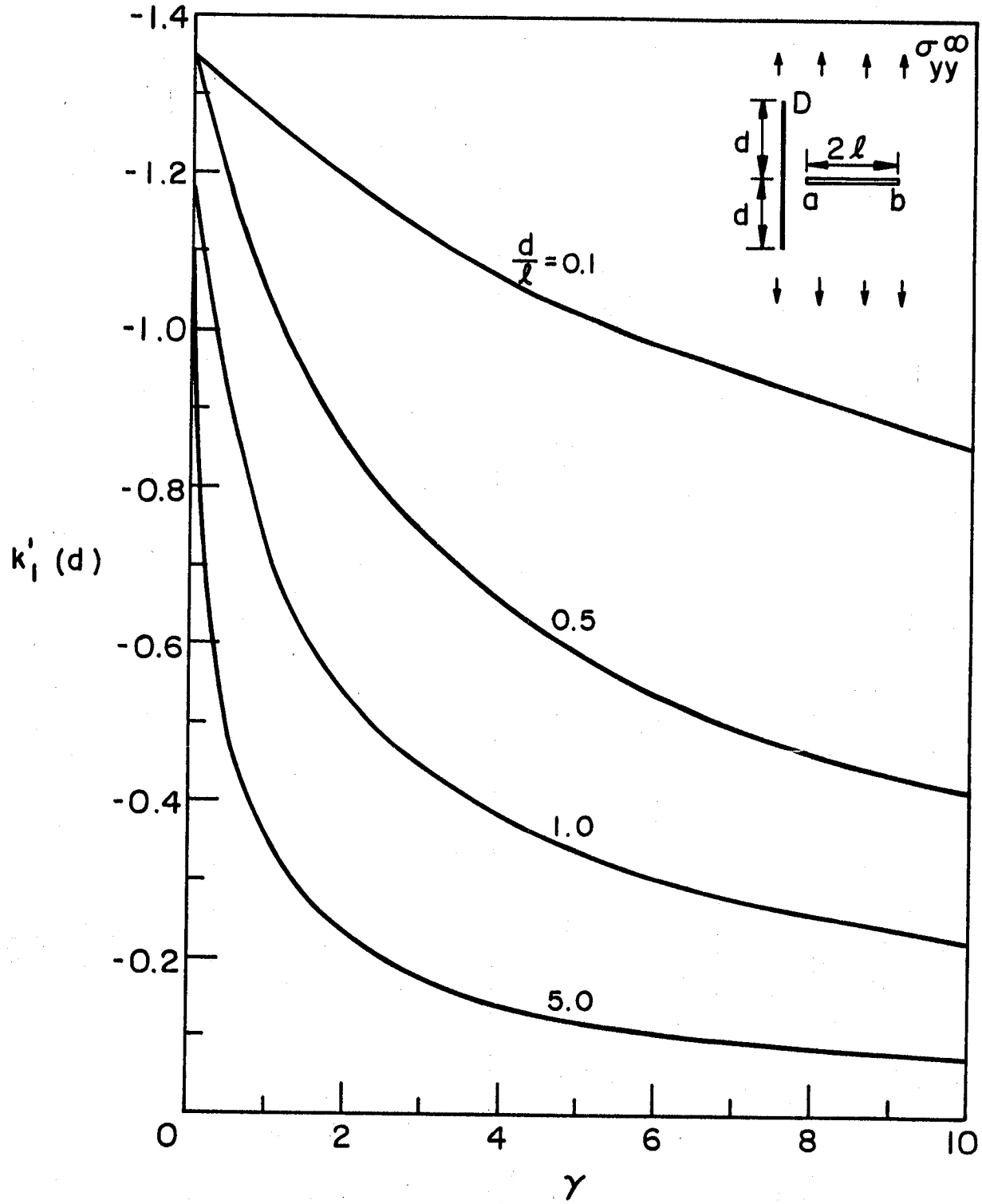

Figure 4. Normalized stress intensity factor at the inclusion end y=d; $\sigma_{yy}^{\infty} \neq 0$, $\sigma_{xx}^{\infty} = \sigma_{xy}^{\infty} = 0$, $a/\ell = 0.5$, $\nu = 0.3$.

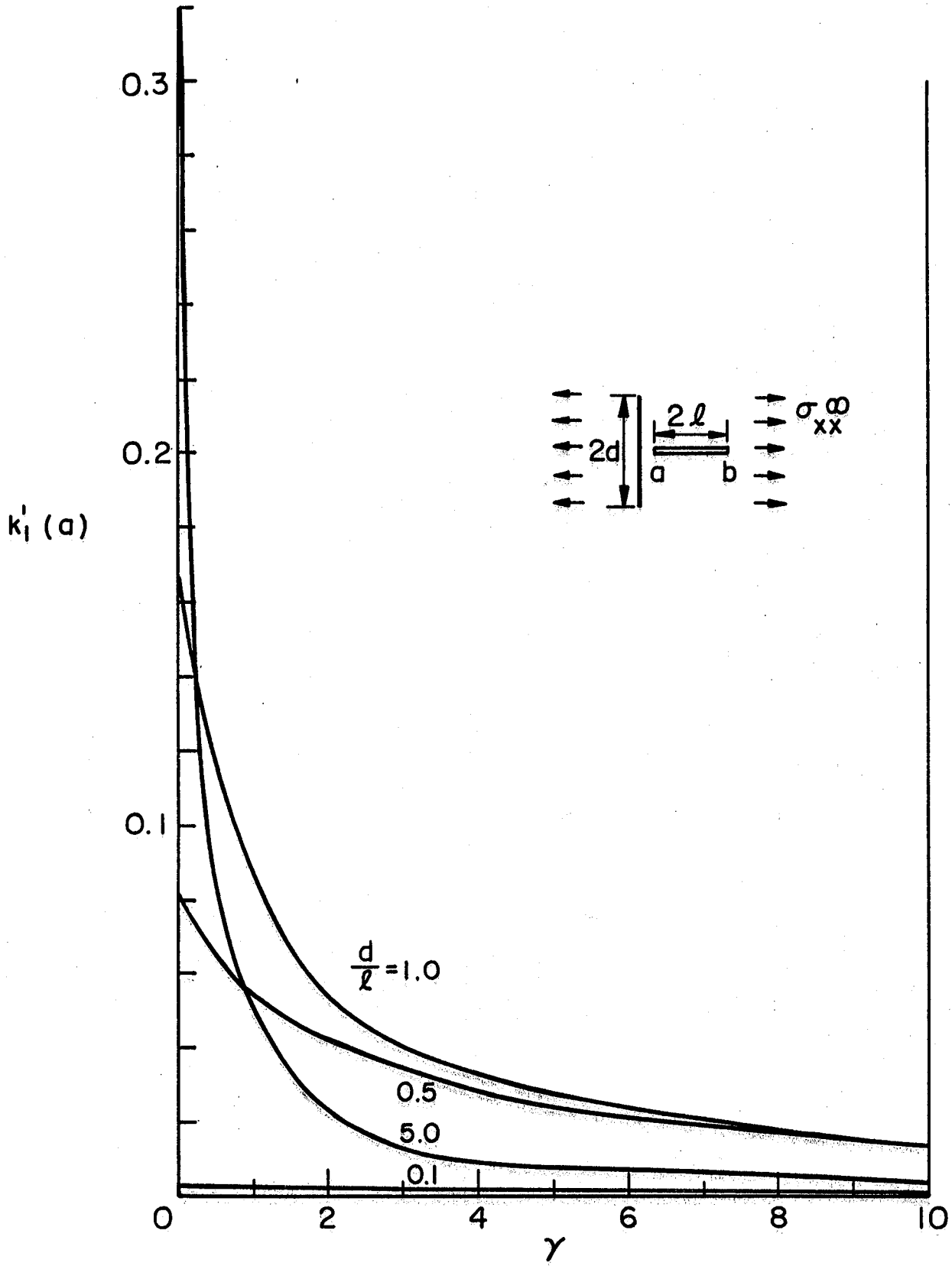

Figure 5. Normalized stress intensity factor at the crack tip x=a; $\sigma_{xx}^{\infty} \neq 0$, $\sigma_{yy}^{\infty} = \sigma_{xy}^{\infty} = 0$, $a/\ell = 0.5$, $\nu = 0.3$.

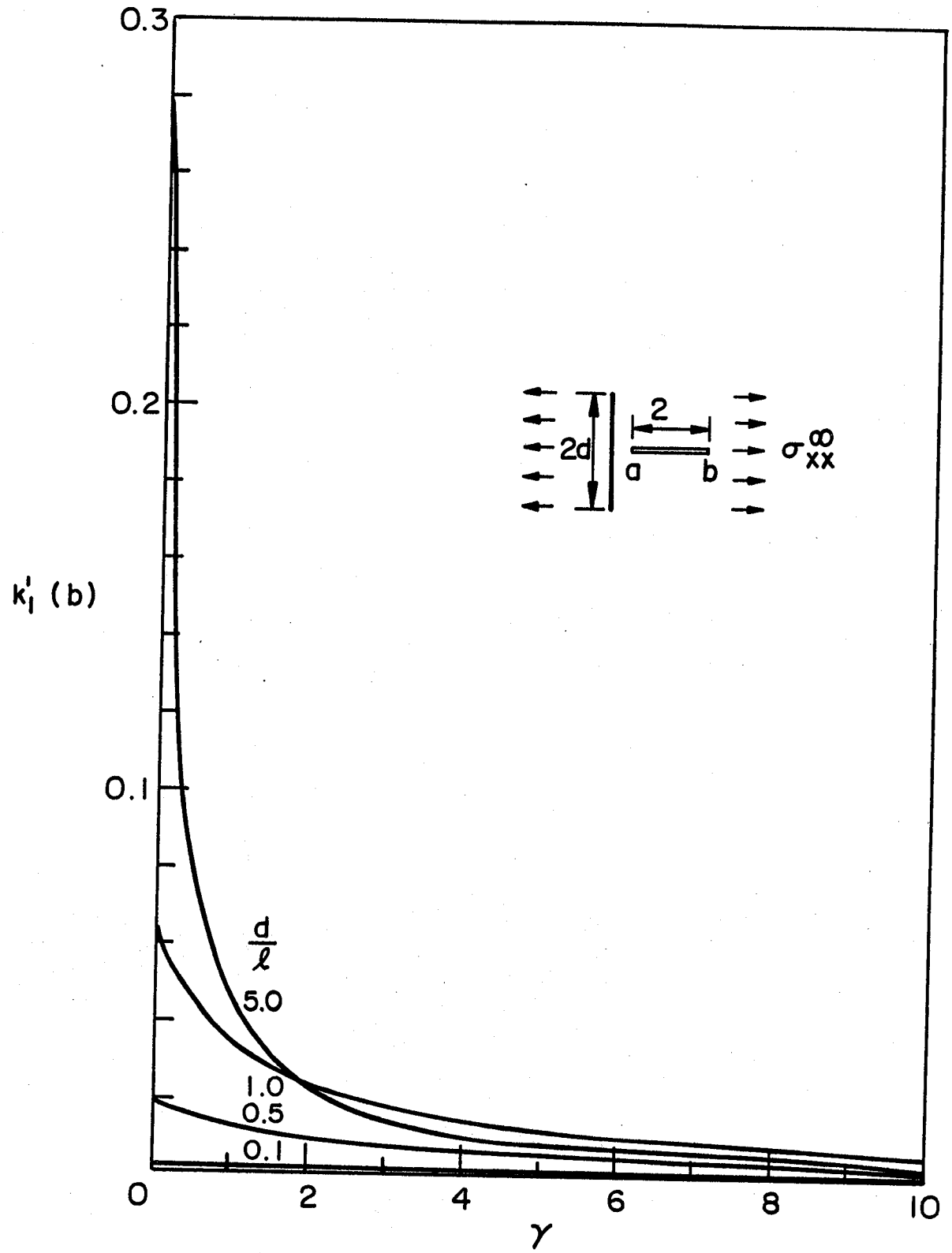

Figure 6. Normalized stress intensity factor at the crack tip x=b; $\sigma_{xx}^{\infty} \neq 0$, $\sigma_{yy}^{\infty} = \sigma_{xy}^{\infty} = 0$, $a/\ell = 0.5$, $\nu = 0.3$.

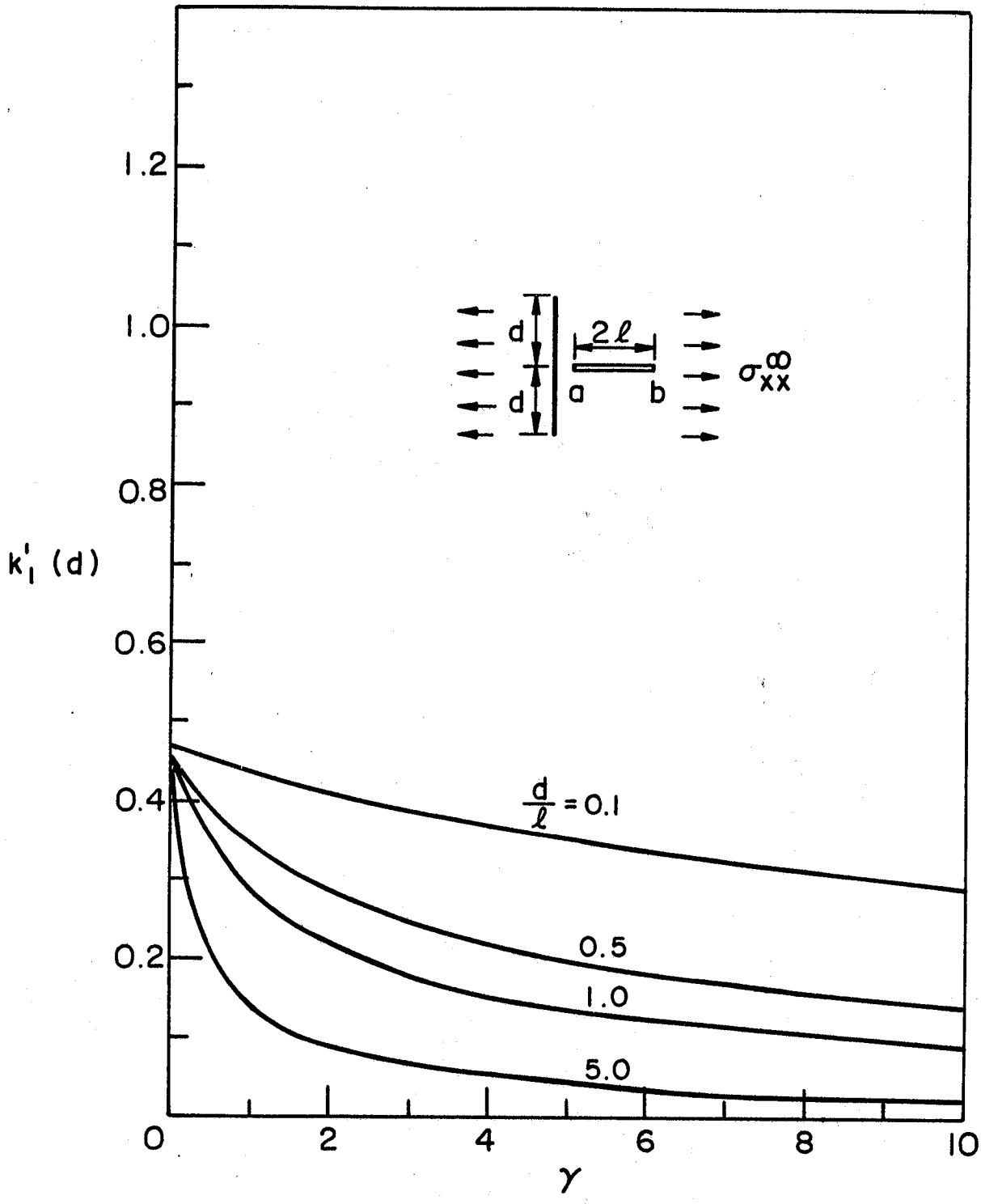

Figure 7. Normalized stress intensity factor at the inclusion end y=d; $\sigma_{xx}^{\infty} \neq 0$, $\sigma_{yy}^{\infty} = \sigma_{xy}^{\infty} = 0$, $a/\ell = 0.5$, $\nu = 0.3$.

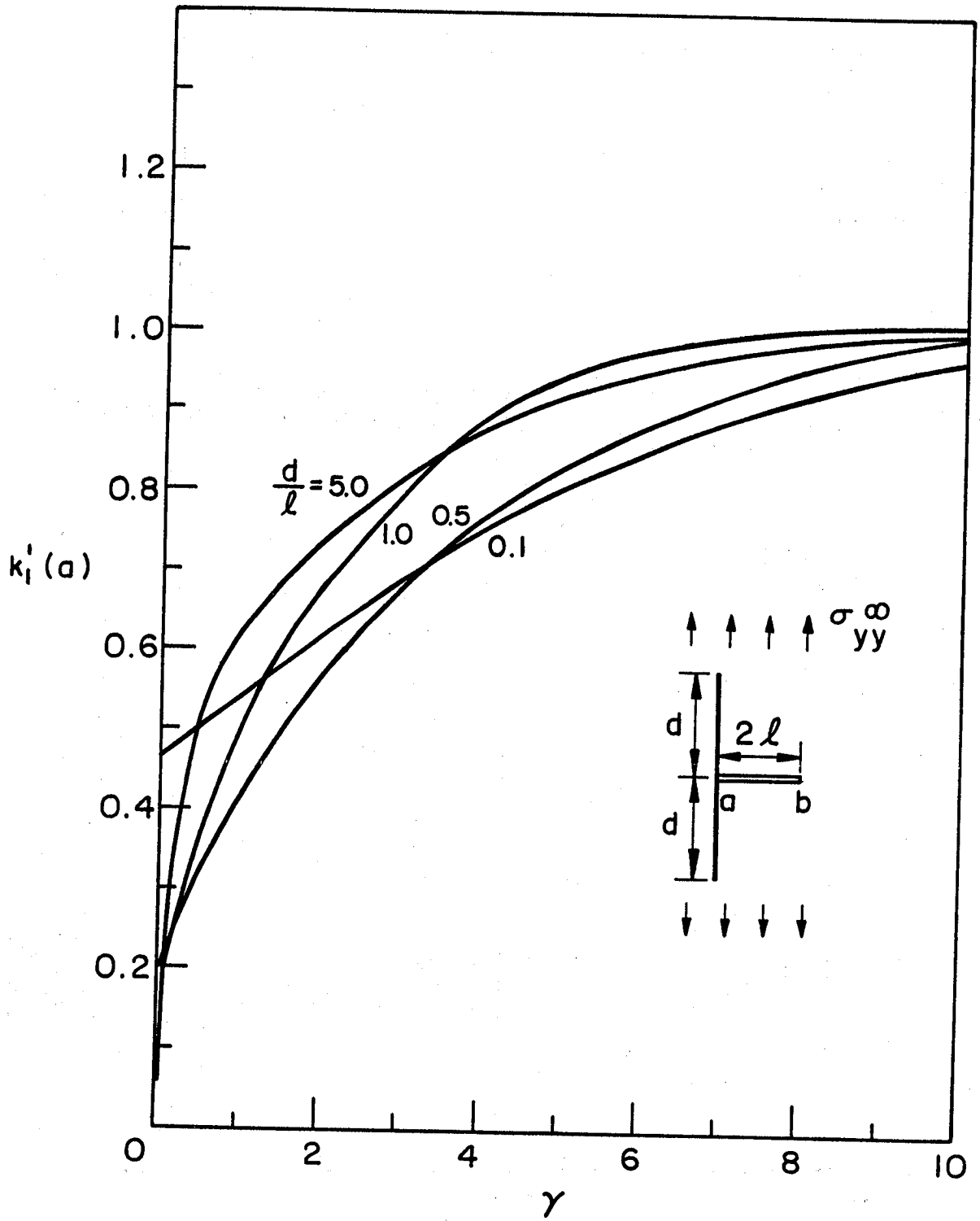

Figure 8. Normalized stress intensity factor at the crack tip x=a=0, $\sigma_{yy}^{\infty} \neq 0$, $\sigma_{xx}^{\infty} = \sigma_{xy}^{\infty} = 0$, $\nu = 0.3$.

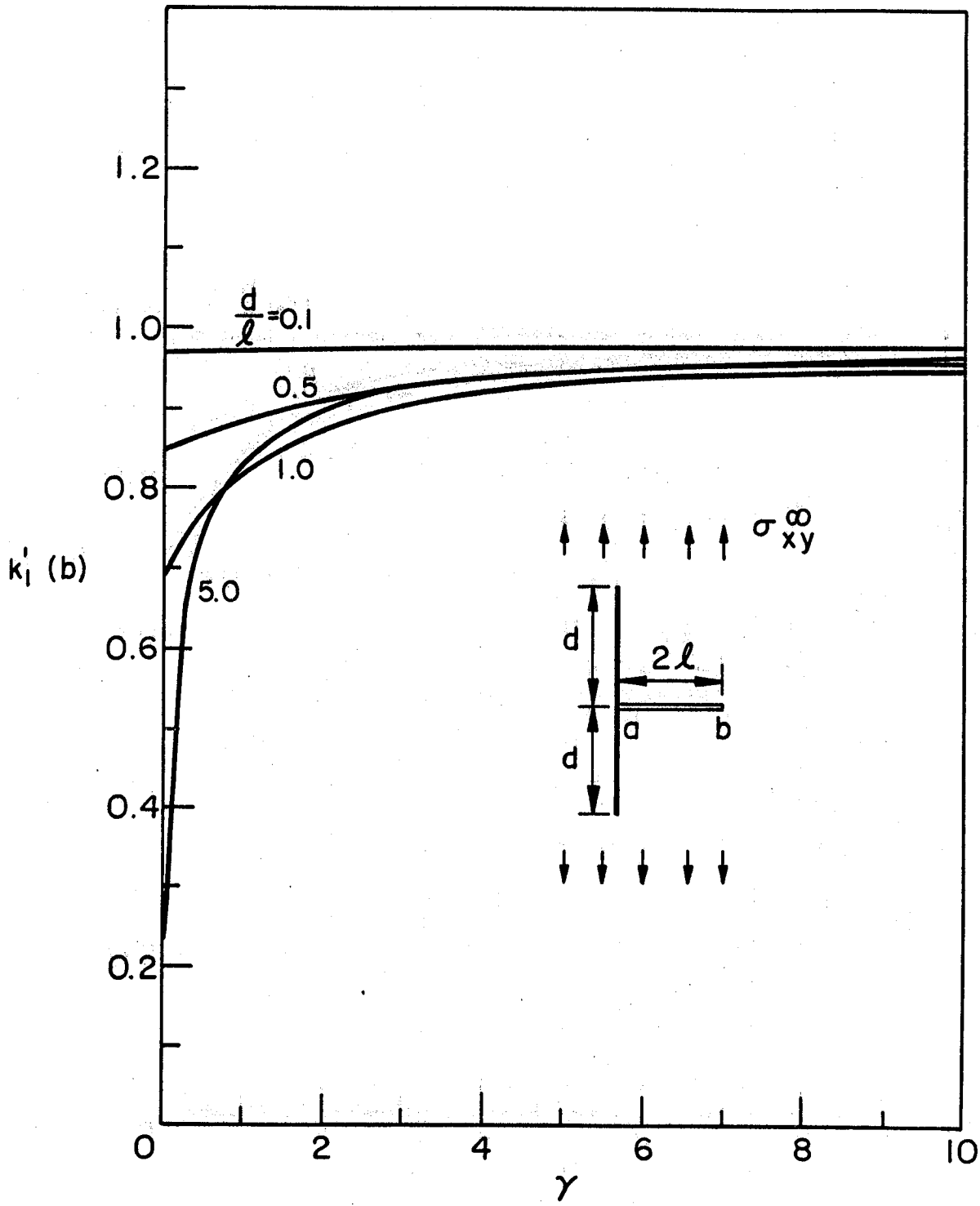

Figure 9. Normalized stress intensity factor at the crack tip x=b, $\sigma_{yy}^{\infty} \neq 0$, $\sigma_{xx}^{\infty} = \sigma_{xy}^{\infty} = 0$, $\nu = 0.3$, a = 0.

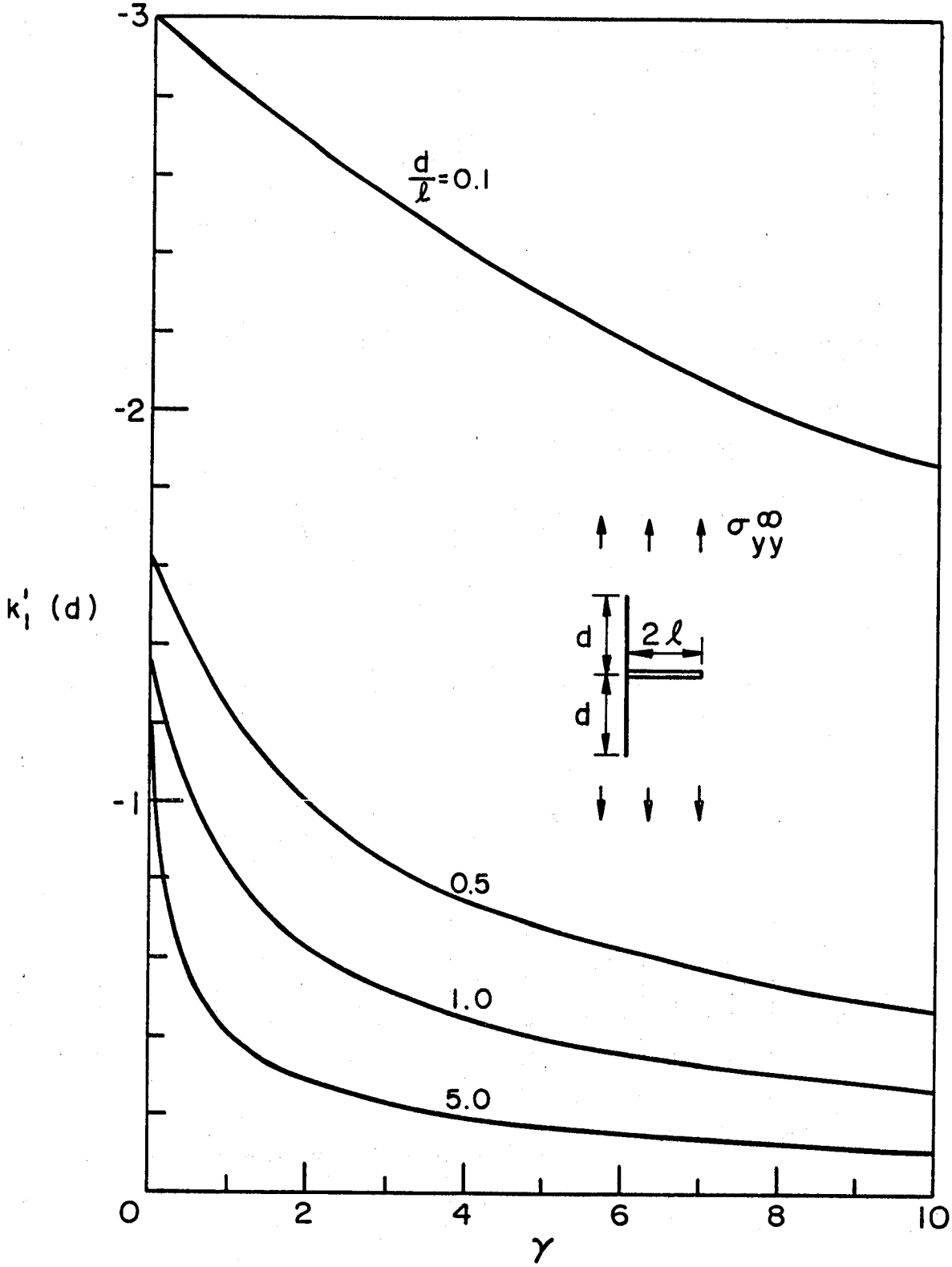

Figure 10. Normalized stress intensity factor at the inclusion end y=d, $\sigma_{yy}^{\infty} \neq 0$, $\sigma_{xx}^{\infty} = \sigma_{xy}^{\infty} = 0$, $\nu = 0.3$, a = 0.

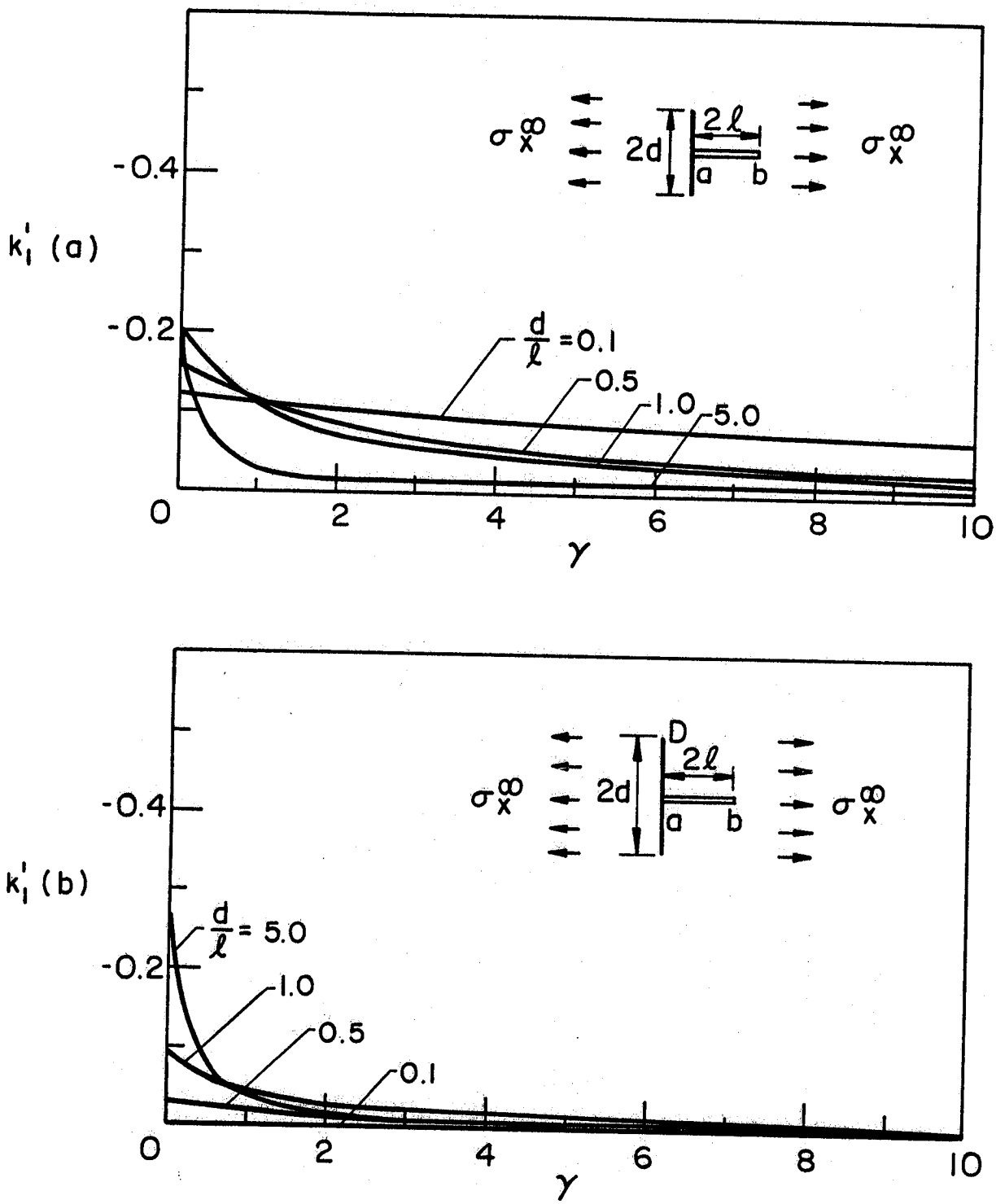

Figure 11. Normalized stress intensity factors at the crack tips x=a=0 and x=b; $\sigma_{xx}^\infty \neq 0$, $\sigma_{yy}^\infty = \sigma_{xy}^\infty = 0$, a = 0, ν = 0.3.

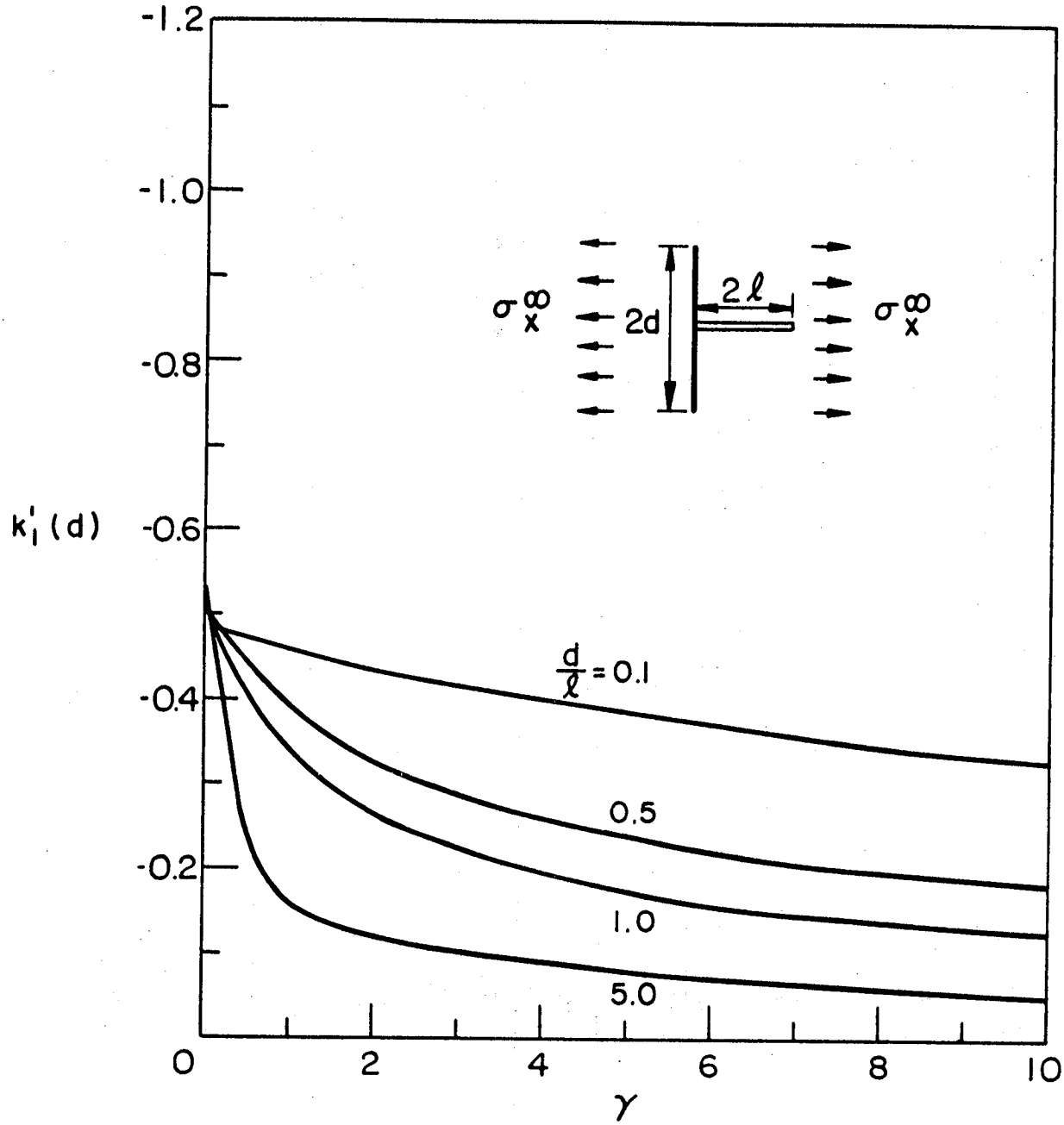

Figure 12. Normalized stress intensity factor at the inclusion end y=d; $\sigma_{xx}^\infty \neq 0$, $\sigma_{yy}^\infty = \sigma_{xy}^\infty = 0$, a = 0, $\nu = 0.3$.

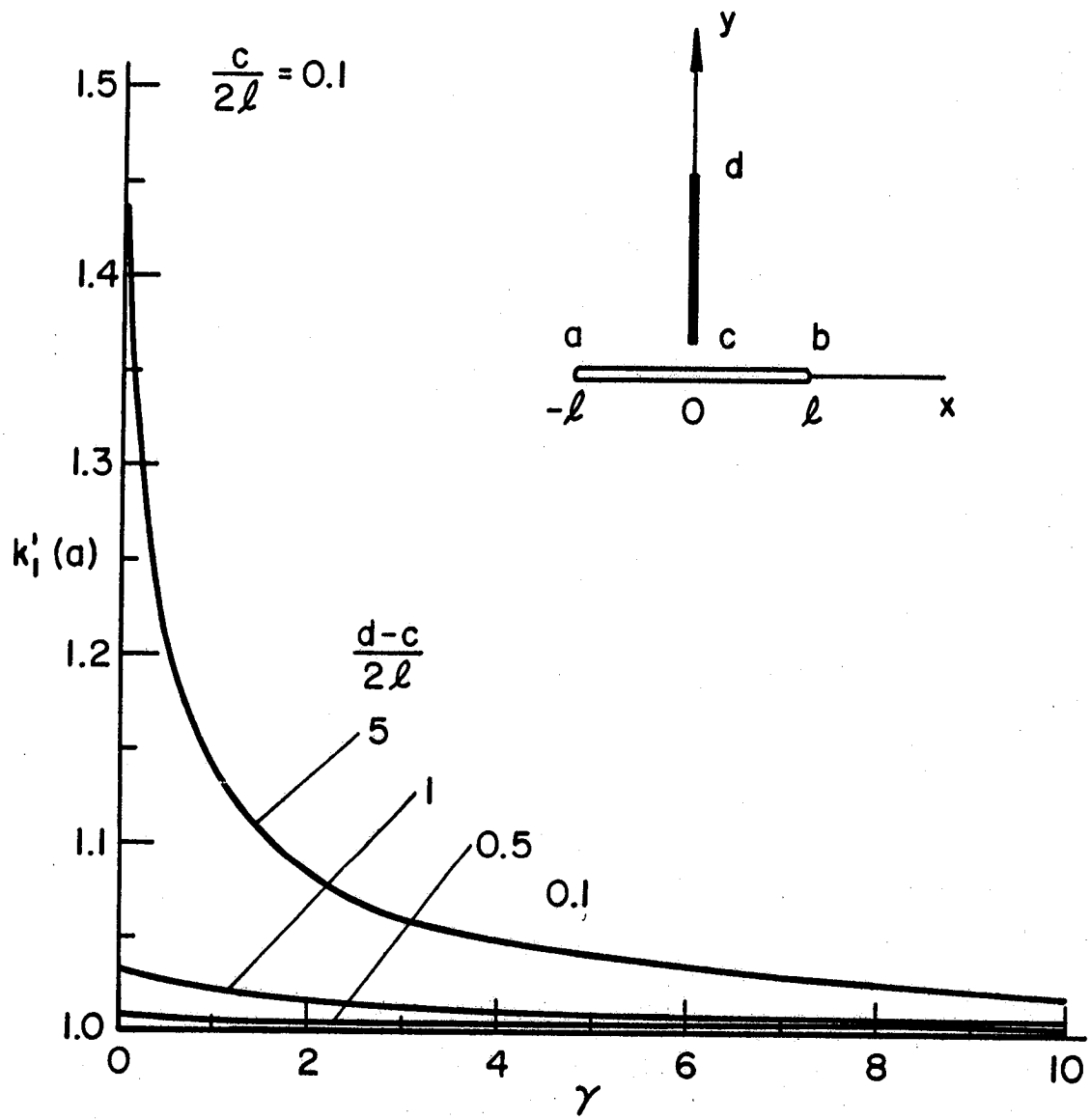

Figure 13. Mode I stress intensity factor at the crack tip $x=a=-\ell$; $\sigma^{\infty}_{yy} \neq 0$, $\sigma^{\infty}_{xx} = 0$, $\sigma^{\infty}_{xy} = 0$, $\theta = \pi/2$, $c = 0.2\ell$, $b = \ell$, $\nu = 0.3$.

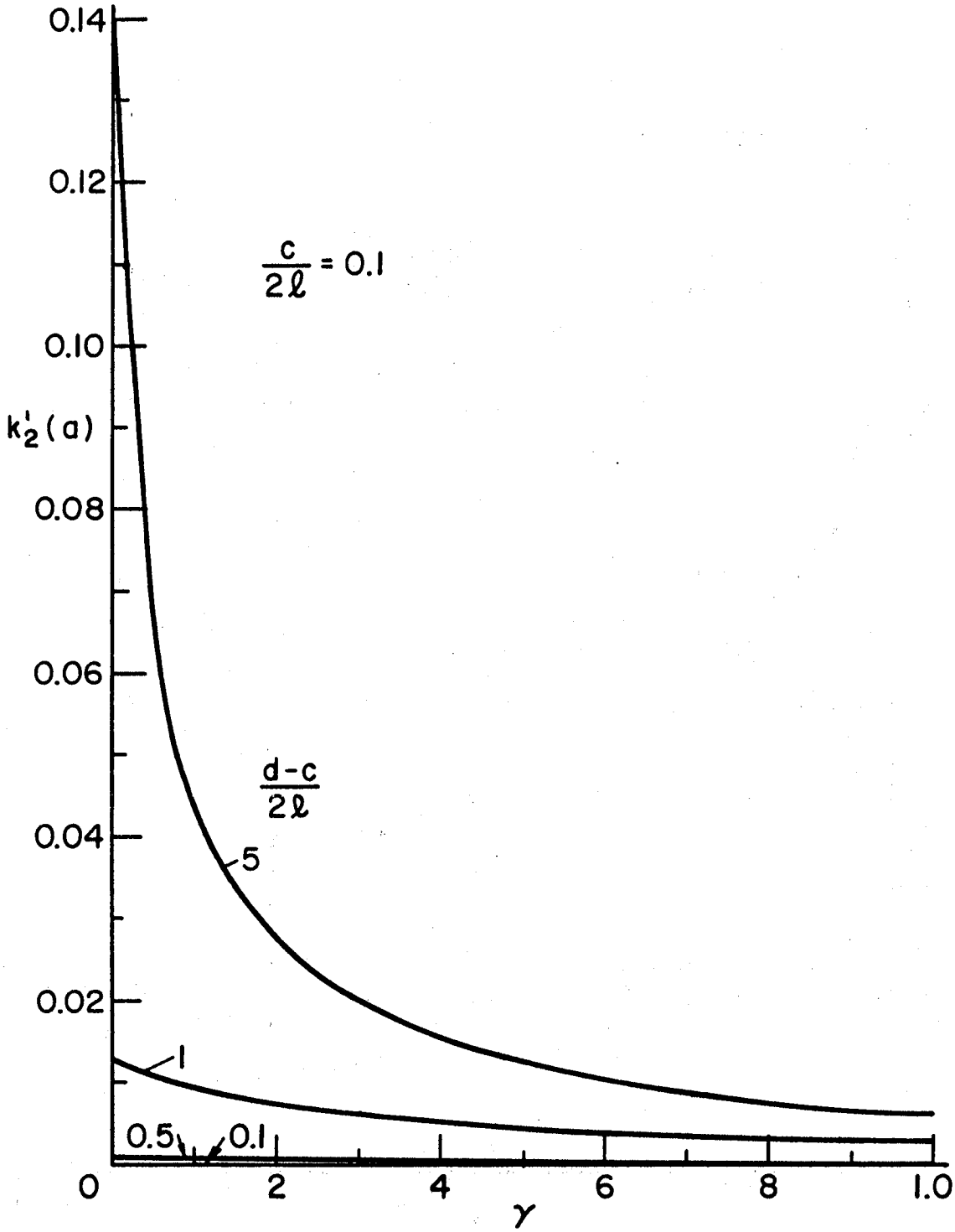

Figure 14. Mode II stress intensity factor at the crack tip $x=a=-\ell$; $\sigma_{yy}^{\infty} \neq 0$, $\sigma_{xx}^{\infty} = \sigma_{xy}^{\infty} = 0$, $\theta = \pi/2$, $c = 0.2\ell$, $b = \ell$, $\nu = 0.3$.

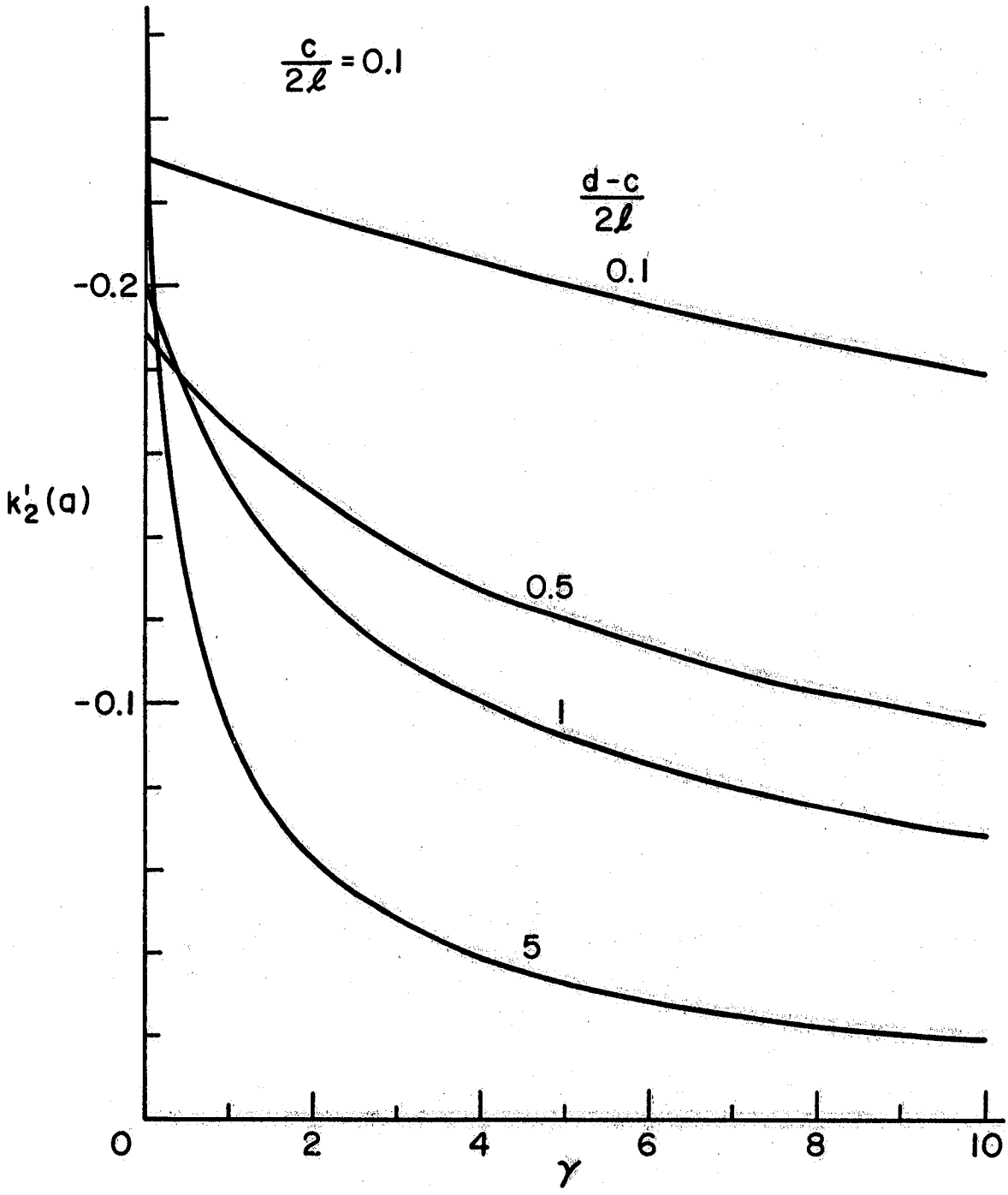

Figure 15. Stress intensity factor at the inclusion end y=c; $\sigma^{\infty}_{yy} \neq 0$, $\sigma^{\infty}_{xx} = \sigma^{\infty}_{xy} = 0$, $\theta = \pi/2$, $c = 0.2\ell$, $\nu = 0.3$, $b = \ell$.

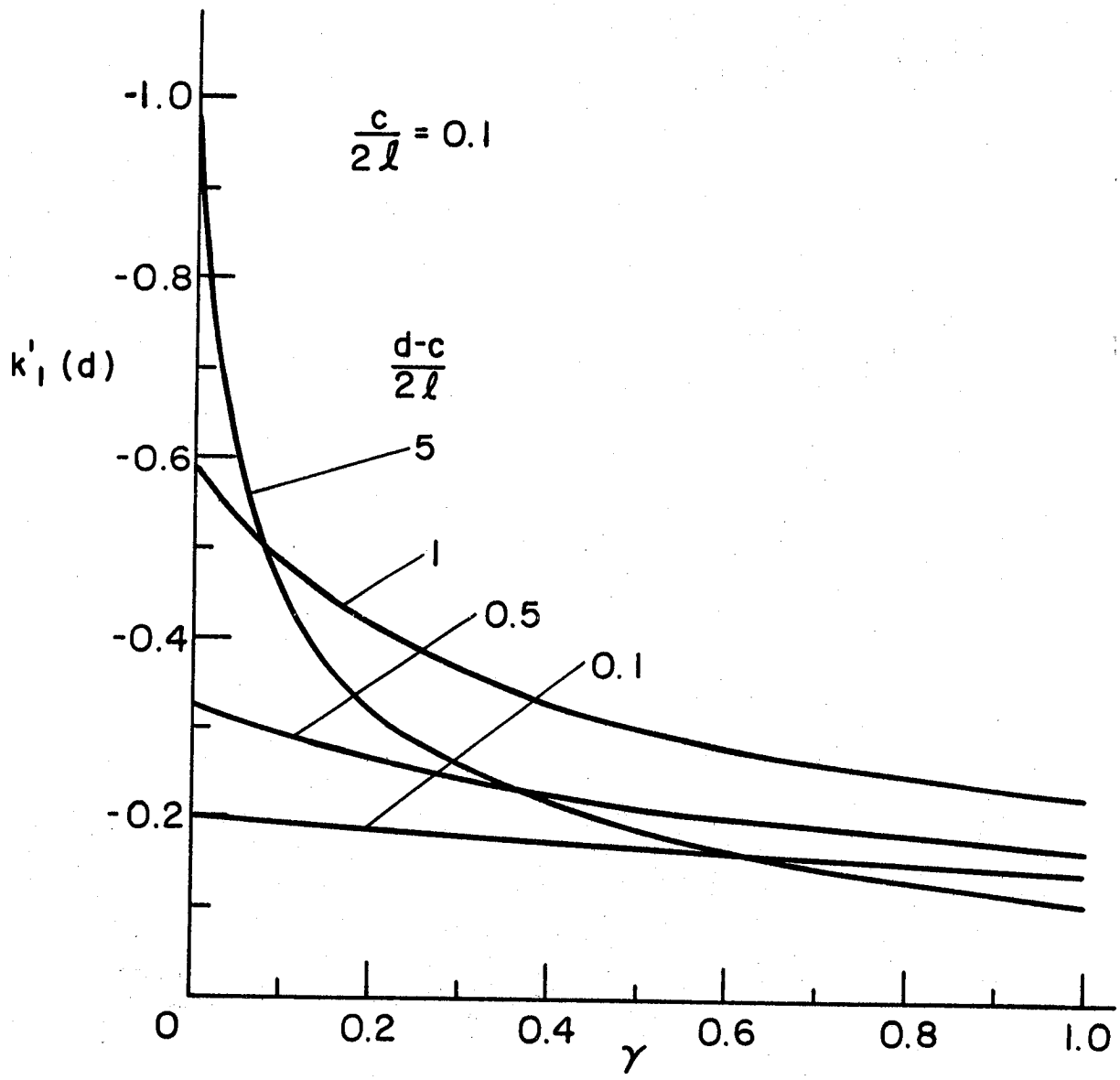

Figure 16. Stress intensity factor at the inclusion end y=d; $\sigma^{\infty}_{yy} \neq 0$, $\sigma^{\infty}_{xx} = \sigma^{\infty}_{xy} = 0$, $\nu = 0.3$, $\theta = \pi/2$, $c = 0.2\ell$, $b = \ell = -a$.

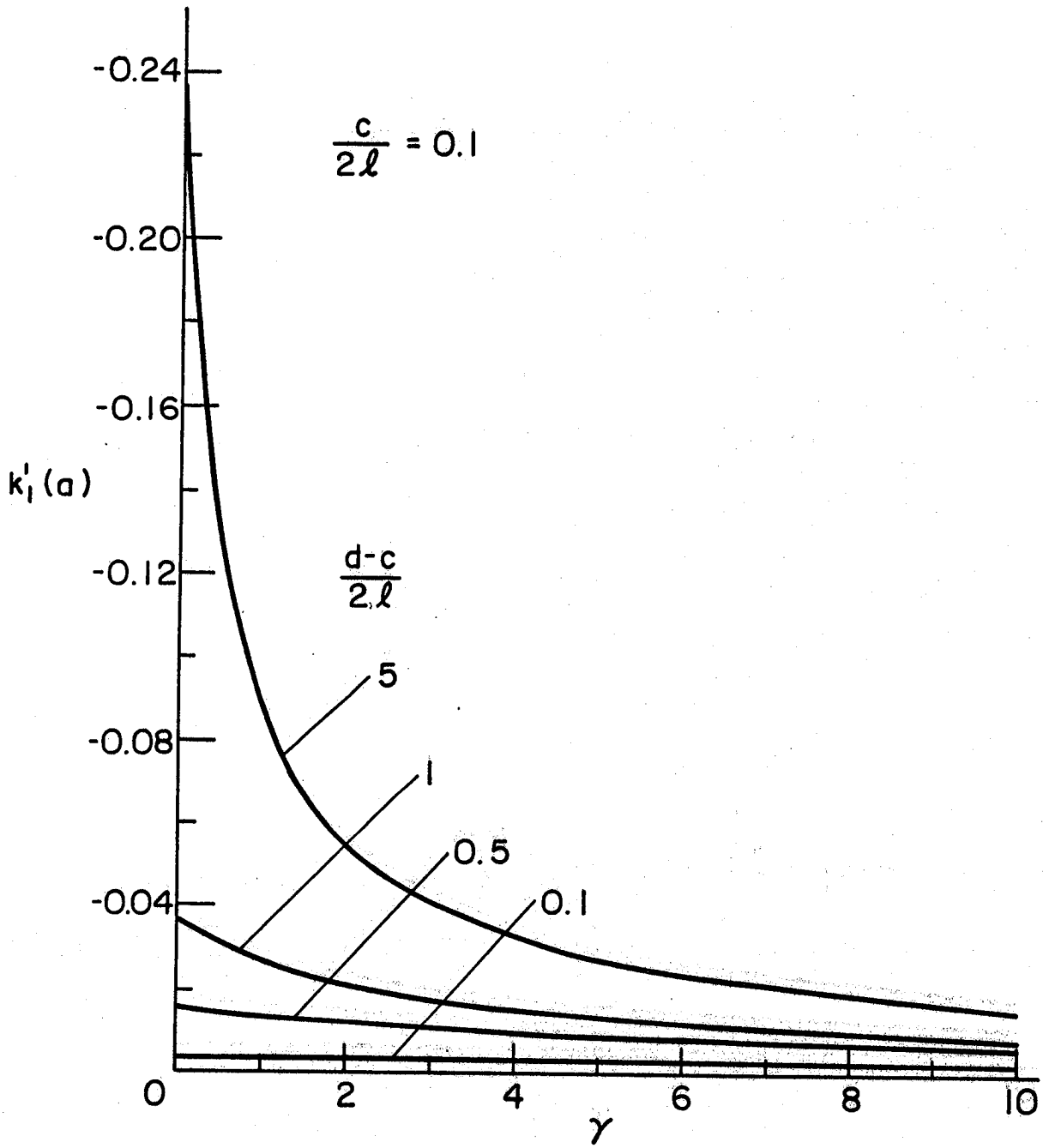

Figure 17. Mode I stress intensity factor at the crack tip $x=a=-\ell$; $\sigma_{xx}^{\infty} \neq 0$, $\sigma_{yy}^{\infty} = \sigma_{xy}^{\infty} = 0$, $\theta = \pi/2$, $\nu = 0.3$, $c = 0.2\ell$, $b = \ell$.

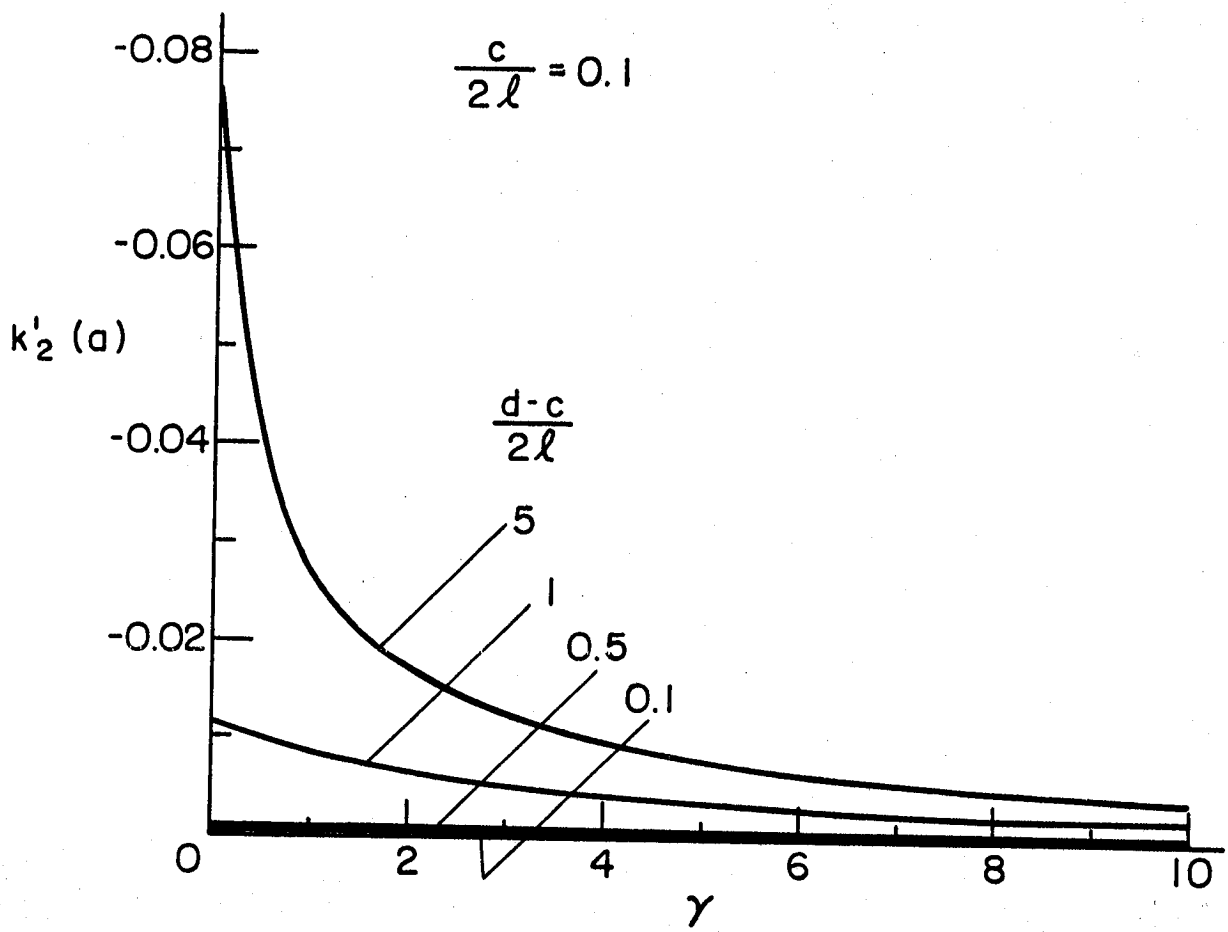

Figure 18. Mode II stress intensity factor at the crack tip $x=a=-\ell$; $\sigma^{\infty}_{xx} \neq 0$, $\sigma^{\infty}_{yy} = \sigma^{\infty}_{xy} = 0$, $\nu = 0.3$, $\theta = \pi/2$, $c = 0.2\ell$, $b = \ell$.

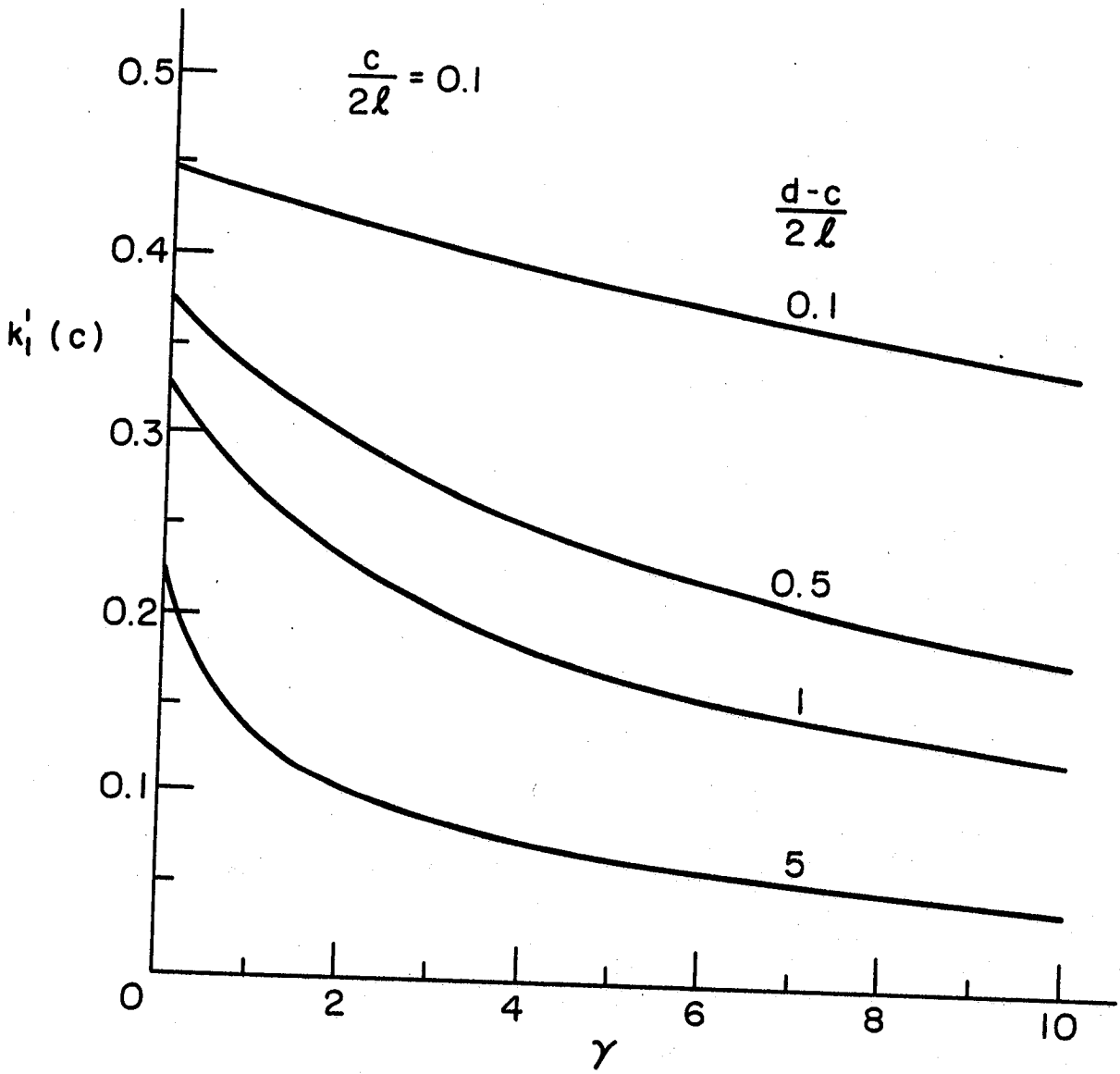

Figure 19. Stress intensity factor at the inclusion end $y = c$; $\sigma^{\infty}_{xx} \neq 0$, $\sigma^{\infty}_{yy} = \sigma^{\infty}_{xy} = 0$, $\nu = 0.3$, $c = 0.2\ell$, $\theta = \pi/2$, $b = \ell = -a$.

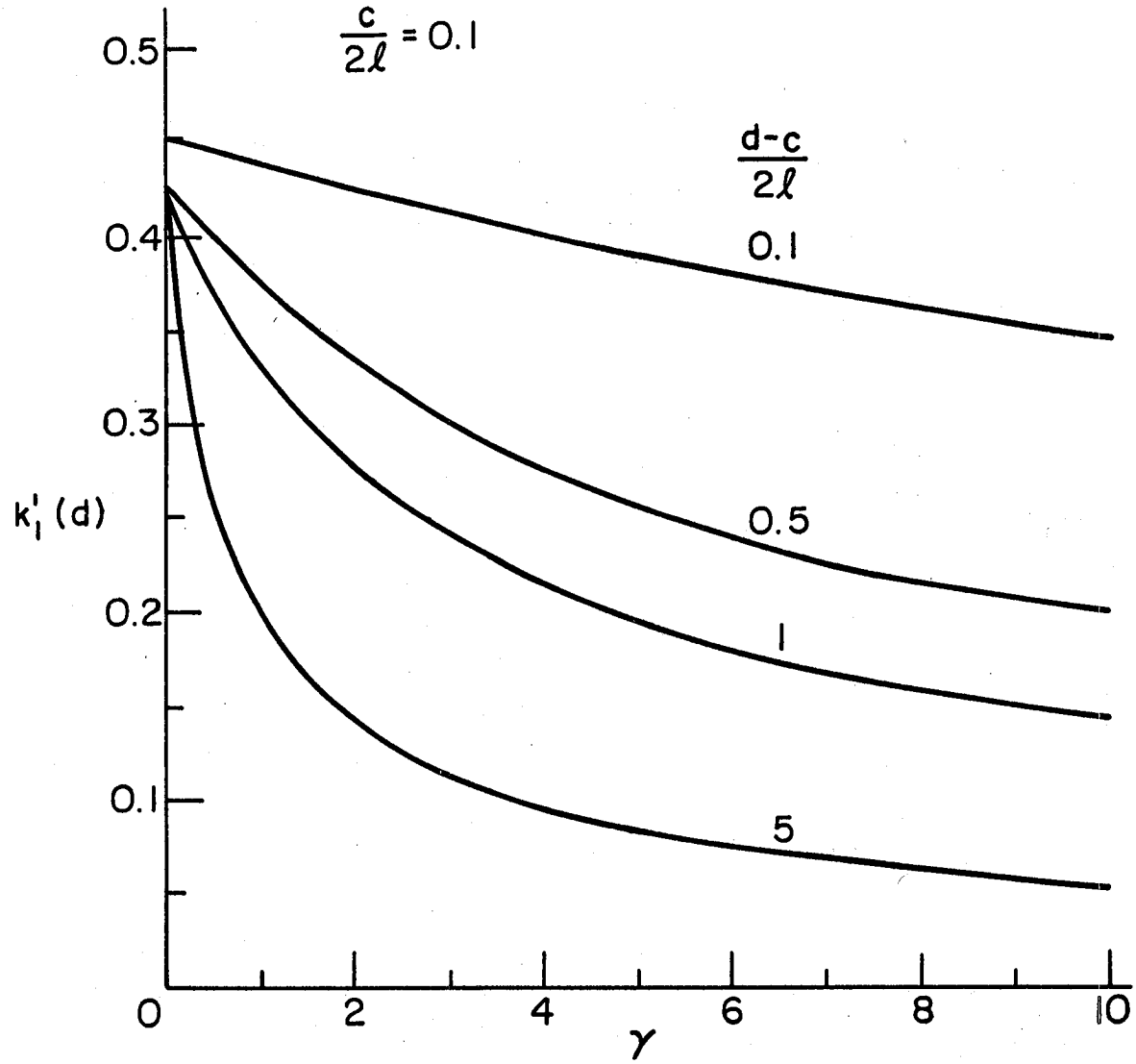

Figure 20. Stress intensity factor at the inclusion end y = d; $\sigma_{xx}^{\infty} \neq 0$, $\sigma_{yy}^{\infty} = \sigma_{xy}^{\infty} = 0$, $\nu = 0.3$, $\theta = \pi/2$, $c = 0.2\ell$, $b = \ell = -a$.

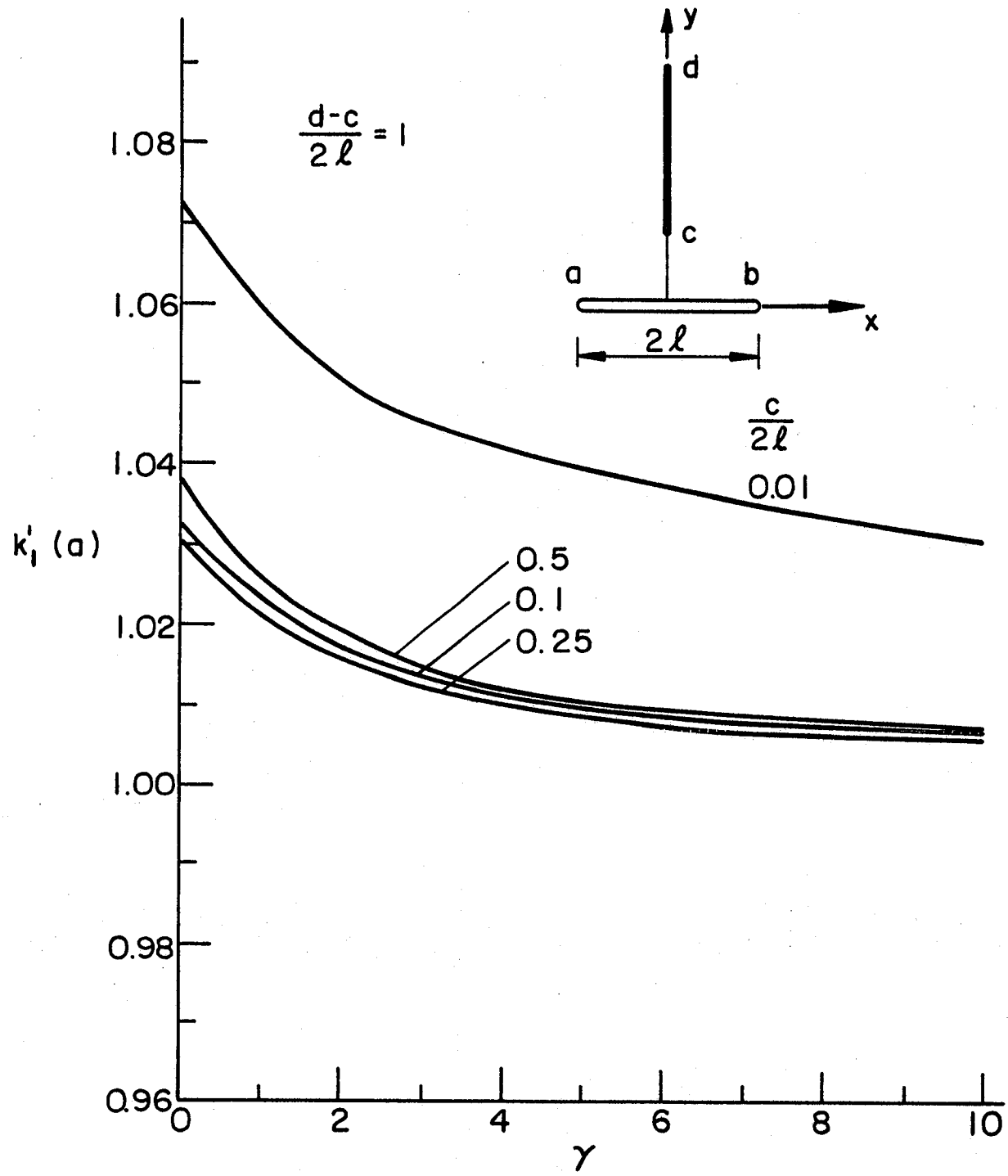

Figure 21. Mode I stress intensity factor at the crack tip $x = a = -\ell$; $\sigma^{\infty}_{yy} \neq 0$, $\sigma^{\infty}_{xx} = \sigma^{\infty}_{xy} = 0$, $\theta = \pi/2$, $\nu = 0.3$, $d\text{-}c = 2\ell$, $b = \ell$.

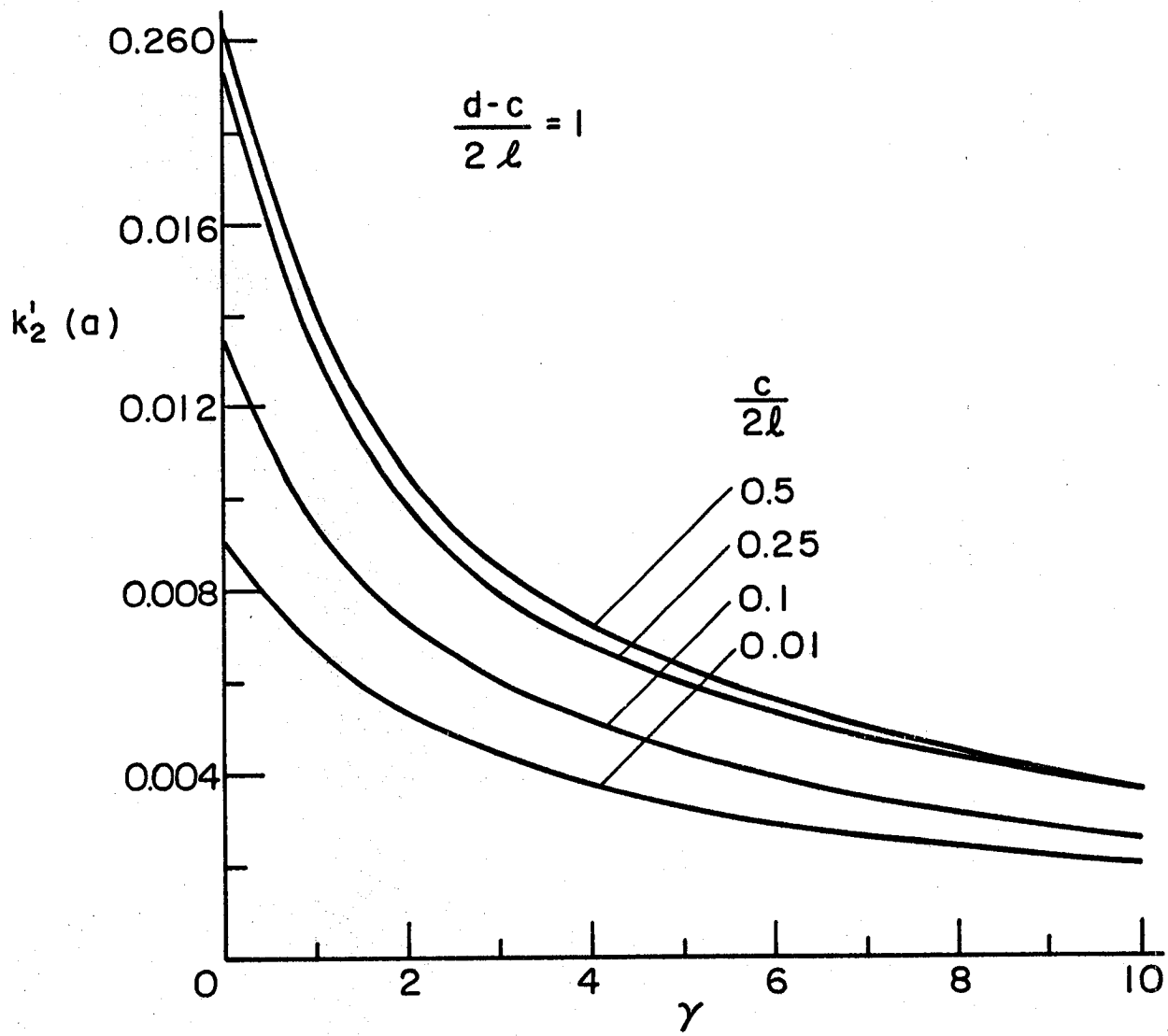

Figure 22. Mode II stress intensity factor at the crack tip $x = a = -\ell$; $\sigma^{\infty}_{yy} \neq 0$, $\sigma^{\infty}_{xx} = \sigma^{\infty}_{xy} = 0$, $\nu = 0.3$, $\theta = \pi/2$, $d-c = 2\ell$, $b = \ell$.

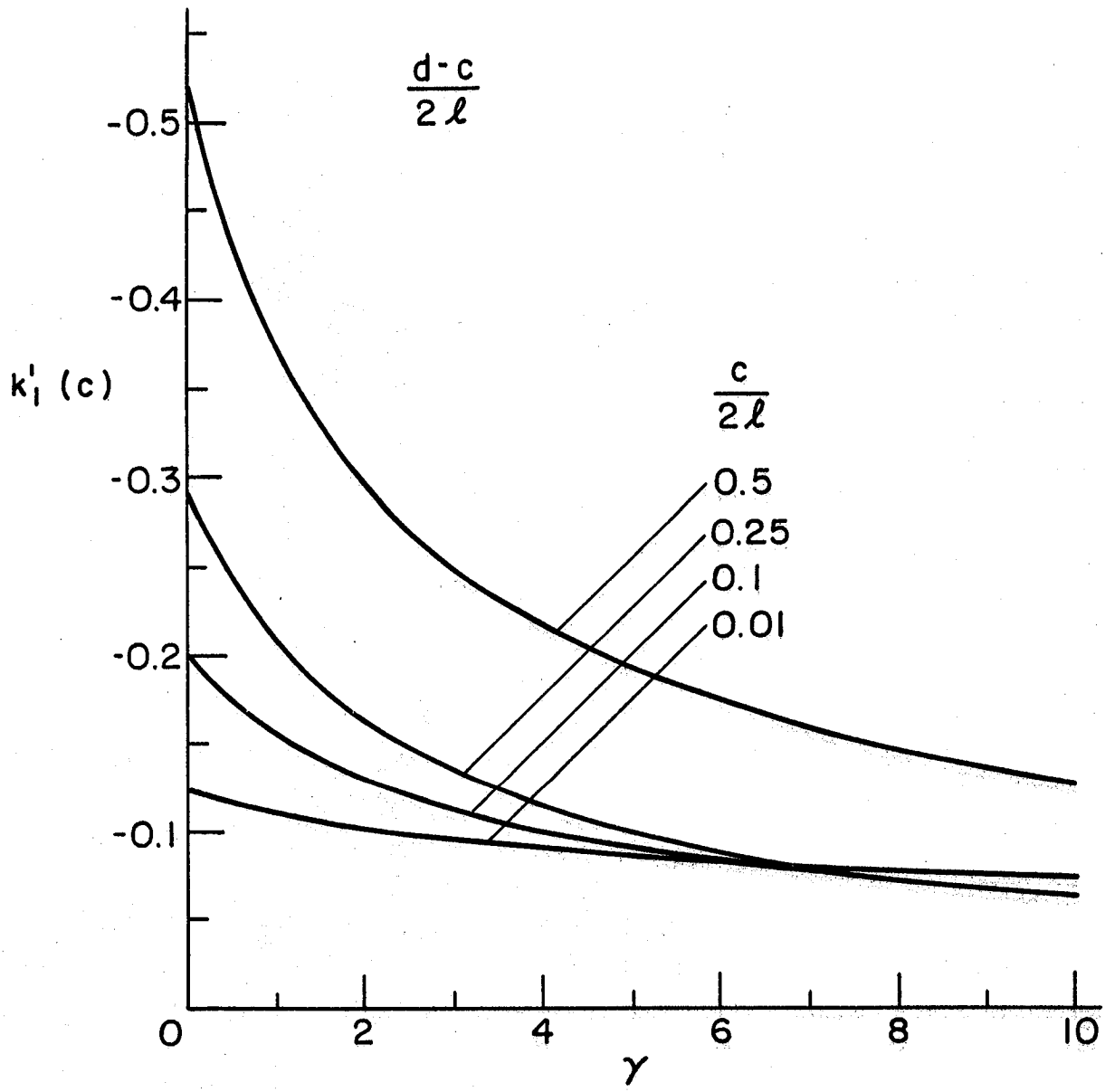

Figure 23. Stress intensity factor at the inclusion end y = c; $\sigma_{yy}^{\infty} \neq 0$, $\sigma_{xx}^{\infty} = \sigma_{xy}^{\infty} = 0$, $\nu = 0.3$, $\theta = \pi/2$, d-c = 2ℓ, b = ℓ = -a.

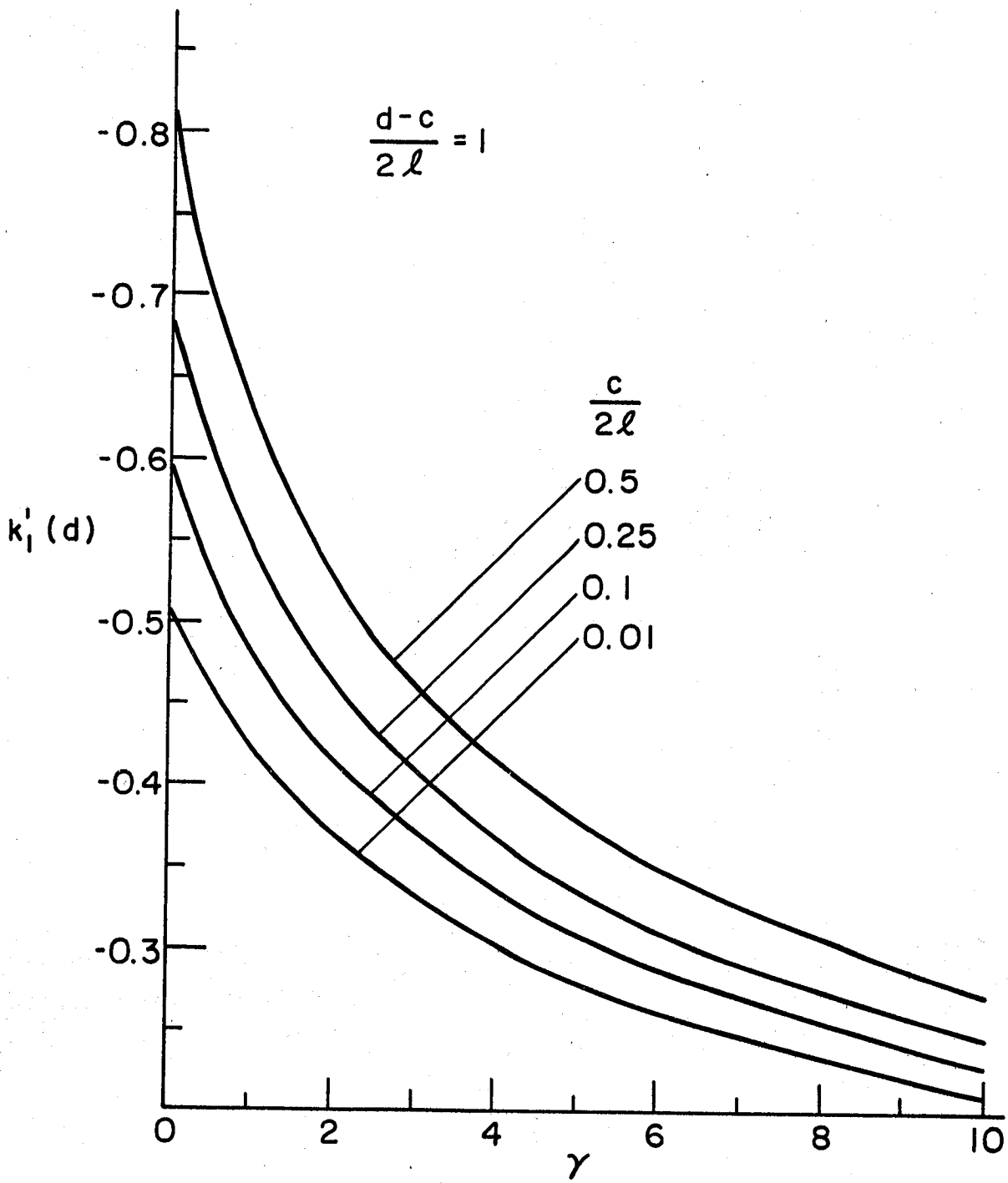

Figure 24. Stress intensity factor at the inclusion end y=d; $\sigma_{yy}^{\infty} \neq 0$, $\sigma_{xx}^{\infty} = \sigma_{xy}^{\infty} = 0$, $\nu = 0.3$, $\theta = \pi/2$, $d-c = 2\ell$, $b = \ell = -a$.

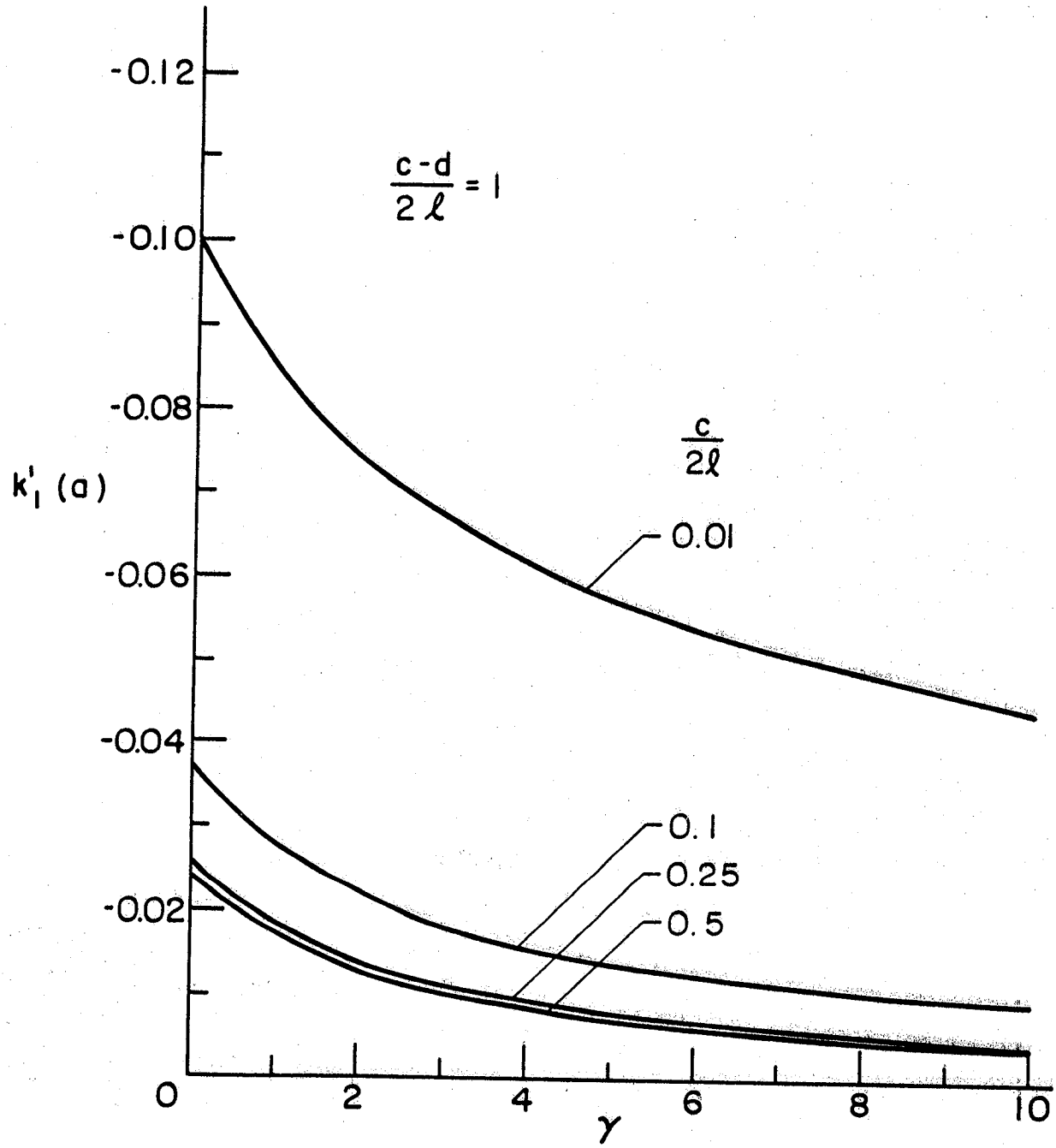

Figure 25. Mode I stress intensity factor at the crack tip $x = a = -\ell$; $\sigma_{xx}^{\infty} \neq 0$, $\sigma_{yy}^{\infty} = \sigma_{xy}^{\infty} = 0$, $\nu = 0.3$, $\theta = \pi/2$, $b = \ell$, $d-c = 2\ell$

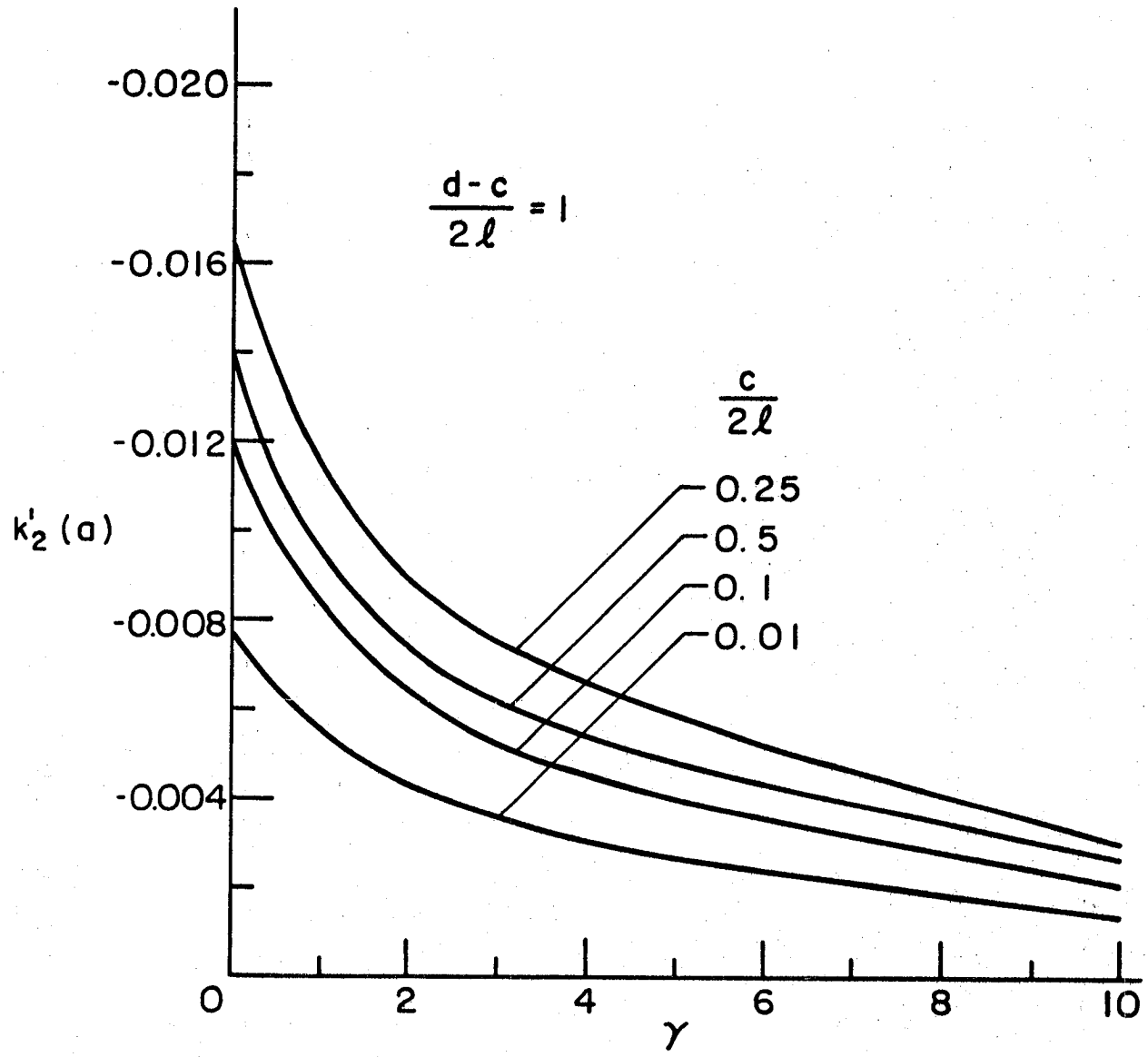

Figure 26. Mode II stress intensity factor at the crack tip $x = a = -\ell$; $\sigma^{\infty}_{xx} \neq 0$, $\sigma^{\infty}_{yy} = \sigma^{\infty}_{xy} = 0$, $\nu = 0.3$, $\theta = \pi/2$, $d-c = 2\ell$, $b = \ell$.

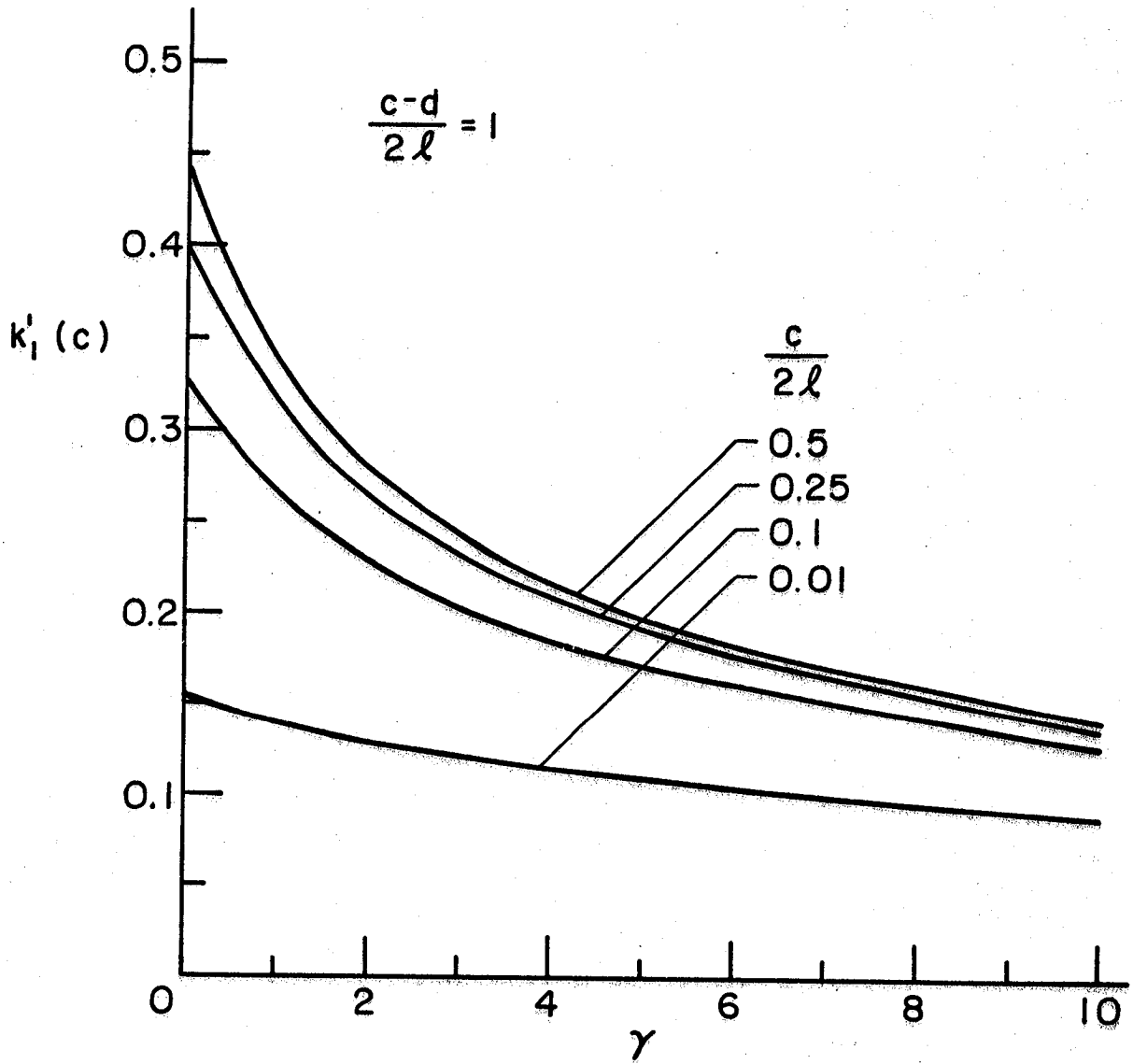

Figure 27. Stress intensity factor at the inclusion end y = c; $\sigma_{xx}^{\infty} \neq 0$, $\sigma_{yy}^{\infty} = \sigma_{xy}^{\infty} = 0$, $\nu = 0.3$, $\theta = \pi/2$, d-c = 2ℓ, b = ℓ = -a.

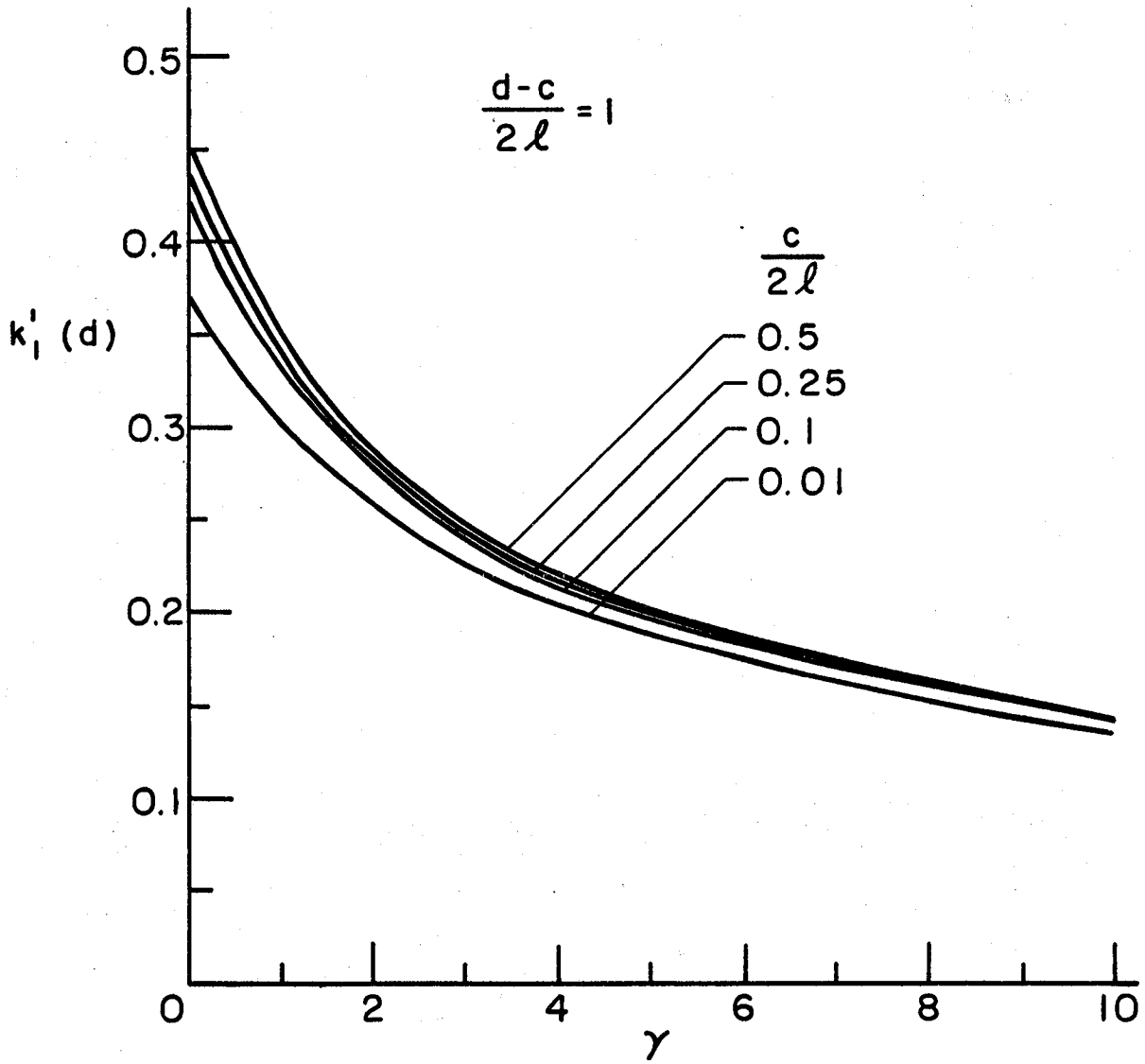

Figure 28. Stress intensity factor at the inclusion end y = d; $\sigma^{\infty}_{xx} \neq 0$, $\sigma^{\infty}_{yy} = \sigma^{\infty}_{xy} = 0$, $\nu = 0.3$, $\theta = \pi/2$, d-c = 2ℓ, b = ℓ = -a.

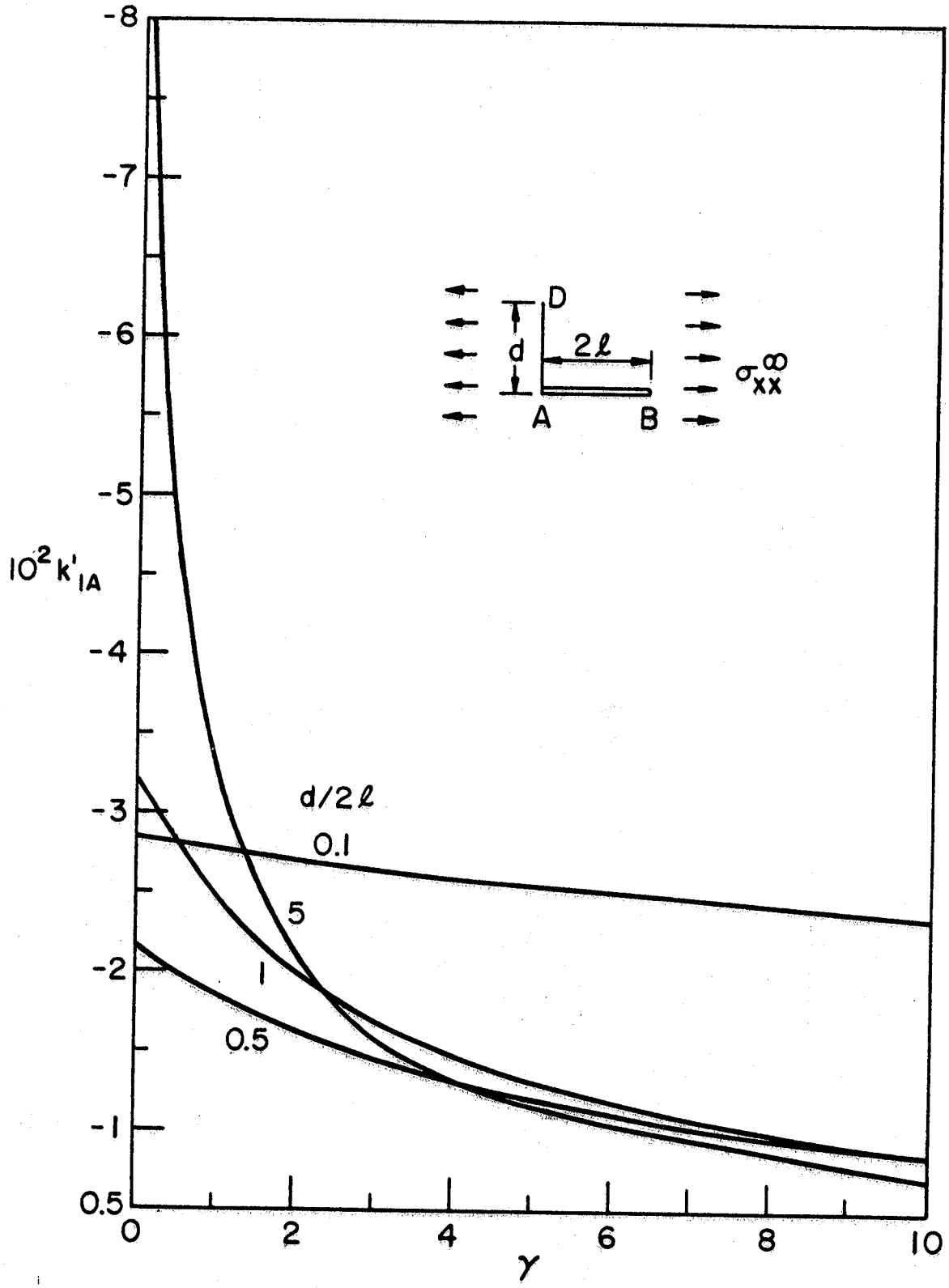

Figure 29. Normalized stress intensity factor for the inclusion-crack intersection problem for which $\theta = \pi/2$, $a = 0$, $b = 2\ell$, $c = 0$, $d/2\ell$ and γ variables. k_{IA} for $\sigma_{xx}^{\infty} \neq 0$, $\sigma_{xy}^{\infty} = 0$, $\sigma_{yy}^{\infty} = 0$.

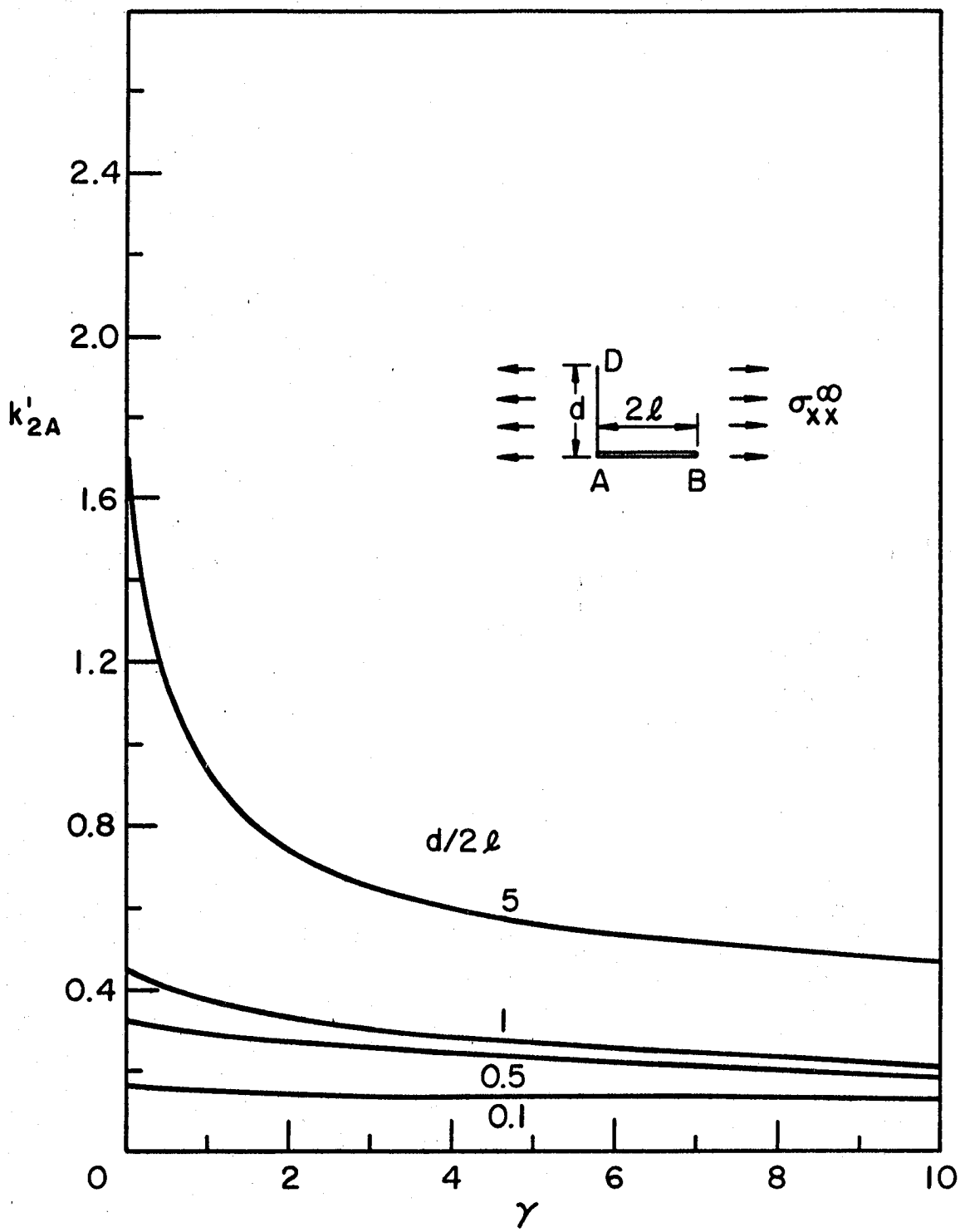

Figure 30. Normalized stress intensity factor for the inclusion-crack intersection problem for which $\theta = \pi/2$, $a = 0$, $b = 2\ell$, $c = 0$, $d/2\ell$ and γ variables. k_{2A}, $\sigma^{\infty}_{xx} = 0$, $\sigma^{\infty}_{xy} = \sigma^{\infty}_{yy} = 0$.

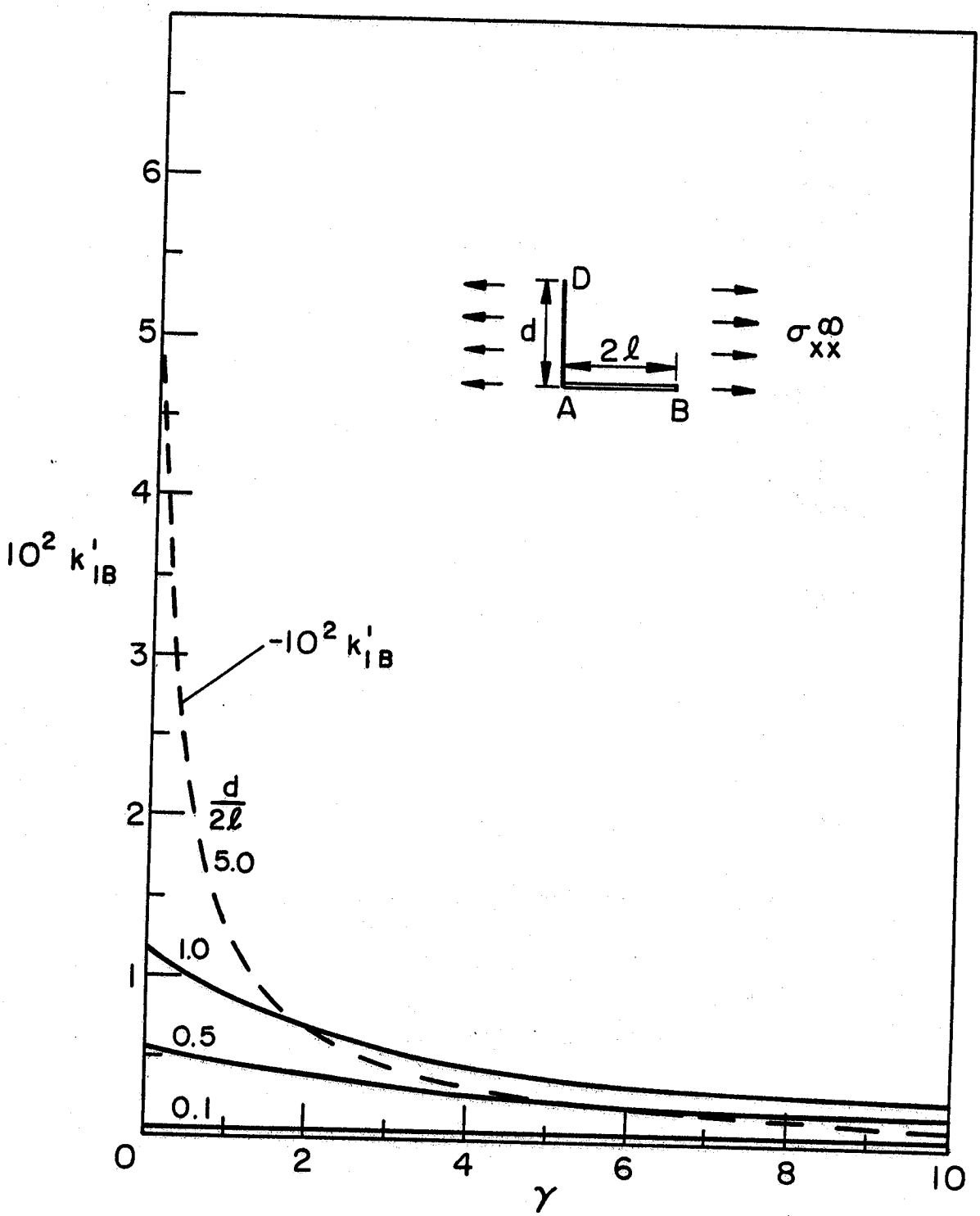

Figure 31. Normalized stress intensity factor for the inclusion-crack intersection problem for which $\theta = \pi/2$, a = 0, b = 2ℓ, c = 0, $d/2\ell$ and γ variables. k_{IB} , $\sigma_{xx}^{\infty} \neq 0$.

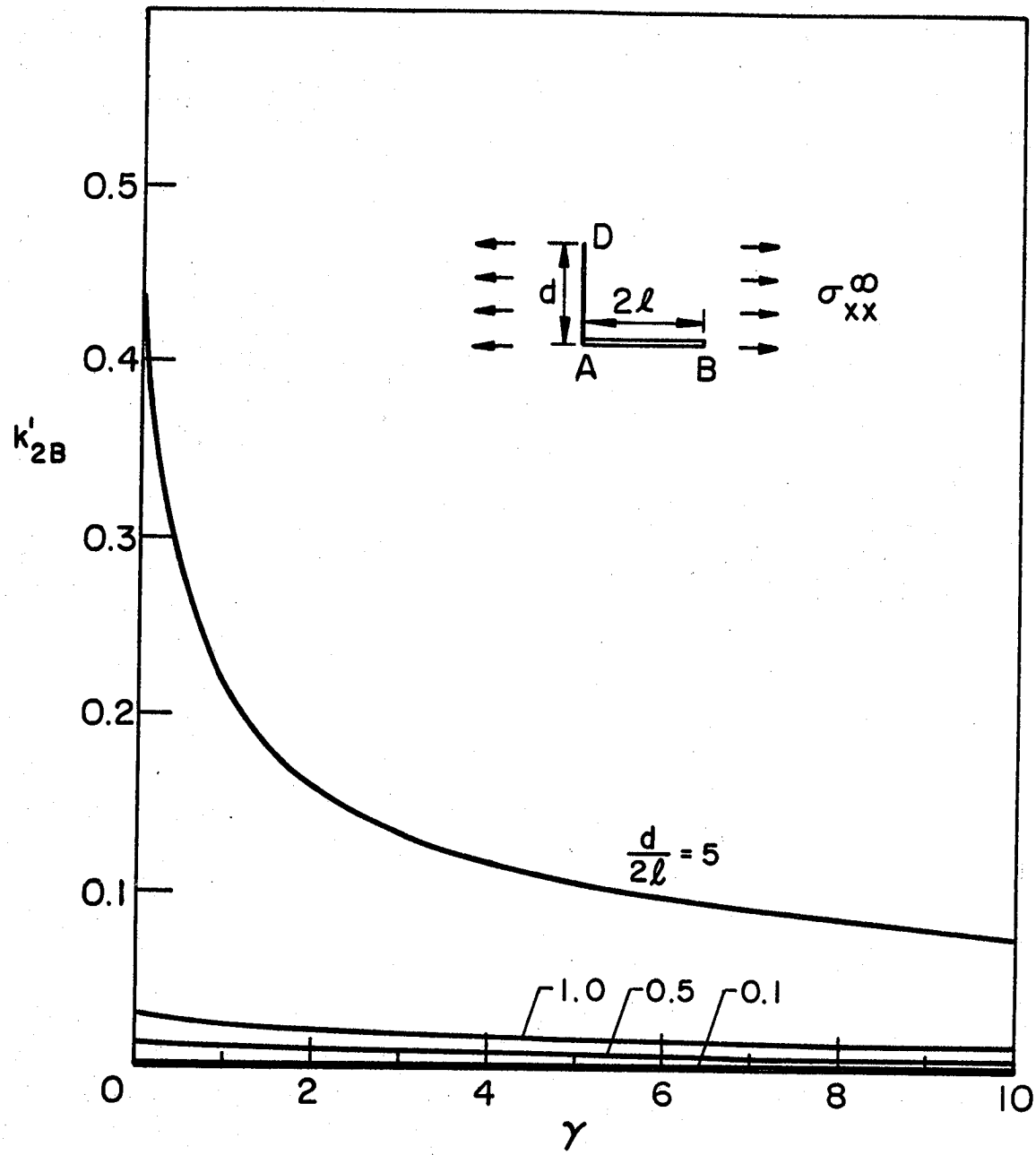

Figure 32. Normalized stress intensity factor for the inclusion-crack intersection problem for which $\theta = \pi/2$, $a = 0$, $b = 2\ell$, $c = 0$, $d/2\ell$ and γ variables. k_{2B} , $\sigma^{\infty}_{xx} \neq 0$.

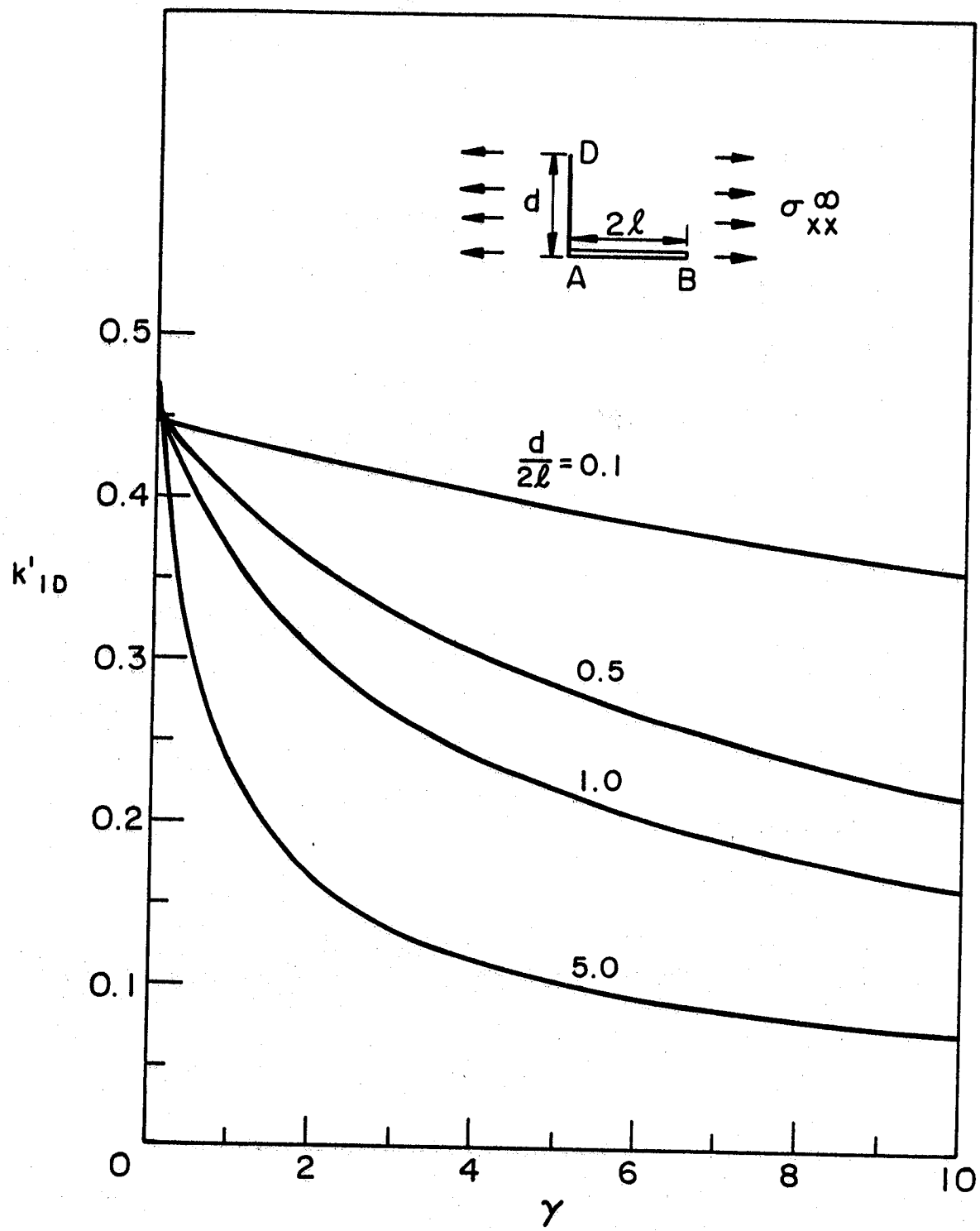

Figure 33. Normalized stress intensity factor for the inclusion-crack intersection problem for which $\theta = \pi/2$, a = 0, b = 2ℓ, c = 0, $d/2\ell$ and γ variables. k'_{ID}, $\sigma^{\infty}_{xx} = 0$.

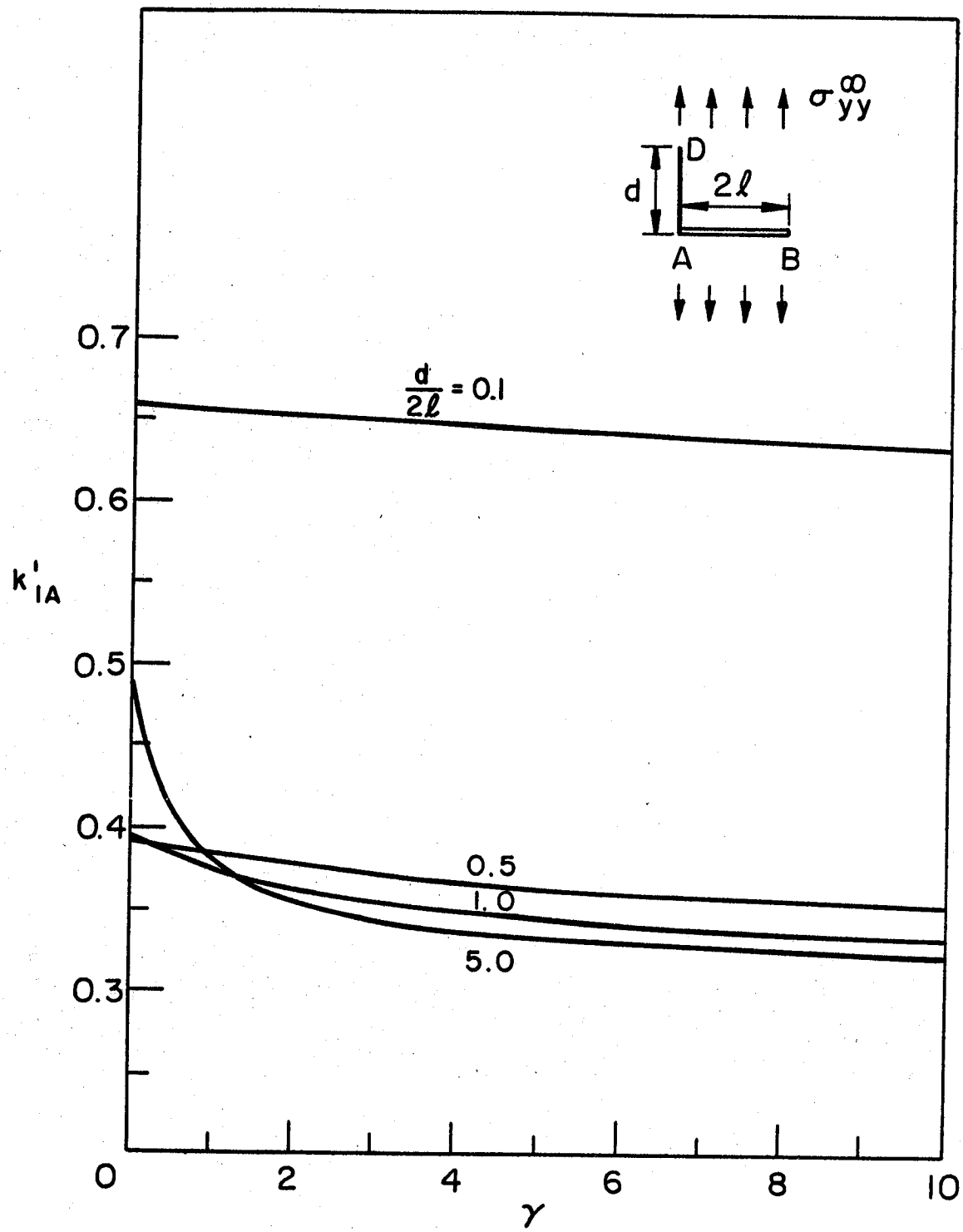

Figure 34. Normalized stress intensity factor for the inclusion-crack intersection problem for which $\theta = \pi/2$, $a = 0$, $b = 2\ell$, $c = 0$, $d/2\ell$ and γ variables. k_{IA}, $\sigma^{\infty}_{yy} \neq 0$.

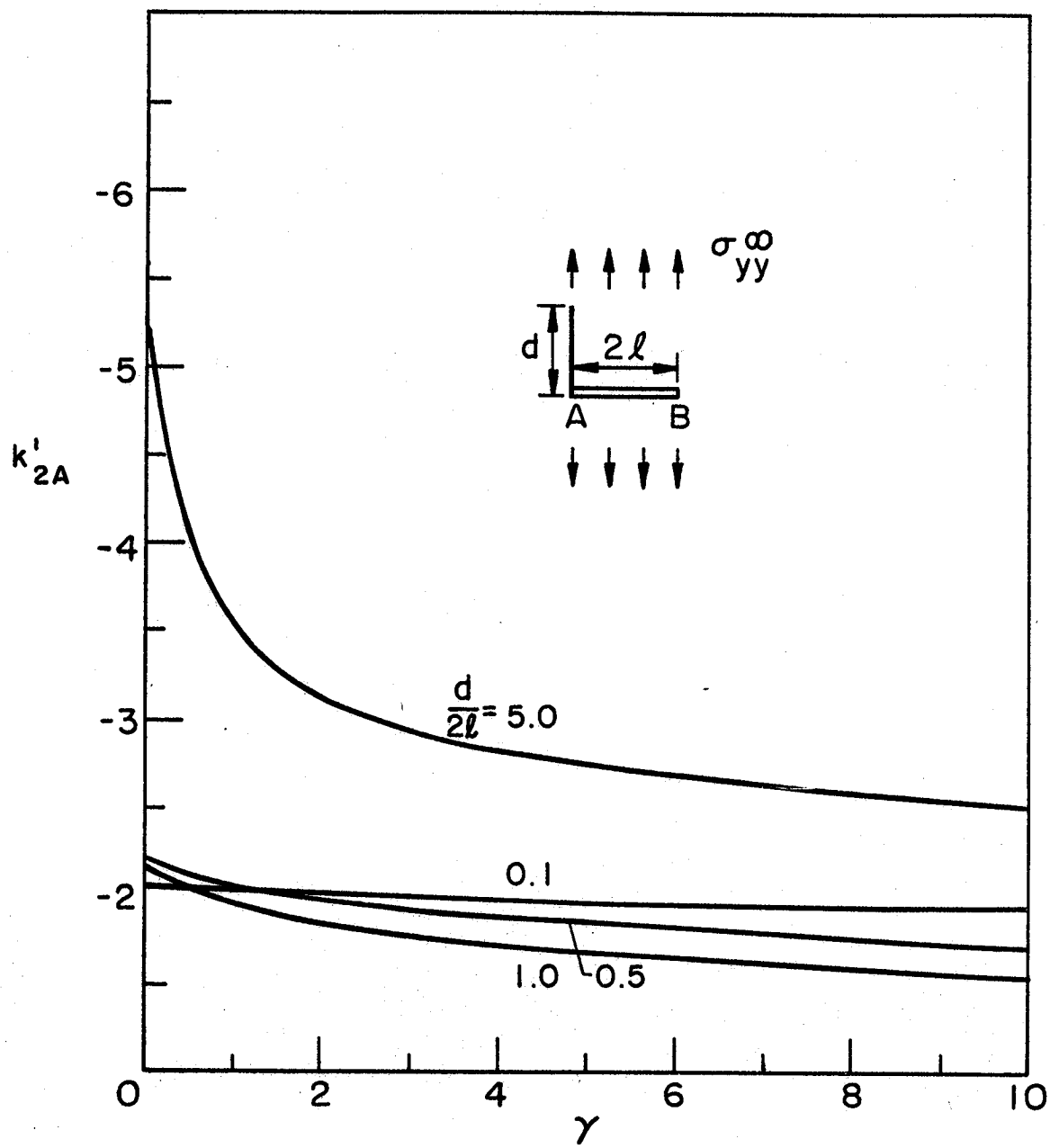

Figure 35. Normalized stress intensity factor for the inclusion-crack intersection problem for which $\theta = \pi/2$, $a = 0$, $b = 2\ell$, $c = 0$, $d/2\ell$ and γ variables. k_{2A}, $\sigma^{\infty}_{yy} \neq 0$.

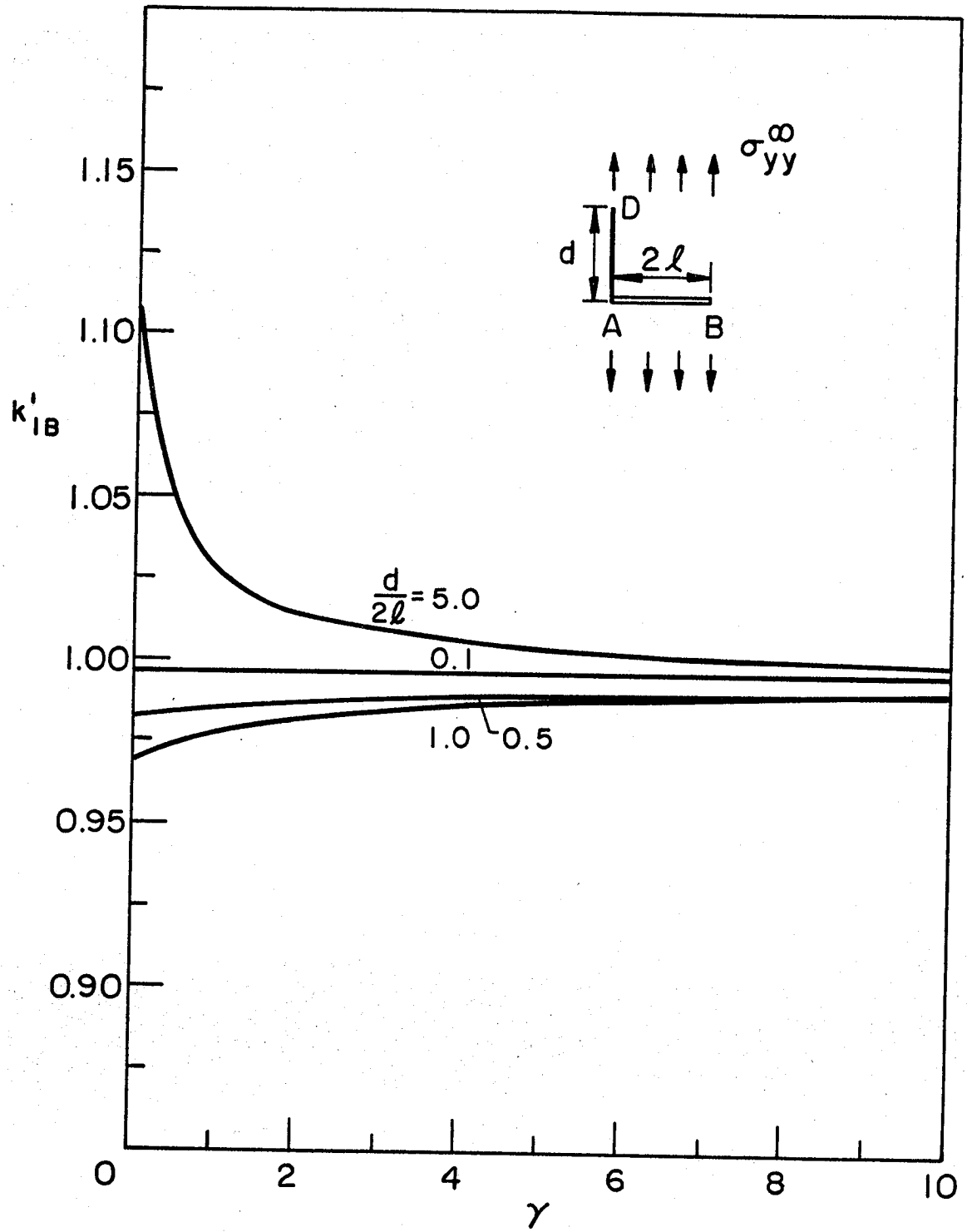

Figure 36. Normalized stress intensity factor for the inclusion-crack intersection problem for which $\theta = \pi/2$, a = 0, b = 2ℓ, c = 0, d/2ℓ and γ variables. k_{IB} , $\sigma^{\infty}_{yy} \neq 0$.

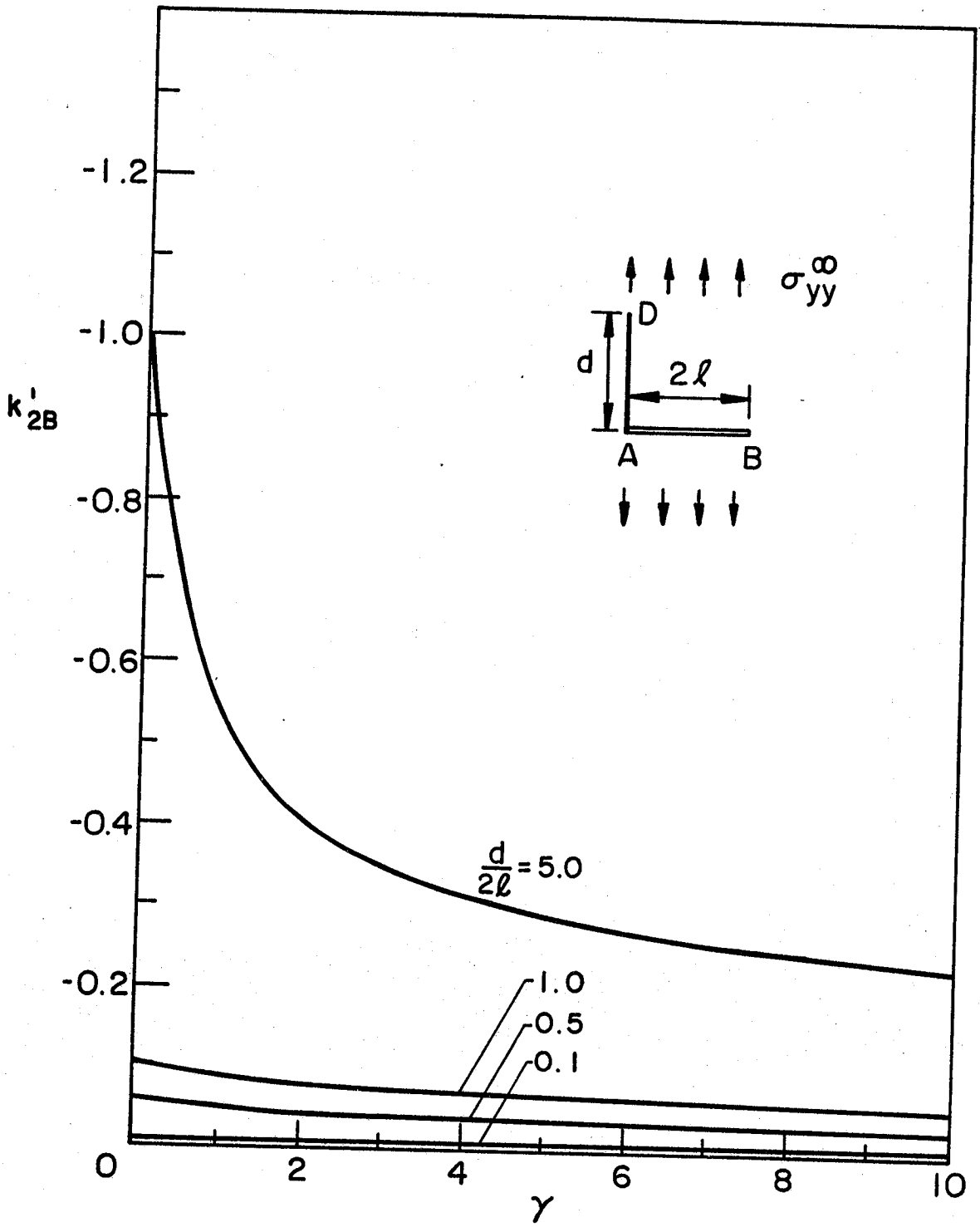

Figure 37. Normalized stress intensity factor for the inclusion-crack intersection problem for which $\theta = \pi/2$, $a = 0$, $b = 2\ell$, $c = 0$, $d/2\ell$ and γ variables. k'_{2B}, $\sigma^{\infty}_{yy} \neq 0$.

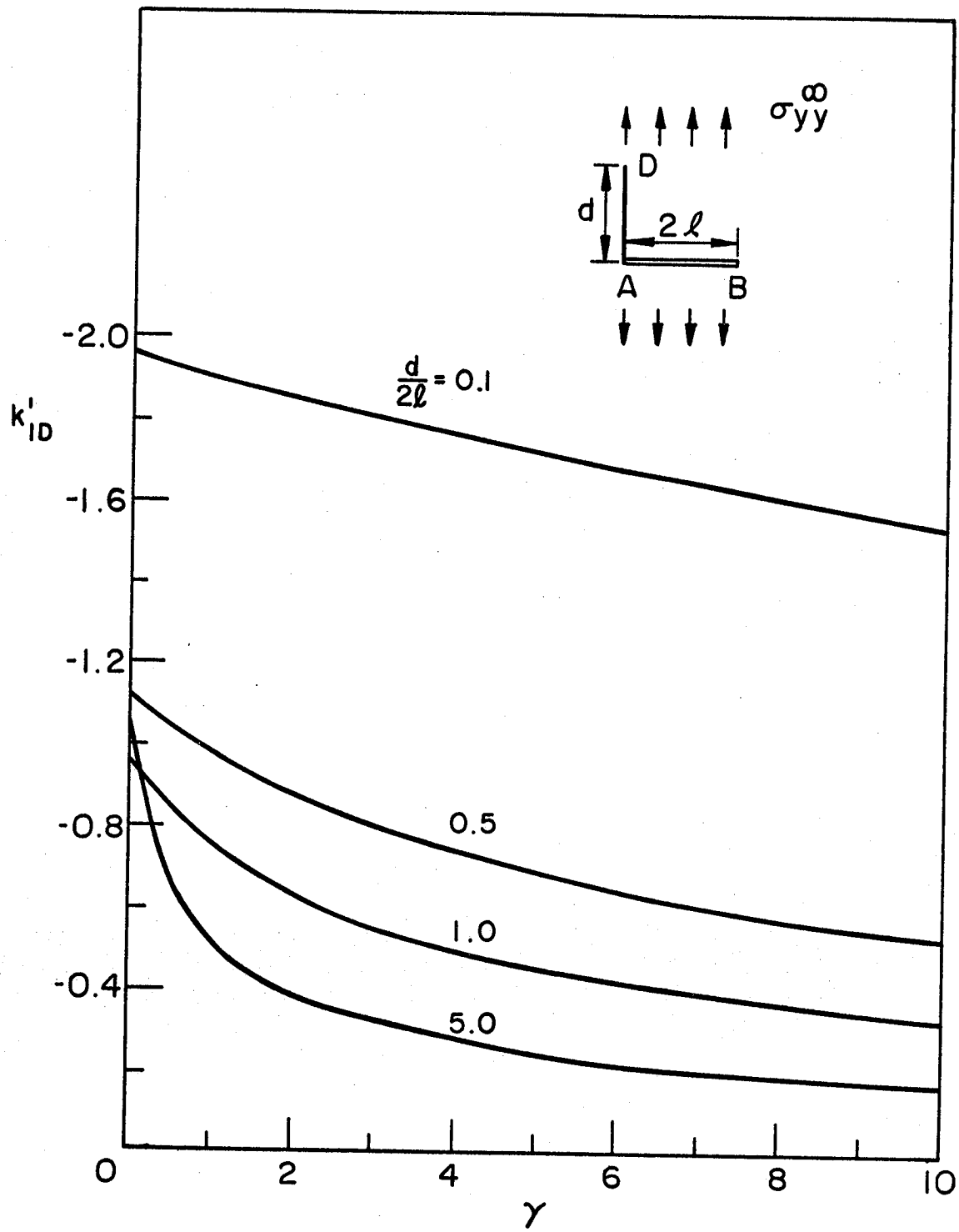

Figure 38. Normalized stress intensity factor for the inclusion-crack intersection problem for which $\theta = \pi/2$, a = 0, b = 2ℓ, c = 0, d/2ℓ and γ variables. k'_{1D}, $\sigma_{yy}^{\infty} \neq 0$.

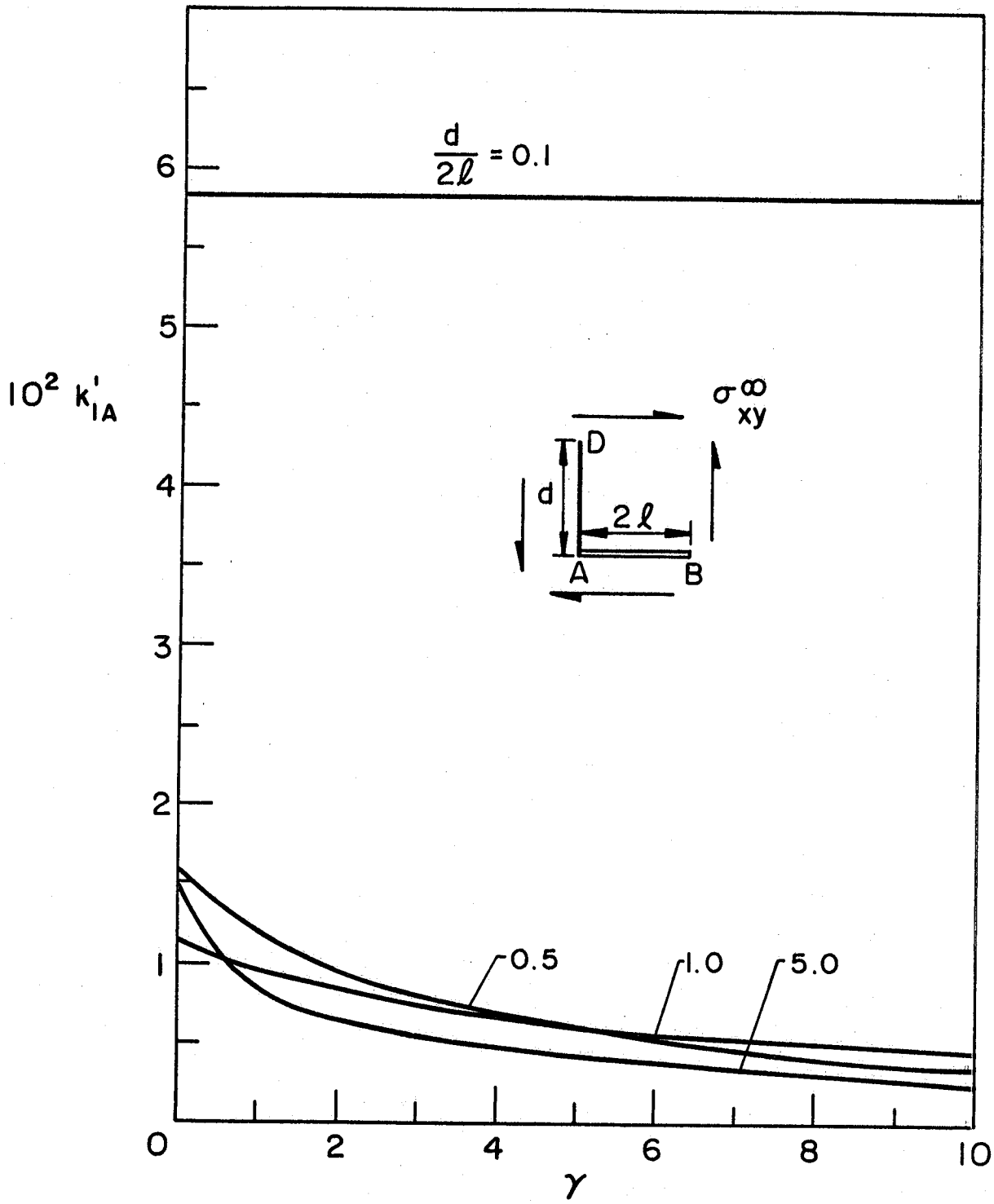

Figure 39. Normalized stress intensity factor for the inclusion-crack intersection problem for which $\theta = \pi/2$, $a = 0$, $b = 2\ell$, $c = 0$, $d/2\ell$ and γ variables. k_{IA} , $\sigma^{\infty}_{xy} \neq 0$.

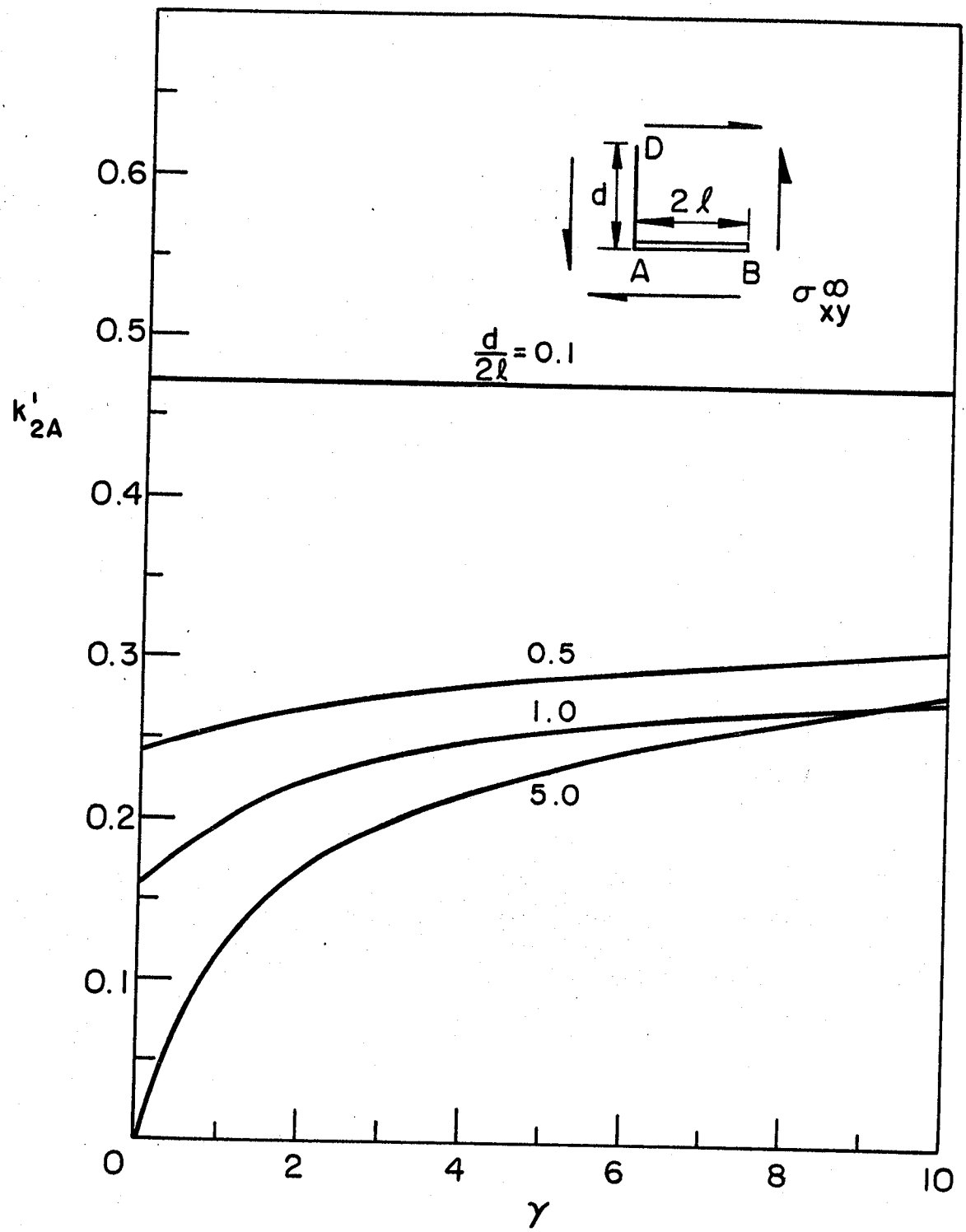

Figure 40. Normalized stress intensity factor for the inclusion-crack intersection problem for which $\theta = \pi/2$, a = 0, b = 2ℓ, c = 0, d/2ℓ and γ variables. k_{2A} , $\sigma^{\infty}_{xy} \neq 0$.

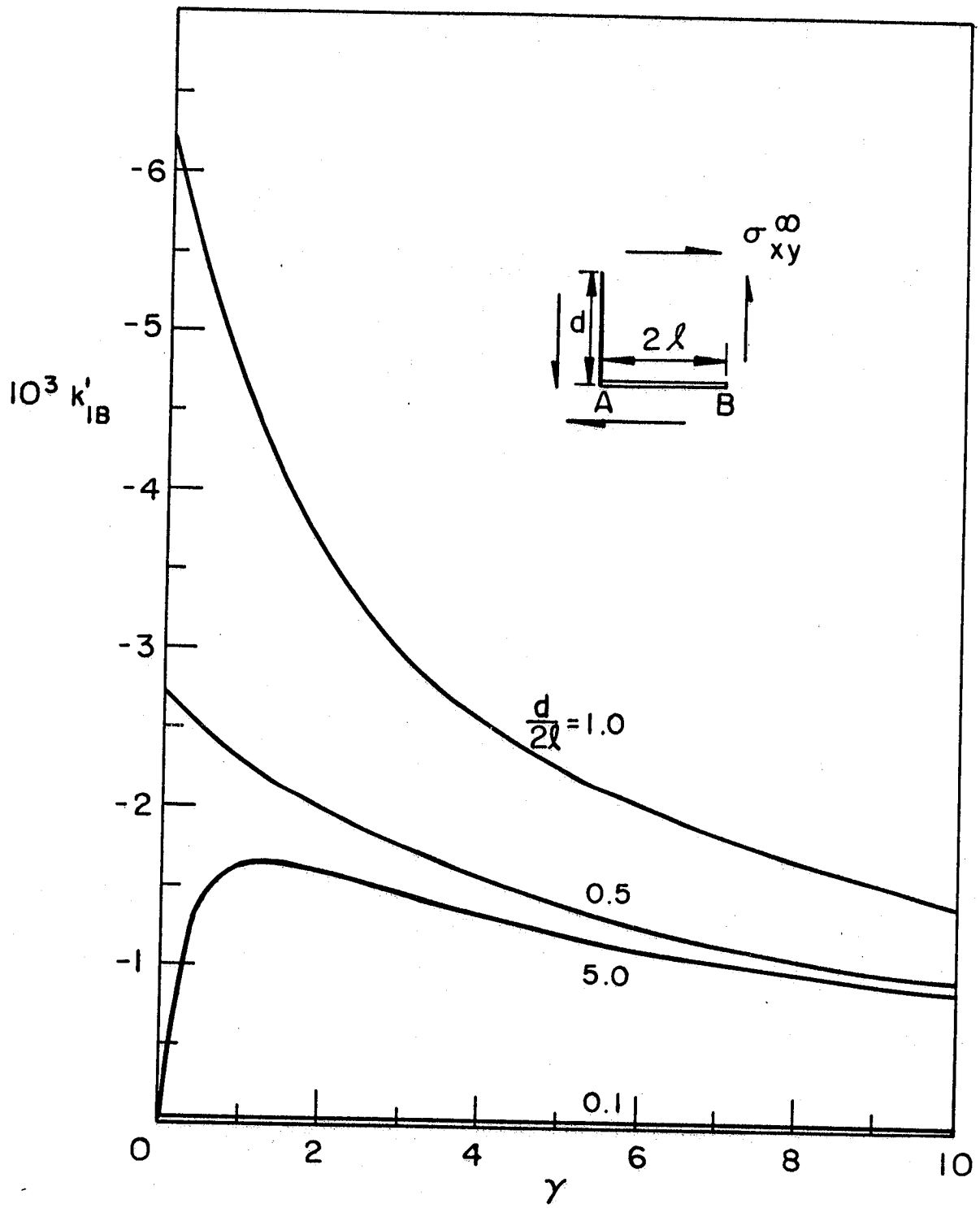

Figure 41. Normalized stress intensity factor for the inclusion-crack intersection problem for which $\theta = \pi/2$, a = 0, b = 2ℓ, c = 0, d/2ℓ and γ variables. k_{IB} , $\sigma^{\infty}_{xy} \neq 0$.

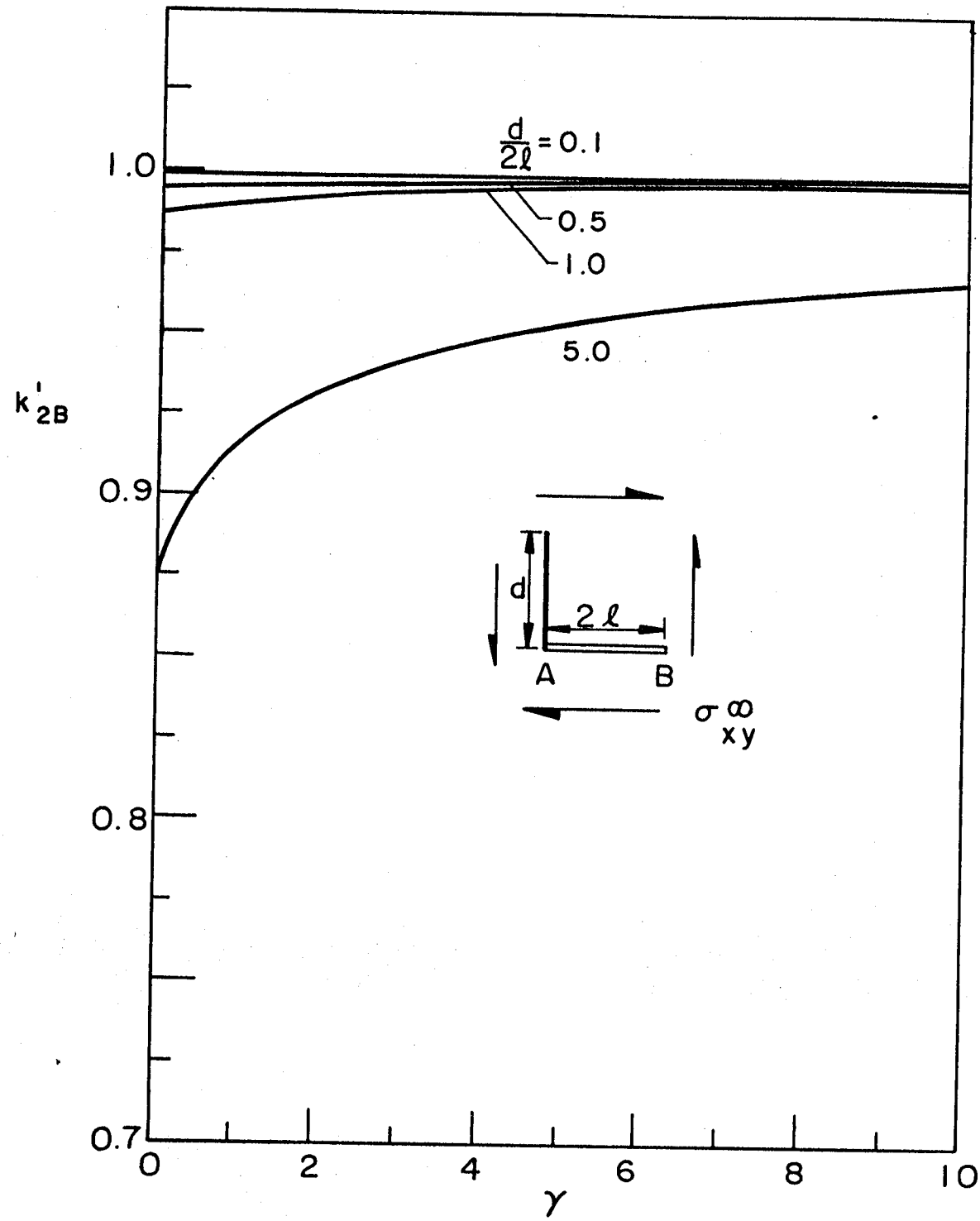

Figure 42. Normalized stress intensity factor for the inclusion-crack intersection problem for which $\theta = \pi/2$, a = 0, b = 2ℓ, c = 0, d/2ℓ and γ variables. k'_{2B} , $\sigma^{\infty}_{xy} \neq 0$.

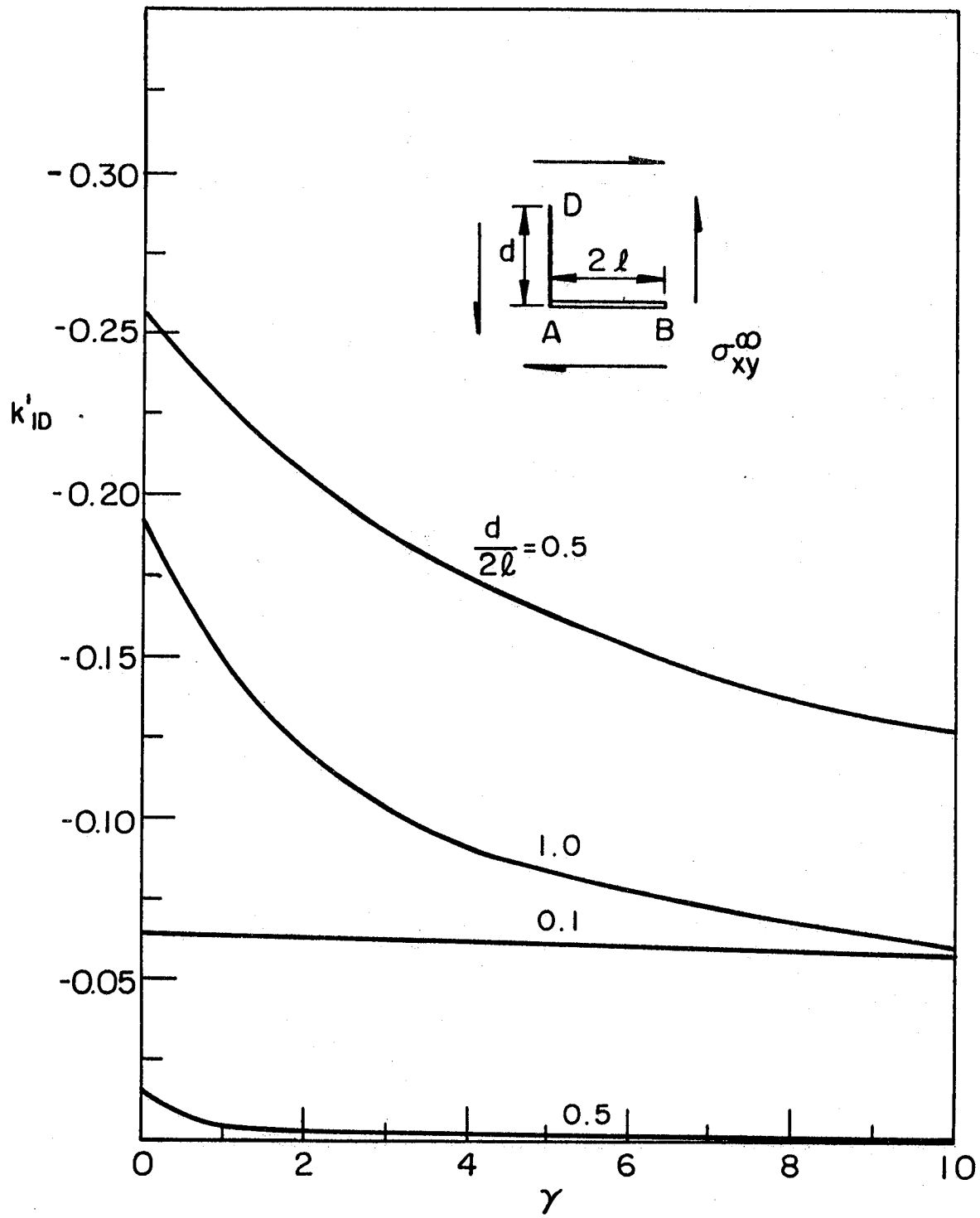

Figure 43. Normalized stress intensity factor for the inclusion-crack intersection problem for which $\theta = \pi/2$, a = 0, b = 2ℓ, c = 0, d/2ℓ and γ variables. k'_{ID} , $\sigma^{\infty}_{xy} \neq 0$.

1. Report No.	2. Government Accession No.	3. Recipient's Catalog No.
NASA CR-172308		

4. Title and Subtitle	5. Report Date
THE CRACK-INCLUSION INTERACTION PROBLEM	February 1984
	6. Performing Organization Code

7. Author(s)	8. Performing Organization Report No.
Liu Xue-Hui and F. Erdogan	
	10. Work Unit No.
9. Performing Organization Name and Address	
Lehigh University Bethlehem, PA 18015	11. Contract or Grant No. NGR-39-007-011
	13. Type of Report and Period Covered Contractor Report
12. Sponsoring Agency Name and Address	
National Aeronautics and Space Administration Washington, DC 20546	14. Sponsoring Agency Code

15. Supplementary Notes

Langley technical monitor: W. S. Johnson

16. Abstract

In this study the general plane elastostatic problem of interaction between a crack and an inclusion is considered. The Green's functions for a pair of dislocations and a pair of concentrated body forces are used to generate the crack and the inclusion. The integral equations of the problem are obtained for a line crack and an elastic line inclusion having an arbitrary relative orientation and size. The nature of stress singularity around the end points of rigid and elastic inclusions is described. Three special cases of this intersection problem have been studied: A crack and an inclusion which are collinear and have a common end point; a crack perpendicular to an inclusion with a common end point (the L configuration); and a crack perpendicular to an inclusion terminating at its midpoint (the T configuration). The problem is solved for an arbitrary uniform stress state away from the crack-inclusion region. First, the nonintersecting crack-inclusion problem is considered for various relative size, orientation, and stiffness parameters, and the stress intensity factors at the ends of the inclusion and the crack are calculated. Then for the crack-inclusion intersection case, special stress intensity factors are defined and are calculated again for various values of the parameters defining the relative size and orientation of the crack and the inclusion and the stiffness of the inclusion.

17. Key Words (Suggested by Author(s))	18. Distribution Statement
Crack-inclusion interaction Stress intensity factors Green's functions	Unclassified - Unlimited Subject Category 39

19. Security Classif. (of this report)	20. Security Classif. (of this page)	21. No. of Pages	22. Price
Unclassified	Unclassified	70	A04

For sale by the National Technical Information Service, Springfield, Virginia 22161